Effects of Composition and Fabrication Process on Glass Properties

Sakaguchi, Koichi

(Degree)
博士（理学）

(Date of Degree)
2007-03-25

(Date of Publication)
2012-04-25

(Resource Type)
doctoral thesis

(Report Number)
甲4017

(URL)
https://hdl.handle.net/20.500.14094/D1004017

Doctoral Dissertation

Effects of Composition and Fabrication Process on Glass Properties

February 2007

Graduate School of Science and Technology,

Kobe University

Koichi SAKAGUCHI

Doctoral Dissertation

Effects of Composition and Fabrication Process on Glass Properties

ガラス特性に対する組成および作製条件の影響

February 2007

Graduate School of Science and Technology,

Kobe University

Koichi SAKAGUCHI

Contents

Acknowledgements **iv**

Chapter 1. General introduction **1**

1. 1. Glass transition and relaxation of structure 2

1. 2. Glass basicity and redox reactions in glass 3

1. 3. Optical basicity concept by Duffy and Ingram 4

1. 4. Metal ion in glass 7

1. 5. Goal of this work 8

References

Chapter 2. The effect of heat treatment on optical absorption of iron in float glass **11**

2. 1. Introduction 11

2. 2. Experimental 12

2. 3. Results and discussion 14

2. 4. Conclusions 23

References

Chapter 3. Compositional dependence of infrared absorption of iron-doped silicate glasses **25**

3. 1. Introduction 25

3. 2. Experimental procedure 29

3. 3. Results 32

3. 3. 1. Absorption-spectra variation with glass composition

3. 3. 1. 1. Alkali alkaline-earth silicate glasses

3. 3. 1. 2. (Alkali) alkaline-earth (alumino-)silicate glasses

3. 3. 2. ESR spectra

3. 4. Discussion 51

3. 5. Conclusions 56

References

Chapter 4. Compositional dependence of optical absorption of bismuth-doped alumino-silicate glasses 59

4. 1. Introduction 59

4. 2. Experimental procedure 60

4. 3. Results 62

4. 4. Discussion 72

4. 5. Conclusions 74

References

Chapter 5. Composition and process dependence of optical absorption and emission properties of bismuth-containing zinc-borate glasses 77

5. 1. Introduction 77

5. 2. Experimental procedure 81

5. 2. 1. Glass composition

5. 2. 2. Glass-melting procedures

5. 2. 2. 1. One-step melting method

5. 2. 2. 2. Two-step melting method

5. 2. 3. Sample preparation and evaluation

5. 3. Results 85

5. 3. 1. Absorption properties

5. 3. 1. 1. Compositional dependence

5. 3. 1. 2. Melting-temperature dependence

5. 3. 1. 3. Effect of reagent for B_2O_3

5. 3. 1. 4. Effect of reducing agent

5. 3. 2. Emission properties

5. 3. 3. XPS spectra
5. 4. Discussion 98
5. 4. 1. Glass-fabrication conditions and optical absorption properties
5. 4. 2. Structures in the vicinity of the Bi ion
5. 5. Conclusions 108
References

Chapter 6. New Glass Sealing Method with Lead-free Solders 113
6. 1. Introduction 113
6. 2. Experimental 114
6. 2. 1. Materials
6. 2. 2. Sealing equipment and procedures
6. 2. 3. Evaluation of Joining Properties
6. 3. Results and discussion 116
6. 4. Summary 118
Refereces

Chapter 7. Conclusions 119

Publication List ***123***

Acknowledgements

This work has been done under the direction of *Doctor Takashi Uchino, Department of Chemistry, Faculty of Science, Kobe University,* from April 2004 to March 2007. I am sincerely grateful to *Dr. T. Uchino* for his enduring commitment to my thesis and so much advice full of insights. *Dr. T. Uchino* and I met about fifteen years ago, when he joined Nippon Sheet Glass Co., Ltd. Since then, he has shown me various aspects of glass, which I always found fascinating. I honestly appreciate the experience.

I would like to express my gratitude to *Professor Yoji Kawamoto,* who approved my doctoral enrollment three years ago. I sincerely thank *Prof. Y. Kawamoto* for giving me the precious opportunity.

My special thanks are due to *Professor Jun-ichiro Setsune, Professor Keisuke Tominaga and Professor Sadayuki Himeno, Kobe University,* for giving me invaluable advice to improve my thesis. I fully appreciate each piece of advice that helped me so much.

I express my sincere thanks to *Koichi Maeda, Former General Manager of Technical Research Laboratory, Nippon Sheet Glass Co., Ltd.,* for admitting my doctoral enrollment. It was a rare opportunity, and I really understand how he cared about it. My thanks are also due to *Chiharu Hisamoto, General Manager of Technical Research Laboratory, Nippon Sheet Glass Co., Ltd.,* for encouraging me to complete my doctoral thesis.

I am very grateful to *Professor Sumio Sakka* for giving me advice on various scientific and technological topics on glasses at monthly meetings in our Laboratory. *Prof. S. Sakka's* comments often helped me look at what I had not imagined was relevant to our problems.

I would like to express my sincere thanks to *Professor Masahiro Nakatsuka and Doctor Yasushi Fujimoto, Osaka University,* who discovered novel infrared emission of Bi-doped silica glass and have been collaborating with us on development of optical amplifiers. Discussions with *Prof. M. Nakatsuka and Dr. Y. Fujimoto* have been fruitful experience for us.

I owe so much to *Dr. Hiroaki Tada, Kinki University. Dr. H. Tada* has always been my roll model as a researcher since I met him eighteen years ago, when I joined Nippon Sheet Glass Co., Ltd. He has always given me encouragement and it really made me feel I can make it. His moral support has never failed to give me hope.

Many thanks are due to *Professor Katsuaki Suganuma, Osaka University,* for helping us develop hermetic sealing of glass sheets. We successfully obtained our new solder composition with his advice on metal properties and effects of processes.

I am so grateful to *Shigeki Nakagaki, Nippon Sheet Glass Co., Ltd.* for his superb experimental work on hermetic sealing of glass sheets and development on new glasses. His outstanding experimental skills and improvisation always helped us overcome haunting problems, which I swear would never have been solved if he had not been there. We worked with *Shinjiro Domi, formerly with Nippon Sheet Glass Co., Ltd.,* on hermetic sealing of glass sheets. He is the one who came up with the idea of Ti-doped Sn-Zn eutectic solder. *S. Nakagaki, S. Domi* and I developed the novel sealing technology, which I am really proud of as the best technological achievement in my career.

I would like to thank *Yoshikazu Toshikiyo* and *Masazo Endo, Nippon Sheet Glass Co., Ltd.,* for their skillful work on glass preparation and glass-property measurements.

Many excellent data were obtained using the samples that *Y. Toshikiyo* and *M. Endo* prepared.

I really thank *Doctor Masahiro Tsuda, Nippon Sheet Glass Co., Ltd.* for luminescence measurements and fruitful discussions on properties of bismuth. Thanks are also due to *Dr. K. Tsunetomo, Dr. S. Kishimoto, T. Inoue* and many others with whom I worked on Bi-doped glasses for amplifiers.

My research interest in process dependence of glass properties developed when I worked on the novel electric glass-melting furnace invented by *Seiichiro Manabe* and *Yukihito Nagashima, Nippon Sheet Glass Co., Ltd.* I respect their truly innovative invention and thank them for having provided me the opportunities to experience the technology.

I thank all my colleagues with whom I worked, including members of Engineering Group, Nippon Sheet Glass Co., Ltd., for the last eighteen years.

Finally, I sincerely thank my wife Miki and my children Yuta, Kotaro and Daisuke for having patience with my absence while I worked on my thesis. I also thank my parents living in Kagoshima for always encouraging me.

Kobe, Hyogo
February 2007

Koichi SAKAGUCHI

Chapter One

General Introduction

Glass properties are determined by the glass composition and the fabrication history (process conditions). Glass products have been developed in a way that the appropriate properties are obtained and the quality of the products is maintained in production. Glass is not an equilibrium state, and thus its state is affected by process parameters, including thermal history. For commercial glass products, redox reactions of metal ions are especially important because they affect glass properties including optical absorption (coloration), and glass quality, for example fining. To understand the effect of glass composition on redox reactions, “basicity” has been used as a basic concept. In addition to redox reactions, the state of a metal ion in glass will be affected by the matrix of the glass that the ion is incorporated to. Metal ions in glass have been treated in terms of ligand field, and concept of “basicity” will be useful in this case as

well.

Here, as an introduction to our work on effects of glass composition and process on glass properties, we first look at briefly how glass will be affected by thermal history. We also present the basic concept of basicity and how it has been used and its limitations in applications. A brief description of metal ions in glass in terms of ligand field is illustrated as well.

1. 1. Glass transition and relaxation of structure

Glass is usually obtained by cooling a melt rapidly enough to avoid crystallization. Figure 1. 1. schematically shows cooling of a liquid and glass transition. As the temperature of the liquid decreases, the volume decreases. If the temperature goes below the melting point without crystallization of the liquid, the state of supercooled liquid is reached. Glass experiences glass transition at point E in Fig. 1. 1., and the temperature-volume curve has a different gradient from that for liquid. Glass is in a higher energy state than the case of crystal. If a glass is heated to a temperature near the glass-transition temperature, it will undergo relaxation of structure and release part of the excessive energy. Thus, glass products usually shrink when they are re-heated because their structures are not fully relaxed in conventional production. The relaxation affects glass properties including thermal expansion, density and optical properties, etc.

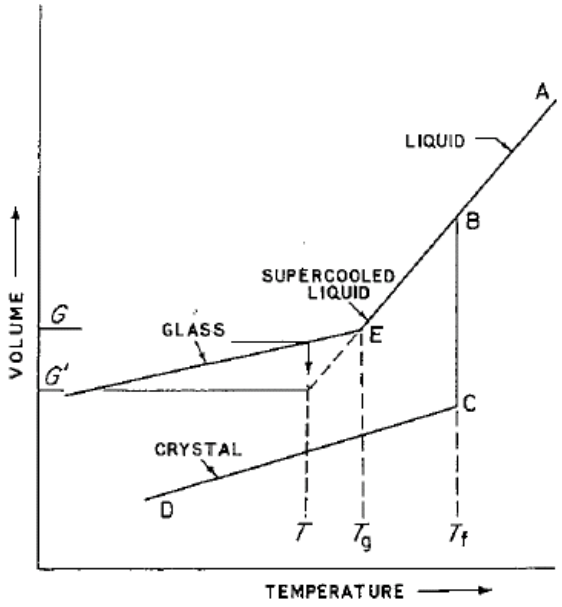

Fig. 1. 1. Relationship between the glassy, liquid and solid states [1].

1. 2. Glass basicity and redox reactions in glass

In glass production, redox reactions are controlled by oxidizing and reducing agents, melting temperature and atmosphere, etc. Glass composition determines the limits the glass can achieve under the conditions. Take iron for example. We express the redox reaction of Fe^{2+}/Fe^{3+} as follows:

$$4Fe^{2+} + O_2 = 4Fe^{3+} + 2O^{2-} \quad (1.\ 1).$$

This equation is often used because of its simplicity. Equation (1. 1) implies that $[Fe^{2+}]/[Fe^{3+}]$ is determined by both p_{O2} and aO^{2-}, namely oxygen potential and oxygen activity. Equation (1) is an overall reaction of the two following reactions:

$$Fe^{2+} = Fe^{3+} + e^{-} \quad (1.\ 2)$$

$$O_2 + 4e^{-} = 2O^{2-} \quad (1.\ 3)$$

The redox reaction of iron is under the condition of reaction (1. 3), which is an

equilibrium reaction between oxygen in atmosphere and oxygen ions in glass. The activity of O^{2-} corresponds to basicity of glass.

1. 3. Optical basicity concept by Duffy and Ingram

Duffy and Ingram proposed a concept of optical basicity, which utilizes Tl^{+}, Pb^{2+} or Bi^{3+} as probe ion to evaluate electron-donating ability of O^{2-} ions surrounding a cation [2]. Figure 1. 2. shows the definition [3]. The technique uses the peak shift of UV absorption of the probe ions to quantify the basicity.

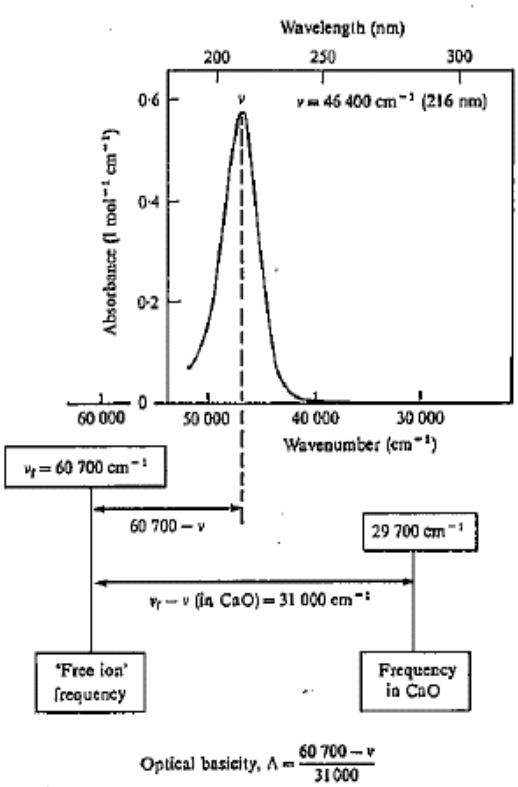

Fig. 1. 2. Definition of optical basicity. The plot shows the ultraviolet absorption spectrum of Pb^{2+} probe ion in 10 mol% Na_2O sodium borate glass (Pb^{2+} concentration 1.0×10^{-3} M, glass thickness 1.0 mm). Below the plot, the spectroscopic red shift with respect to the 'free ion' frequency of Pb^{2+} is indicated and compared with the red shift for Pb^{2+} hosted in CaO. The ratio of the red shifts is defined as optical basicity, $\Lambda = (\nu_f - \nu)/(\nu_f - \nu_{CaO})$ [3].

Using this method, we can obtain optical basicity when we have a specific glass sample. Optical basicity values [4] are obtained for various oxides and are tabulated as in Table 1. 1. With these data, we can calculate optical basicity from glass composition. We employ this "calculated optical basicity" in our investigations of compositional dependence of optical properties.

Table 1. 1.Basicity moderating parameters for elements in oxidation states denoted, and values of Λ for individual oxides [4].

Element	γ	Oxide	Λ
Caesium(I)	0.60	Cs_2O	1.7
Potassium(I)	0.73	K_2O	1.4
Sodium(I)	0.87	Na_2O	1.15
Lithium(I)	1.0	Li_2O	1.0
Barium(II)	0.87	BaO	1.15
Strontium(II)	0.91	SrO	1.1
Calcium(II)	1.00	CaO	1.00
Iron(II)	1.0	FeO	1.0
Manganese(II)	1.0	MnO	1.0
Magnesium(II)	1.3	MgO	0.78
Aluminium(III)	1.65	Al_2O_3	0.60
Silicon(IV)	2.1	SiO_2	0.48
Boron(III)	2.36	B_2O_3	0.42
Hydrogen(I)	2.5	H_2O	0.40
Phosphorus(V)	3.0	P_2O_5	0.33

Values of Λ are expressed to the nearest 0.05 for oxides of formula M_2O and MO (except CaO and MgO)

Using the optical basicity obtained this way, it is proposed that we can treat effects of different oxides in a universal manner. Figure 1. 3. is an example, showing that compositional dependence of $[Fe^{2+}]/[Fe^{3+}]$ ratio in alumino-silicate glasses is expressed in a simple linear relationship using optical basicity [4].

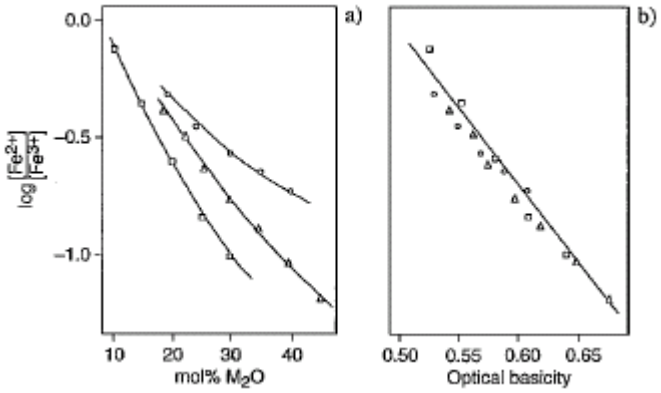

Fig. 1. 3. Effect of glass basicity on the $[Fe^{2+}]/[Fe^{3+}]$ ratio in alkali silicate glasses: (a) The upper oxidation state, Fe^{3+}, is enhanced either as the alkali oxide content is increased, or by substituting Na_2O (Δ) for Li_2O (○) and K_2O (□) for Na_2O. (b) The distinct trends for the three glass systems are united into a single trend when the plot is versus optical basicity instead of alkali oxide content [4].

Optical basicity has been widely accepted and used, especially in glass science and technology, since its introduction. However, we also have the following problems:

(a) Unable to deal with temperature dependence of basicity,

(b) Different basicity values are sometimes obtained with different probe ions,

(c) Not necessarily give the average basicity of the glass.

Duffy and Ingram themselves admit that deviations occur when different probe ions are used [5]. Figure 1. 4. shows an example.

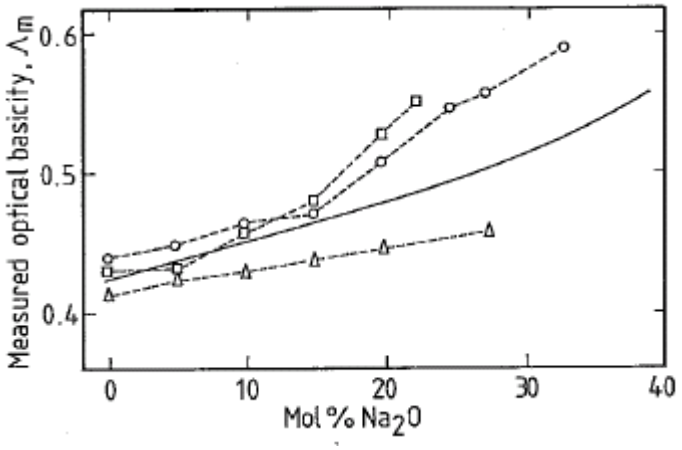

Fig. 1. 4. Trends in experimental optical basicities in Na_2O/B_2O_3 glasses using: □ Tl^+, ○ Pb^{2+}, and Δ Bi^{3+} probes. The continuous line shows the variation in the ideal or calculated basicity [5].

1. 4. Metal ion in glass

Transition metals in glass often exhibit coloration in glass. The coloration originates in d-d transition and the phenomena have been successfully dealt with using ligand-field theory [6]. Figure 1. 5. shows splitting of d orbitals when the ion takes octahedral (a), or tetrahedral (b) coordination. If the ion is in glass, the ligand of the ion is not uniform but has distortion and its structure has some distribution, which result in shifts and/or broadening of the absorption band due to the transition. In the case of oxide glasses, the ligand is influenced by states of the surrounding oxygen atoms. Thus, glass composition and process conditions affect the absorption of the metal ion in the glass.

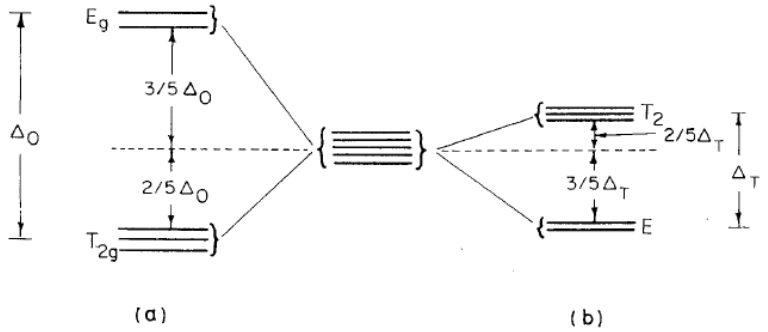

Fig. 1. 5. Energy levels diagrams showing the splitting of a set of d orbitals by (a) octahedral field, and (b) tetrahedral field [7].

1. 5. Goal of this work

In this work, we mainly deal with effects of glass composition and fabrication conditions on optical properties of glasses. For this purpose, we employ systematic composition changes and represent it using optical basicity as composition parameter. Several fabrication and treatment techniques are used to investigate process effects. We look at iron and bismuth in our investigations. Iron is the most common colorant and also the most frequently incorporated impurity in glass. Bismuth in specific glasses has been recently discovered to exhibit absorption in the visible region and infrared emission that has not been reported before [8]. We also deal with glass/metal joining, which involves oxidation effects at the interface between the two materials during a joining process.

In Chapter 2, the effects of heat treatment on optical absorption of iron-doped float glasses are discussed. We compare absorption changes of Fe^{2+} and Fe^{3+} after heat treatments and deduce structural differences. Tempered glasses are also investigated and the effect is compared with compositional effects.

In Chapter 3, compositional dependence of optical absorption of Fe^{2+} is dealt with using optical basicity as composition parameter. Systematic composition changes are applied to glasses based on a float glass and an alumino-silicate glass to investigate absorption behaviors. Interactions between alkali ions and alkaline-earth ions are estimated to affect the state of the Al^{3+} ion. An interaction between Mg^{2+} and Fe^{2+} is also predicted.

In Chapter 4, compositional dependence of optical absorption of Bi-doped alumino-silicate glasses are presented. The broad absorption band that hinders luminescence properties is mainly investigated. We consider that the Al^{3+} ion stabilizes the Bi ion in a way to prevent the ion from being reduced to metallic states. From the variations of the broad absorption with composition changes, we conclude that alkaline-earth ions, Ca^{2+}, Sr^{2+} and Ba^{2+} can associate with the Al^{3+} ion only when alkali ions are present in the glass.

In Chapter 5, process dependence of optical properties of Bi-containing zinc-borate glasses are revealed. We successfully present glasses with an identical composition and different optical properties. It is the first demonstration of its kind in investigations on Bi-doped glasses. We discuss that reducing conditions and low-temperature melting is essential to obtain the characteristic absorption bands of the glasses. Based on the deduced conditions and using *Ab initio* molecular orbital calculations, we estimate the origin of the characteristic visible-to-near-infrared absorption and the related near-infrared luminescence.

In Chapter 6, a new glass/metal-joining technology is presented. We introduce

low-temperature melting lead-free solders that join with glasses well and also employ a new sealing method called “friction-activated capillary soldering”. We demonstrate how hermetic sealing of glass sheets is obtained.

In Chapter 7, we summarize our achievements briefly.

References

[1] A. Paul, “Chemistry of Glasses”, Chipman and Hall Ltd., New York, NY, 1990, p. 3.

[2] J. A. Duffy and M. D. Ingram, “Establishment of an optical scale for Lewis basicity in inorganic oxyacids, molten salts and glasses”, J. Am. Chem. Soc., 93 (1971) 6448-6454.

[3] F. G. K. Baucke and J. A. Duffy, “The effect of basicity on redox equilibria in molten glasses”, Phys. Chem. Glasses, 32 (1991) 211-218.

[4] J. A. Duffy, “Basicity of Glass-Forming Melts”, in *“Electrochemistry of Glasses and Glass Melts, Including Glass Electrodes”*, H. Bach, F. G. K. Baucke and D. Krause Eds., Springer-Verlag, Berlin, 2000, pp 275-301.

[5] J. A. Duffy and M. D. Ingram, “Optical Basicity” in *“Optical Properties of Glass”*, D. R. Uhlmann and N. J. Kreidl Eds., American Ceramic Society, Westerville, OH, 1991, pp 159-184.

[6] A. Paul, ibid, p. 276.

[7] A. Paul, ibid, p. 278.

[8] Y. Fujimoto, M. Nakatsuka, Jpn. J. Appl. Phys. 40 (2001) L279.

Chapter Two

The Effect of Heat Treatment on Optical Absorption of Iron in Float Glass

2. 1. Introduction

Iron is a color constituent, which has been widely used for commercial glass products, especially for infrared- and ultraviolet-absorbing automotive windows. in soda-lime-silicate glasses, iron takes the form of Fe^{2+} and Fe^{3+} ions, which give rise to ligand-field bands at around 1050nm and 400nm, respectively [1-2]. The color of the glass is dependent on such factors as base glass composition, fabrication history and the total content of iron and the redox ratio (Fe^{2+}/Fe^{3+}). Several researchers reported that the absorption of the Fe^{2+} ion changes with glass composition, but few detailed quantitative analyses have been given. In addition, there have been few reports on the effects of production factors such as thermal history of the glass [3].

Float process is a smart and probably the best way to fabricate flat glass in a

large scale commercially. The glass produced by this process (float glass) does not have the completely-relaxed structure because it experiences rather rapid cooling during the annealing process after being formed as a sheet (called ribbon) in the tin bath. Re-heating the glass usually yields thermal compaction [4], which is one of the disadvantages of float glasses when they are used as substrates for flat panel displays, such as PDP. The structural relaxation also gives changes in the optical absorption of ions in the glass. It is necessary to obtain relationships between the absorption of iron and thermal history for developing new high-performance glasses. Compositional effects should be elucidated as well.

In this study, changes of optical absorption of Fe^{2+} and Fe^{3+} with heat treatment were investigated using an iron-containing float glass. The glass samples were heat-treated at and below its glass transition temperature. The results were interpreted in terms of local-basicity changes due to rearrangement of alkali ions. Compositional dependence of absorption of Fe^{2+} was also obtained for crucible-melted glasses. The absorption changes were analyzed as a function of calculated optical basicity of the glasses.

2. 2. Experimental

A float soda-lime-silicate glass containing 0.5 mass% of total iron oxide (T-Fe_2O_3) was used. The base nominal composition (mol%) is $70.9SiO_2 \cdot 0.88Al_2O_3 \cdot 5.9MgO \cdot 8.5CaO \cdot 13.6Na_2O \cdot 0.63K_2O \cdot 0.19Fe_2O_3$, which is a typical green-tinted automotive glass in the glass industry. A sheet product of 3.4 mm thick was cut into

samples of 50 mm × 50 mm in size. Each sample was set in an electric furnace at room temperature and heated at a rate of 5 ºC /min to a specified temperature. When a designated time passed, it was cooled in the furnace at a rate of 1 ºC/min or less to room temperature. Heat-treatment temperatures were in the range of 260 ºC to 550 ºC. The glass transition temperature (T_g) was determined as 550 ºC by thermal-expansion measurements prior to the heat-treatment experiments.

For obtaining the relationship between the optical basicity of glass [5] and the absorption-peak position of Fe^{2+}, glasses with different Na_2O/K_2O ratios and/or different total contents of alkali oxides ($Na_2O + K_2O$) were fabricated using crucible melting. The base composition is the one described above. The total content of alkali oxides was varied by substitution between SiO_2 and R_2O (Na_2O and K_2O). Optical basicity was calculated according to the formula by Duffy and Ingram [5]. The values of basicity that we used were 0.48 for SiO_2, 0.60 for Al_2O_3, 0.78 for MgO, 1.0 for CaO, 1.15 for Na_2O and 1.4 for K_2O. Each glass was melted in a platinum crucible at 1450 ºC for 4 hours and was cast onto a stainless-steel plate. The glass was annealed at 650 ºC for 45 minutes and cooled at a rate of 1 ºC/min or less to room temperature. These glass samples were tempered by the following procedures. A sample was put in an electric furnace kept at 650 ºC for 3 minutes. The sample was taken out of the furnace and was rapidly cooled by air-blowing the glass surfaces. A typical air-blowing condition for commercial tempered glasses was used. Optical transmission spectra of the samples were measured before and after the heating/tempering treatments with a Shimadzu UV3100PC spectrophotometer in the range of 290-2100nm.

2. 3. Results and discussion

Figure 2. 1. shows optical transmission spectra for as-drawn and a float-glass sample heat-treated at 550 ºC for 32 hours. The as-drawn glass showed a broad absorption band of Fe^{2+} at around 1080 nm and bands of Fe^{3+} in the 420-440 nm region. The heat-treatment at 550 ºC, T_g of the glass, shifted the absorption peak of Fe^{2+} to a shorter wavelength and increased the intensity of the absorption band of Fe^{3+}. Figure 2. 1. depicts the spectra for the as-drawn glass and a float-glass sample heat-treated at 370 ºC for 32 hours. As can be seen from the figure, the heat-treatment below T_g shifted the absorption peak of Fe^{2+} to a shorter wavelength largely compared with the heat-treatment at 550 ºC, but did not vary the absorption of Fe^{3+}. Figure 2. 3. depicts changes of absorption due to Fe^{3+} by showing the difference of absorbance at 420 nm between before and after heat treatment as a function of time for different heat-treatment temperatures. The treatments at the temperatures between 260 ºC and 450 ºC gave no particular increase or decrease of the absorption intensity except for small scattering of the data, whereas the treatment at 550 ºC gave a gradual increase in intensity. We consider that the result is not inconsistent with the notion that the Fe^{3+} ion takes tetrahedral coordination in alkali-containing silicate glasses as the Al^{3+} ion does and participates in the glass network. The structure in the vicinity of the Fe^{3+} ion changes little below the glass-transition temperature, at which the glass network begins to deform.

Figure 2. 4. shows variations of absorption-peak wavenumber (ν_p) of Fe^{2+} for

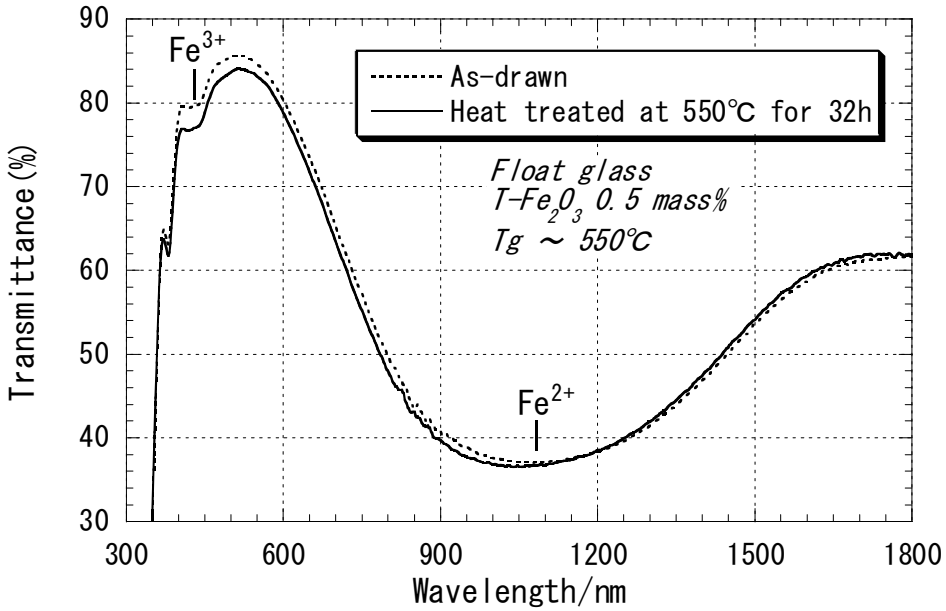

Fig. 2. 1. Transmission spectra for iron-doped float glasses: (a) as-drawn; (b) heat-treated at 550 ºC for 32 h.

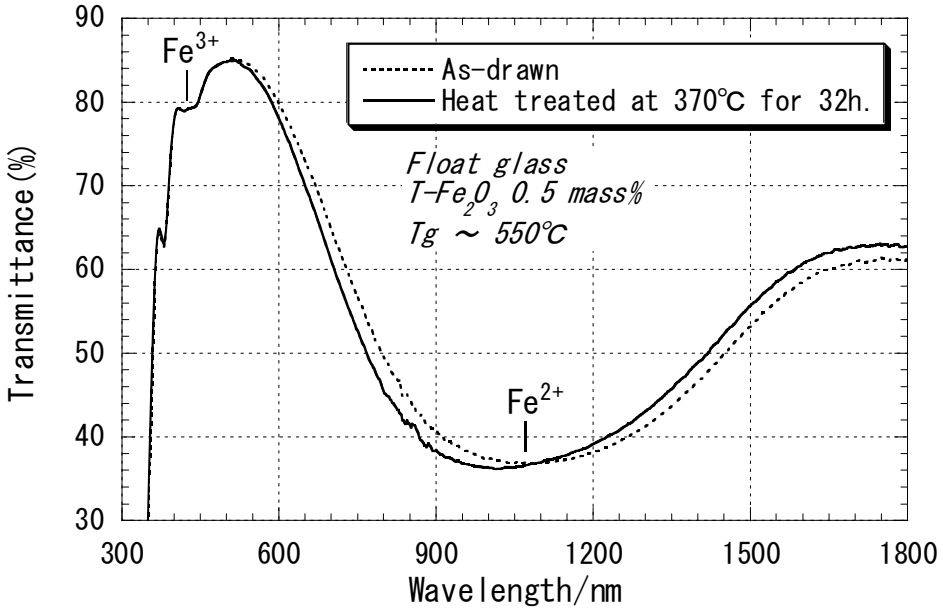

Fig. 2. 2. Transmission spectra for iron-doped float glasses: (a) as-drawn ; (b) heat-treated at 370 ºC for 32 h.

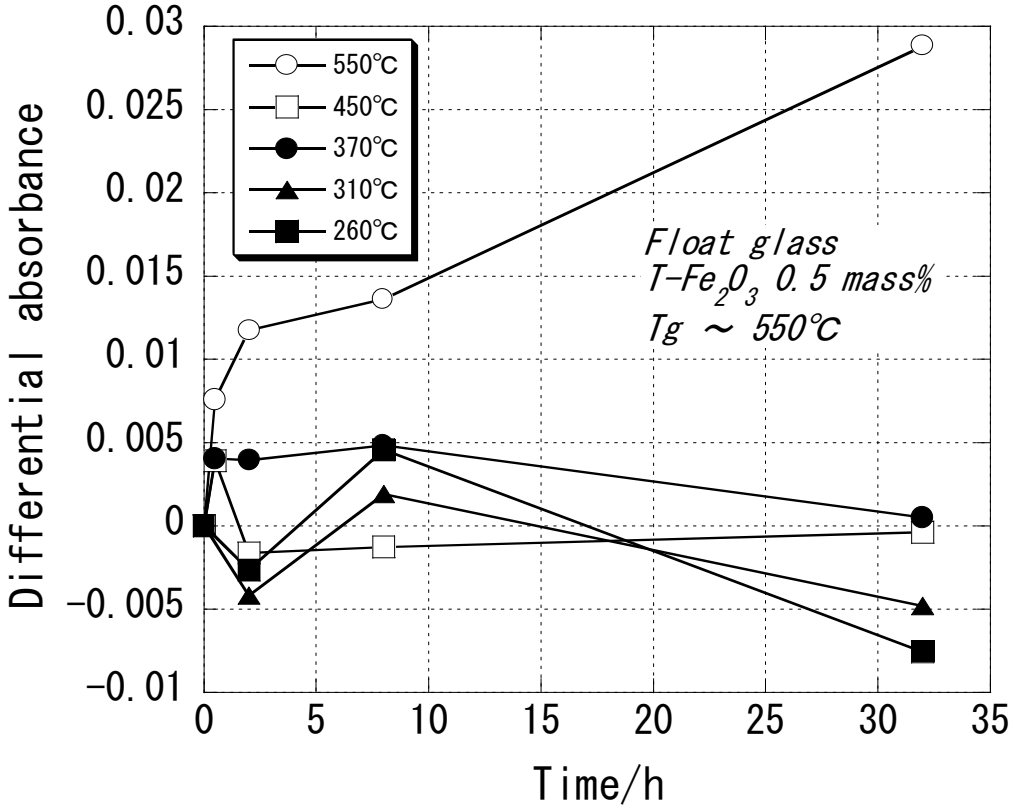

Fig. 2. 3. Difference of absorbance at 420nm before and after a heat treatment as a function of heat-treatment time for iron-doped float glasses. The heat-treatment temperatures are indicated in the figure. The absorption is due to Fe^{3+}. The lines are drawn as a guide for the eye.

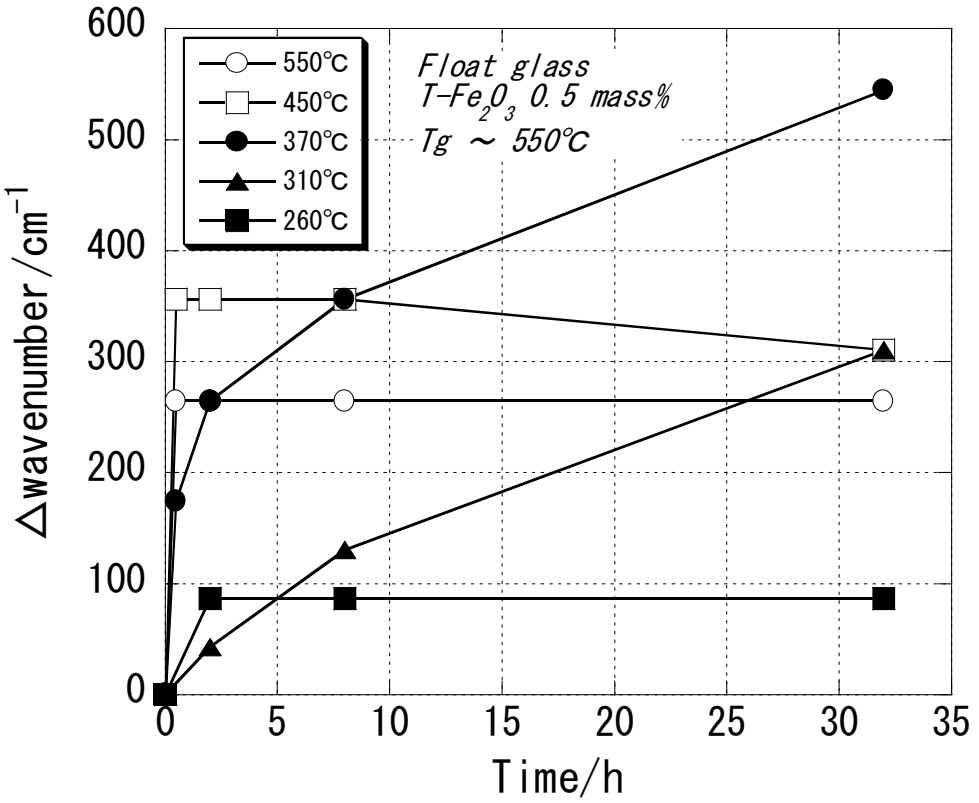

Fig. 2. 4. Variation of absorption-peak wavenumber of Fe^{2+} by heat treatment as a function of heat-treatment time for iron-doped float glasses. The heat-treatment temperatures are indicated in the figure. The lines are drawn as a guide for the eye.

different heat-treatment temperatures and time. At 450 ºC and 550 ºC, ν_p increased steeply at the initial period of the heat treatments and stayed almost the same in the subsequent period. Gradual increases in ν_p were observed for glass samples heat-treated at 310 ºC and 370 ºC. The largest increase in ν_p was observed at 370 ºC (32 h), which is nearly 200 ºC below T_g. The results suggest that rearrangement of the alkali ions is responsible for the structural relaxation of the glass below T_g. It is widely accepted that the dominant coordination of the Fe^{2+} ion is octahedral in alkali-silicate glasses. The ligand field of the Fe^{2+} ion is susceptible to local environmental changes caused by rearrangement of alkali ions. When a glass is heat-treated, the alkali ions migrate to energetically more stable sites by thermal activation. As the heat-treatment temperature increases, the thermal-activation energy increases and so does the probability of migration, but displacement of the alkali ions from the lowest-energy sites also increases by thermal vibrations of the ions. Therefore, there should be a temperature at which the rearrangement of the alkali ions takes the maximum degree. Vogel [6] states that in iron-doped phosphate glasses for infrared filters in movie projector lamps, the Fe-O interaction is weakened by high field strength of P^{5+}. The loosening of FeO_6 shifts ν_p to a lower wavenumber. Using the same argument, we consider that structural relaxation by heat treatment decreases Fe-O distance, and thus the ligand field of Fe^{2+} increases, which increases ν_p.

The infrared absorption of Fe^{2+} is due to d-d transitions [7], which are affected by electron donation from the coordinated oxygen atoms. The degree of the electron donation is defined as basicity of glass [5]. Figure 2. 5. shows relationships between ν_p

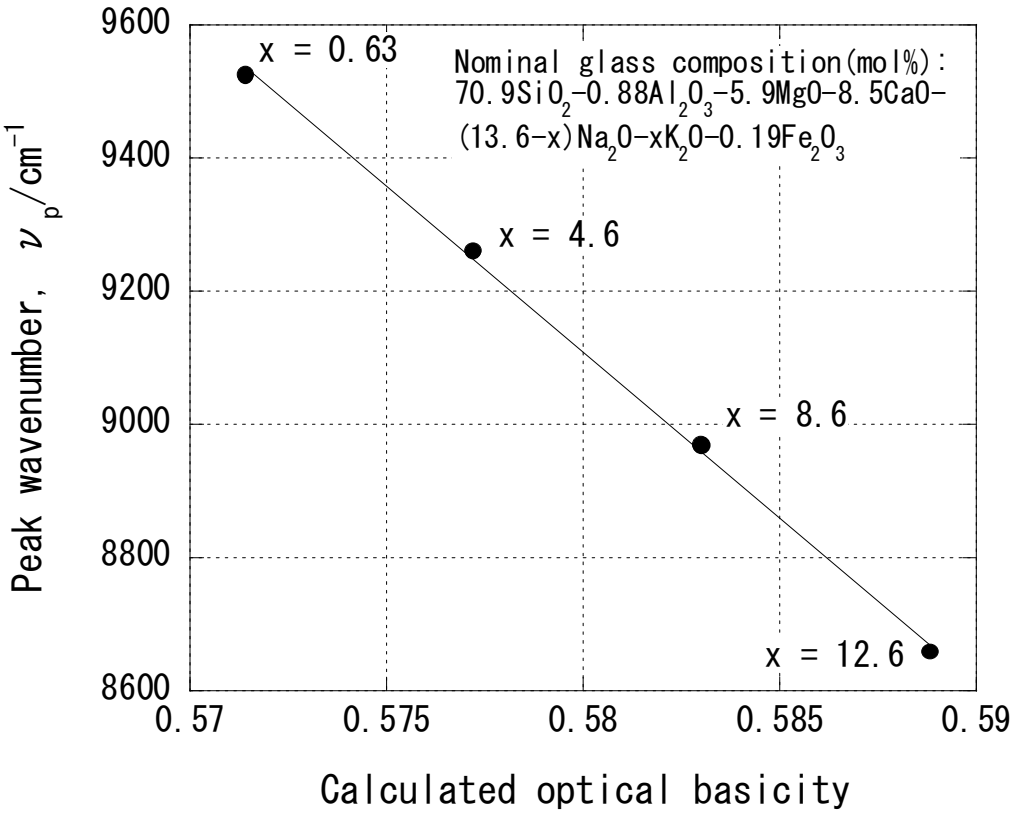

Fig. 2. 5. Relationship between calculated optical basicity and absorption-peak wavenumber of Fe^{2+} for crucible-melted alkali-containing silicate glasses. The glass compositions are defined by the formulae indicated in the figure. The line is obtained by a least-square method.

and caluculated optical basicity Λ_c for iron-containing alkali-silicate glasses with different Na_2O/K_2O ratio. We can see a good linear relationship between ν_p and Λ_c. From Fig. 2. 5., we find that a decrease of 0.012 in Λ_c, substituting 60% of K_2O for Na_2O, gives an increase of 550 cm^{-1} in ν_p, which is comparable to the variation in ν_p for the heat treatment of the float glass at 370 ºC for 32 hours.

Figure 2. 6. shows relationships between ν_p and caluculated optical basicity Λ_c for iron-containing alkali-silicate glasses with different Na_2O/K_2O ratios and different total contents of alkali oxides ($Na_2O + K_2O$). We can see good linear relationships between ν_p and Λ_c for each glass series with a constant total content of alkali oxides and varied Na_2O/K_2O ratios. We also find that increase of Λ_c by substitution of Na_2O for K_2O decreased ν_p, whereas increasing Λ_c by substituting SiO_2 for R_2O showed the opposite trend. We consider that this is the first clear observation and demonstration of the compositional effects on ν_p. Increase in the total content of the alkali oxides yields fundamentally different glass-network structures from that of the base glass, giving essentially different environments for the Fe^{2+} ion. We discuss compositional effects on infrared absorption of the Fe^{2+} ion in detail in the following chapter.

Figure 2. 6. shows effects of rapid cooling (tempering) on ν_p as well. Rapid cooling decreased ν_p from that of the as-annealed one. This is the opposite effect of heat treatment, which was described in the preceding part, and can be interpreted as weakening of Fe-O interaction. The variation of ν_p decreased with decreasing the Na_2O/K_2O ratio. One possible explanation is that potassium ions, which are much larger than sodium ions, fill the voids of the glass network than sodium ions do, leaving

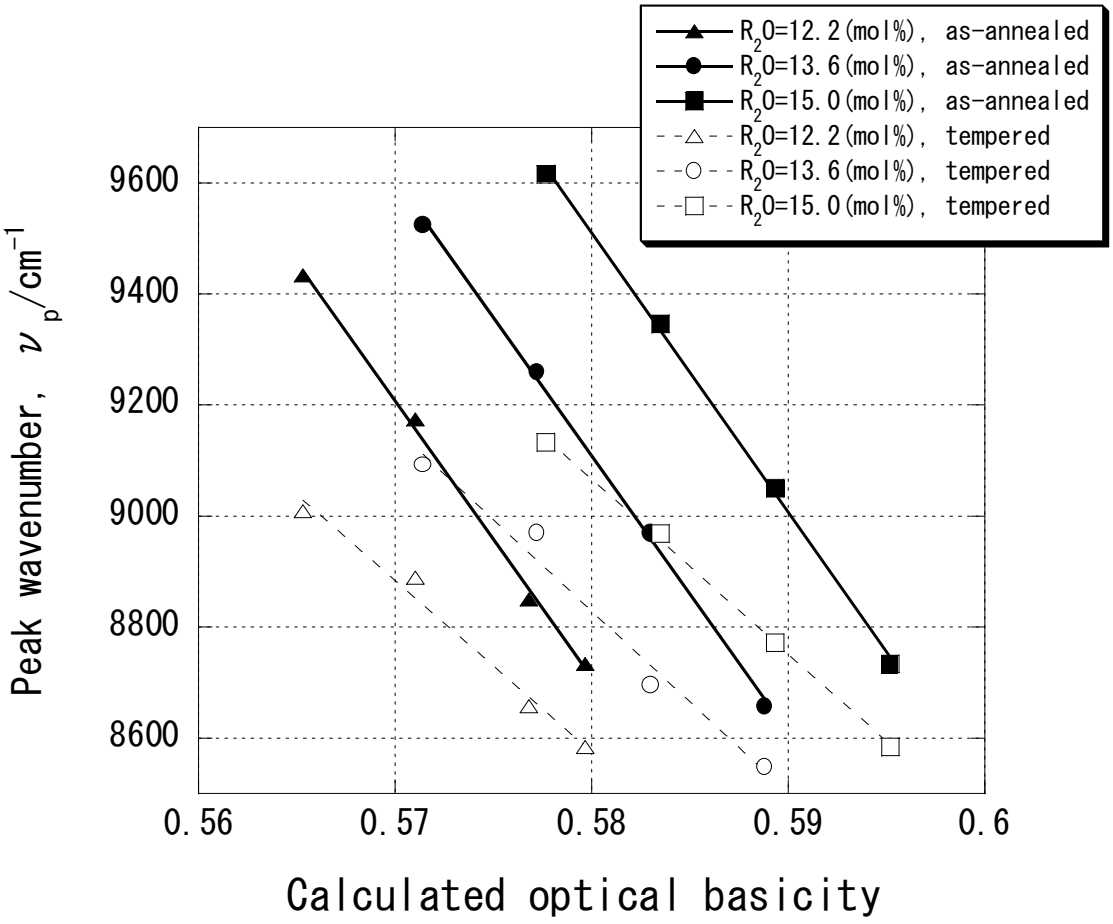

Fig. 2. 6. Relationship between calculated optical basicity and absorption-peak wavenumber of Fe^{2+} for crucible-melted alkali-containing silicate glasses. The data for as-annealed and tempered glasses are indicated by closed and open marks, respectively. The base-glass compositions in each glass series are expressed as follows:

$xK_2O{\cdot}(12.2\text{-}x)Na_2O{\cdot}8.5CaO{\cdot}5.9MgO{\cdot}0.88Al_2O_3{\cdot}72.5SiO_2$ (x = 0.63-10.7);

$xK_2O{\cdot}(13.6\text{-}x)Na_2O{\cdot}8.5CaO{\cdot}5.9MgO{\cdot}0.88Al_2O_3{\cdot}71.0SiO_2$ (x = 0.63-12.7);

$xK_2O{\cdot}(15.0\text{-}x)Na_2O{\cdot}8.5CaO{\cdot}5.9MgO{\cdot}0.88Al_2O_3{\cdot}69.6SiO_2$ (x = 0.63-12.7).

Each glass was doped with 0.19 mol% of Fe_2O_3. The total content of Na_2O and K_2O of each glass series is indicated in the figure. The lines are obtained by a least-square method.

smaller spaces for the potassium ions to displace themselves from their stabilized sites.

2. 4. Conclusions

Heat treatment of an iron-containing float glass yielded absorption changes of Fe^{2+} and Fe^{3+}. By a heat treatment at T_g, the absorption peak of Fe^{2+} at around 1080nm shifted to a shorter wavelength and the absorption of Fe^{3+} in the 420-440nm region increased in intensity. For heat treatments below T_g, only the absorption peak of Fe^{2+} shifted and no changes were observed for absorption of Fe^{3+}. It is consistent with the notion that the Fe^{3+} ion takes tetrahedral coordination and participates in the glass network in alkali-containing silicate glasses. The largest increase in absorption-peak wavenumber of Fe^{2+} (ν_p) was observed at a temperature nearly 200 ºC below T_g. The results suggest that rearrangement of the alkali ions is responsible for the structural relaxation of the glass below T_g. Compositional effects on ν_p were analyzed using caluculated optical basicity Λ_c as composition parameter. Increase of Λ_c by substitution of Na_2O for K_2O decreased ν_p, whereas increasing Λ_c by substituting SiO_2 for R_2O showed the opposite trend. Rapid cooling of glass decreased ν_p. The variation of ν_p by rapid cooling decreased with decreasing the Na_2O/K_2O ratio.

References

[1] C. R. Banford, Colour Generations and Control in Glass, Elsevier, Amsterdam, Netherlands, 1977.

[2] W. A. Weyl, Coloured Glasses, Society of Glass Technology, London, England,

1951.

[3] K. Sakaguchi, Abstracts of the Annual Meeting of The Ceramic Society of Japan, 1998, p.390.

[4] M. Anma, Glass Tecl. 40 (1999) 121.

[5] J. A. Duffy, M. D. Ingram, In: Optical Basicity, Eds D. R. Uhlmann and N. J. Kreidl, American Ceramic Society, OH, 1991, pp. 159-184

[6] W. Vogel, Chemistry of Glass, translated and edited by N. Kreidl, The American Ceramic Society Inc., Columbus, OH, 1985, p.179.

[7] J. P. Traverse, T. Toganidis, C. Ades, Glastech. Ber. 65 (1992) 201.

Chapter Three

Compositional Dependence of Infrared Absorption of Iron-Doped Silicate Glasses

3. 1. Introduction

Many commercial glass products contain iron either as dopant or impurity. For example, iron-doped glasses are widely used for infrared-absorbing automotive windows which shield heat flux of sunshine. It is mainly the effect of the Fe^{2+} ion, which exhibits a broad absorption band at around 10000cm^{-1}. The absorption usually gives blue coloration to the glass. Some other applications require colorless glasses. In these cases, iron ions, especially the Fe^{2+} ion, should be decreased to yield high transmission in the visible range. Motivated partly by these practical needs, properties and structures of iron-containing glasses have been extensively investigated [1-14].

The peak position (wavenumber) of the infrared absorption band (ν_p) at around

$10000cm^{-1}$ varies with glass composition. Vogel [15] states that in iron-doped phosphate glasses for infrared filters in movie projector lamps, the Fe-O interaction is weakened by high field strength of P^{5+}. The loosening of FeO_6 shifts ν_p to a lower wavenumber, and thus high transmission of near infrared region is obtained. Fox et al. [2] investigated compositional dependence of ν_p for $xNa_2O{\cdot}ySiO_2$ glasses and showed that ν_p increased with Na_2O content of the glass. They claimed from the results that effective negative charge of oxygen atoms increased with the composition variation, and thus the crystal field of the Fe^{2+} ion increased. Danielson et al. [3] investigated absorption properties of iron-doped $xMO{\cdot}yAl_2O_3{\cdot}zSiO_2$ glasses (M: Mg, Ca, Sr, and Ba) and found that ν_p increased with increasing the x/y value. Nakaguchi et al. [4] developed iron-doped alkali-alkaline-earth silicate glasses for infrared-absorbing windows and disclosed that substitution of MgO for BaO decreased ν_p, increasing transmission in the visible region. Combes et al. [8] reported that for silicate glasses containing alkali ions and alkaline-earth ions, ν_p decreased with SiO_2 content of the glass and increased with the field strength of modifier cations. In these reports, changes of ν_p with composition were presented and the structural changes with composition of the relevant glasses were inferred from the compositional dependence of ν_p as described above. However, the differences between the effects of alkali ions and alkaline-earth ions on ν_p have yet to be revealed clearly. The effects of interactions between the two kinds of ions on ν_p have not been illustrated, either. In addition, it has not been depicted how the dependence of ν_p on composition varies gradually, from the case of glasses having relatively high content of network-modifying cations to the case of glasses having low content of those. These

questions remain to be solved because the previous studies utilized limited ranges of glass compositions and variations in the individual investigation. Different ways of composition variation and its representation would not let us readily understand how the results relate to each other. This ambiguity of composition variation and representation is favored to be avoided, if possible, for better understanding of the glass properties. For developing new glasses, it is beneficial to illustrate the relationships between ν_p and glass composition in a unified way, using a single parameter representing the glass composition as well as classification of composition variations.

Basicity of glass has been employed by many researchers to express state of glass. Among the approaches, concept of optical basicity, proposed by Duffy and Ingram [16], has been widely accepted and used in the field of glass science and technologies. For example, Baucke et al. [17] reported that the ratio of Fe^{2+} to Fe^{3+} in alkali silicate melts can be represented as a simple linear function of optical basicity regardless of the types of alkali ion in the glasses. Optical basicity was first established using ultraviolet absorption of probe ions, such as Tl^{+}, Pb^{2+} and Bi^{3+}, then the idea was extended to obtain the value from glass composition using empirically-assigned basicities of oxides. These are two types of basicity, namely measured optical basicity Λ_m and calculated optical basicity Λ_c [18]. Although the concept of optical basicity made a remarkable success in investigating states of glass, its limitations as "universal basicity indicator" have been recognized by the inventors and other researchers. Duffy and Ingram [18] presented several examples of deviations between Λ_m and Λ_c, indicating that the environment of the site where the probe ion is accommodated does

not necessarily follow the trend that is expected from the change in the glass composition. As Morinaga et al. [19] pointed out in their review report, this is generally the case with doped metal ions in glass; the doped ion tends to interact preferentially with specific sites in the glass, depending on its character. Bearing in mind the limitations, the usefulness of optical basicity and other proposed indicators of glass basicity will be most appreciated when they are used as a tool to infer relationships between glass composition and glass structures or used as glass-composition parameter [19]. We take this approach in our investigations. We think that calculated optical basicity Λ_c, which is obtained from the glass composition, can be used for the composition parameter. It is a scale of glass composition, which is actually a complex function of components. In other words, we simplify the function using one parameter, Λ_c.

In a previous paper [9] and the preceding chapter, we reported ν_p for iron-doped alkali-alkaline-earth-silicate glasses, which had composition variations from a typical float glass. Variations of Na_2O/K_2O ratio and substitution of SiO_2 for R_2O (Na_2O and K_2O) were used for the experiments. The obtained ν_p values were investigated as a function of calculated optical basicity Λ_c, which was used as composition parameter. The results showed that two different ways of increasing Λ_c, namely, increase of R_2O and decrease of Na_2O/K_2O ratio, have opposite effects on ν_p; the former increased ν_p, whereas the latter decreased it.

In this study, we further investigated the dependence of ν_p on glass composition using two types of glass systems, namely, alkali-containing and alkali-free glasses. We

first looked at iron-doped alkali alkaline-earth-silicate glasses with alkaline-earth-oxides variations, using the same base-glass system investigated in the previous study [9], to compare the results with those for alkali-oxides variations. For a base composition of alkali-free glass, we chose so-called S-glass for high tensile-strength fibers, a glass of $MgO{\cdot}Al_2O_3{\cdot}SiO_2$ system. We consider that it is the simplest glass composition among alkali-free multi-component glasses that can be fabricated by conventional melting methods. For investigations of the composition range between the two kinds of base-glass systems, we set series of experimental glasses with steps of Na_2O content, varying Na_2O/Al_2O_3 ratio. In each series, we substituted MgO for another alkaline-earth oxide with varying quantities. The results were interpreted in terms of Λ_c-ν_p diagrams. Some novel implications on structural changes with the composition variations were obtained.

3. 2. Experimental procedure

Base glass compositions are categorized into two groups. One is an alkali alkaline-earth silicate glass system based on a typical float-glass composition, $0.63K_2O{\cdot}13.0Na_2O{\cdot}8.5CaO{\cdot}5.9MgO{\cdot}0.88Al_2O_3{\cdot}71.0SiO_2$, which was used in the previous study [9] All the glass compositions are expressed in mol% in this chapter. Composition variations include substitution between MgO and R'O, where R' is either of Ca, Sr or Ba, and substitution between SiO_2 and alkaline-earth oxides. Thus, the nominal experimental compositions are as follows:

$$0.63K_2O{\cdot}13.0Na_2O{\cdot}xR'O{\cdot}(12.4\text{-}x)MgO{\cdot}0.88Al_2O_3{\cdot}73.1SiO_2 \ (x = 0\text{-}12.4);$$

$0.63K_2O{\cdot}13.0Na_2O{\cdot}xR'O{\cdot}(14.4\text{-}x)MgO{\cdot}0.88Al_2O_3{\cdot}71.0SiO_2$ (x = 0-14.4);

$0.63K_2O{\cdot}13.0Na_2O{\cdot}xR'O{\cdot}(16.4\text{-}x)MgO{\cdot}0.88Al_2O_3{\cdot}69.0SiO_2$ (x = 0-16.4).

The other glass system is based on S-glass for high tensile-strength glass fiber, of which approximate composition is $15.8MgO{\cdot}15.6Al_2O_3{\cdot}68.6SiO_2$. This base glass composition was used for alkali-free glasses. For glasses with Al_2O_3/Na_2O substitutions, a slightly modified base-glass composition, $16MgO{\cdot}16Al_2O_3{\cdot}68SiO_2$, was used. Composition variations in alkaline-earth oxides were done in the same way as in the first glass system. Thus, the nominal experimental glass compositions are $xR'O{\cdot}(15.8\text{-}x)MgO{\cdot}15.6Al_2O_3{\cdot}68.6SiO_2$ (R': Ca, Sr and Ba, x = 0-15.8) for alkali-free glasses; $yNa_2O{\cdot}xR'O{\cdot}(16\text{-}x)MgO{\cdot}(16\text{-}y)Al_2O_3{\cdot}68SiO_2$, where x = 0-16 and y = 2-16 for R' = Ca, and x = 0-16 and y = 2, 4 for R' = Sr, Ba. To each glass of either system, 0.19 mol% of Fe_2O_3 was added.

For each glass, batch was obtained thoroughly mixing raw materials selected from reagent or high-grade industrial materials of SiO_2, Al_2O_3, MgO, $CaCO_3$, $SrCO_3$, $BaCO_3$, Na_2CO_3, K_2CO_3 and Fe_2O_3. For the float-glass-based glasses, small quantity of Na_2SO_4 and carbon was added to the batch to enhance fining of the glass melt. Each glass batch of 350-g glass was put in a platinum or a Pt-10% Rh crucible and melted in an electric furnace in air. Melting temperature and duration were 1450 ºC - 4hours for float-glass-based alkali-alkaline-earth silicate glasses. Melting conditions for S-glass-based (alkali) alkaline-earth (alumino-)silicate glasses are summarized in Table 1. The glass melt was stirred with a silica rod several times during melting to enhance its homogeneity. After the melting, the glass melt was poured onto a stainless-steel plate

and annealed in an electric furnace. The float-glass-based alkali-alkaline-earth silicate glasses were annealed at 650 ºC for 30 minutes and cooled to room temperature at the rate of 1.67 ºC/min or less. The annealing conditions for S-glass-based (alkali) alkaline-earth (alumino-)silicate glasses are described in Table 1. A sample of 30 mm × 30 mm × 3.5 mm was cut, ground and polished from each glass block. Transmission spectra were measured in the range from 290 nm to 2500 nm with a Hitachi U-4100 spectrophotometer. For each glass, the peak position of the infrared absorption band was obtained from the transmission curve, and the peak wavenumber was calculated. The estimated error for the peak wavenumber is ±50 cm^{-1}. After the first transmission measurements, the samples were ground and polished to the thickness of 2.45 mm, and transmission spectra were measured again. For each glass, the absorption spectrum was obtained using Lambert's law from the set of transmittance data for the two thicknesses. Optical basicity was calculated for each base glass according to the formula by Duffy and Ingram [20]. The values of basicity that we used were 0.48 for SiO_2, 0.60 for Al_2O_3, 0.78 for MgO, 1.0 for CaO, 1.1 for SrO, 1.4 for BaO, 1.15 for Na_2O and 1.4 for K_2O. ESR spectra were measured in X-band (9.5GHz) with a JEOL JES-TE300 ESR spectrometer, using a crushed glass sample put in a quartz tube. Marker of Mn^{2+}: MgO was used as an internal standard in the measurements.

Table 1
Melting and annealing conditions for S-glass-based (alkali) alkaline-earth (alumino-)silicate glasses doped with 0.19mol% of Fe_2O_3

y, Na_2O (mol%)	Melting	Annealing
0	1620 ºC - 7 hrs	700 ºC - 30 min
2	1620 ºC - 7 hrs	700 ºC - 30 min
4	1620 ºC - 6 hrs	700 ºC - 30 min
8	1570 ºC - 4.5 hrs	700 ºC - 30 min
12	1500 ºC - 4.5 hrs	650 ºC - 30 min
16	1450 ºC - 4 hrs	600 ºC - 45 min

After annealing, the glasses were cooled to room temperature at the rate of 1.67 ºC /min or less.

3. 3. Results

3. 3. 1. Absorption-spectra variation with glass composition

3. 3. 1. 1. Alkali alkaline-earth silicate glasses

Figures 3. 1. - 3. 3. show the dependence of ν_p on Λ_c for alkaline-earth oxides variations. In each set of the data points, the left side (low optical-basicity side) corresponds to MgO-rich glasses and the right side (high optical-basicity side) to MgO-poor glasses. For each series of MgO-CaO, MgO-SrO, and MgO-BaO, substitution of SiO_2 for R'O, which increases Λ_c, increased ν_p. On the other hand, increasing Λ_c by substituting the Mg^{2+} ion for a larger ion, either of Ca^{2+}, Sr^{2+} or Ba^{2+}, decreased ν_p. Steep decreases of ν_p were found in the region with a very low or no MgO content of the Λ_c-ν_p diagrams for MgO-CaO and MgO-SrO series, especially in the former. Figure 3. 1. also shows the data for the Na_2O-K_2O series in a previous study [9].

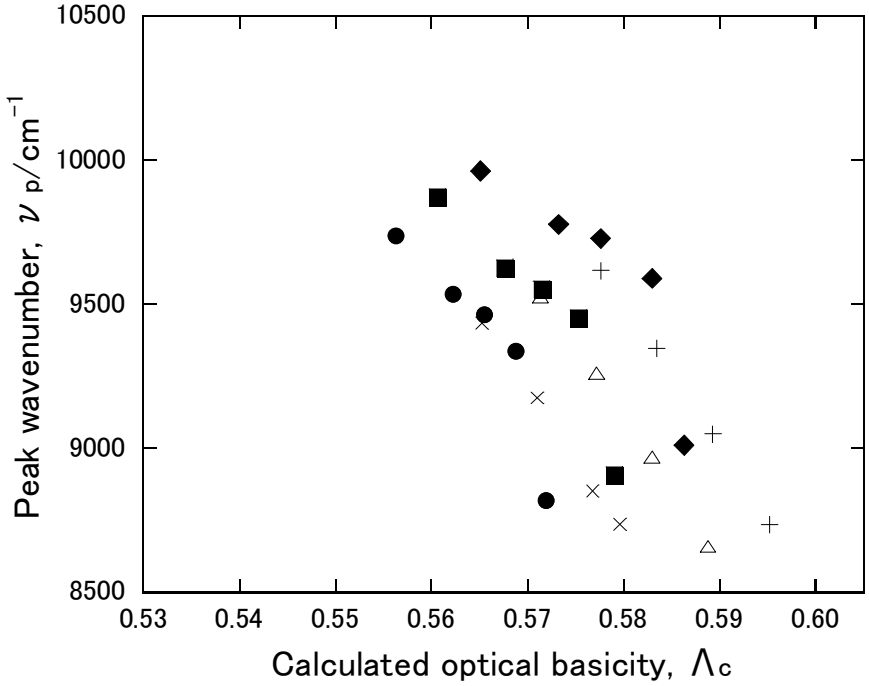

Fig. 3. 1. Absorption-peak wavenumber of Fe^{2+} as a function of calculated optical basicity for float-glass-based alkali-alkaline-earth silicate glasses:

$0.63K_2O{\cdot}13.0Na_2O{\cdot}xCaO{\cdot}(12.4\text{-}x)MgO{\cdot}0.88Al_2O_3{\cdot}73.1SiO_2$ (x = 0-12.4)(●);

$0.63K_2O{\cdot}13.0Na_2O{\cdot}xCaO{\cdot}(14.4\text{-}x)MgO{\cdot}0.88Al_2O_3{\cdot}71.0SiO_2$ (x = 0-14.4)(■);

$0.63K_2O{\cdot}13.0Na_2O{\cdot}xCaO{\cdot}(16.4\text{-}x)MgO{\cdot}0.88Al_2O_3{\cdot}69.0SiO_2$ (x = 0-16.4)(◆).

The data for glasses with K_2O/Na_2O variations by Sakaguchi [9] are also shown in the figure:

$xK_2O{\cdot}(12.2\text{-}x)Na_2O{\cdot}8.5CaO{\cdot}5.9MgO{\cdot}0.88Al_2O_3{\cdot}72.5SiO_2$ (x = 0.63-10.7) (×);

$xK_2O{\cdot}(13.6\text{-}x)Na_2O{\cdot}8.5CaO{\cdot}5.9MgO{\cdot}0.88Al_2O_3{\cdot}71.0SiO_2$ (x = 0.63-12.7)(△);

$xK_2O{\cdot}(15.0\text{-}x)Na_2O{\cdot}8.5CaO{\cdot}5.9MgO{\cdot}0.88Al_2O_3{\cdot}69.6SiO_2$ (x = 0.63-12.7)(+).

Each glass was doped with 0.19 % Fe_2O_3.

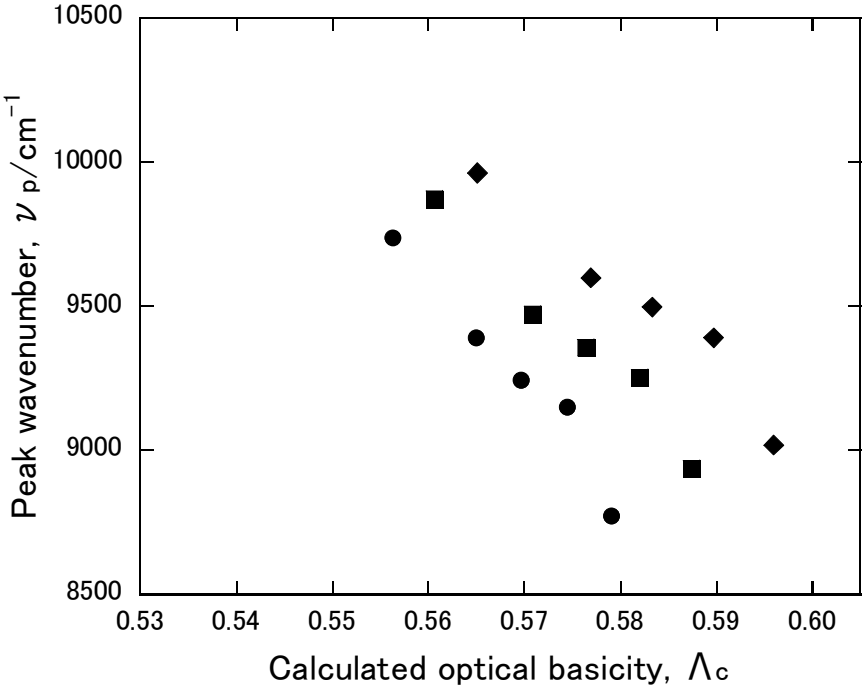

Fig. 3. 2. Absorption-peak wavenumber of Fe^{2+} as a function of calculated optical basicity for float-glass-based alkali-alkaline-earth silicate glasses: $0.63K_2O{\cdot}13.0Na_2O{\cdot}xSrO{\cdot}(12.4\text{-}x)MgO{\cdot}0.88Al_2O_3{\cdot}73.1SiO_2$ (x = 0-12.4)(●); $0.63K_2O{\cdot}13.0Na_2O{\cdot}xSrO{\cdot}(14.4\text{-}x)MgO{\cdot}0.88Al_2O_3{\cdot}71.0SiO_2$ (x = 0-14.4)(■); $0.63K_2O{\cdot}13.0Na_2O{\cdot}xSrO{\cdot}(16.4\text{-}x)MgO{\cdot}0.88Al_2O_3{\cdot}69.0SiO_2$ (x = 0-16.4)(◆). Each glass was doped with 0.19 % Fe_2O_3.

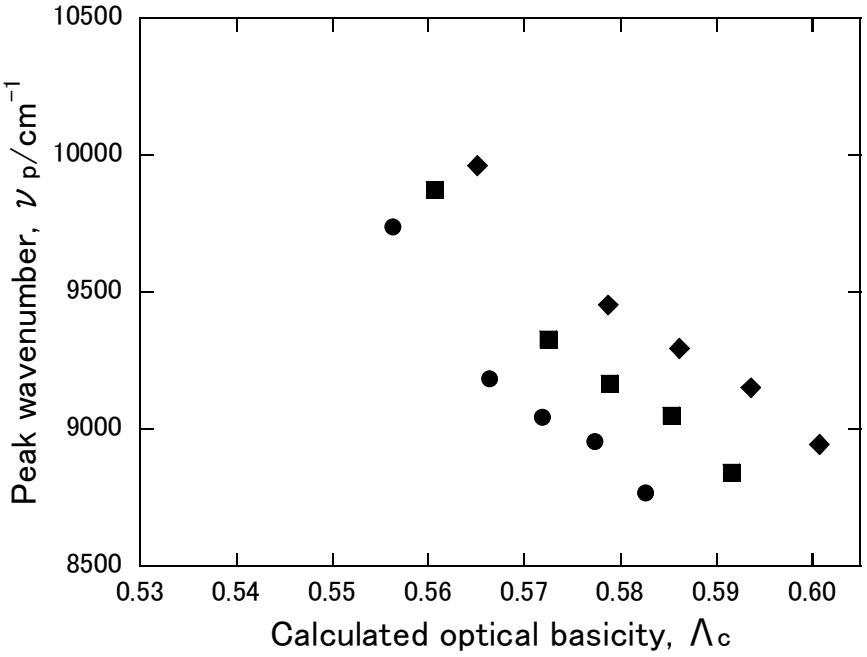

Fig. 3. 3. Absorption-peak wavenumber of Fe^{2+} as a function of calculated optical basicity for float-glass-based alkali-alkaline-earth silicate glasses: $0.63K_2O{\cdot}13.0Na_2O{\cdot}xBaO{\cdot}(12.4\text{-}x)MgO{\cdot}0.88Al_2O_3{\cdot}73.1SiO_2$ (x = 0-12.4)(●); $0.63K_2O{\cdot}13.0Na_2O{\cdot}xBaO{\cdot}(14.4\text{-}x)MgO{\cdot}0.88Al_2O_3{\cdot}71.0SiO_2$ (x = 0-14.4)(■); $0.63K_2O{\cdot}13.0Na_2O{\cdot}xBaO{\cdot}(16.4\text{-}x)MgO{\cdot}0.88Al_2O_3{\cdot}69.0SiO_2$ (x = 0-16.4)(◆). Each glass was doped with 0.19 % Fe_2O_3.

We can see similar trends in the two series depicted in the figure; the peak wavenumber ν_p increased with substitution of SiO_2 for R'O (R_2O) and decreased with substituting the R'^{2+} (R^+) ion for a larger ion. However, the MgO-CaO series shows a steep decrease in ν_p in the region with a very low or no MgO content.

3. 3. 1. 2. (Alkali) alkaline-earth (alumino-)silicate glasses

Dependence of ν_p on Λ_c for MgO-CaO series in the glass system is depicted in the Λ_c-ν_p diagram shown in Fig. 3. 4. As in Figs. 3. 1 - 3. 3., in each set of the data points, the left side corresponds to MgO-rich glasses and the right side to MgO-poor glasses. Starting from the initial base glass (the S-glass composition), we can see the overall trend that substituting Al_2O_3 for Na_2O makes variations of ν_p with Λ_c larger as the Mg^{2+} ion is substituted for the Ca^{2+} ion. Figure 3. 4. also shows that ν_p varies with Λ_c to a greater degree for MgO-rich glasses, while it changes to a lesser degree for CaO-rich glasses. As was found for the alkali alkaline-earth silicate glasses, ν_p steeply decreases in the regions with a very low or no MgO content of the Λ_c-ν_p diagram, especially for the glasses of high substituted ratios of Na_2O/Al_2O_3. In the regions with a larger MgO content, dependence of ν_p on Λ_c changes with the Na_2O/Al_2O_3 ratio. For glasses with no or small Na_2O content (0, 2 and 4 %), ν_p slightly increases with increase of Λ_c. For glasses with 8 % Na_2O, ν_p changes little with Λ_c. At 12 % and 16 % Na_2O, ν_p decreases with increase of Λ_c.

Figure 3. 5. and Fig. 3. 6. illustrate Λ_c-ν_p diagrams for MgO-SrO and MgO-BaO series. The basic trend is similar to the one for MgO-CaO series in the same

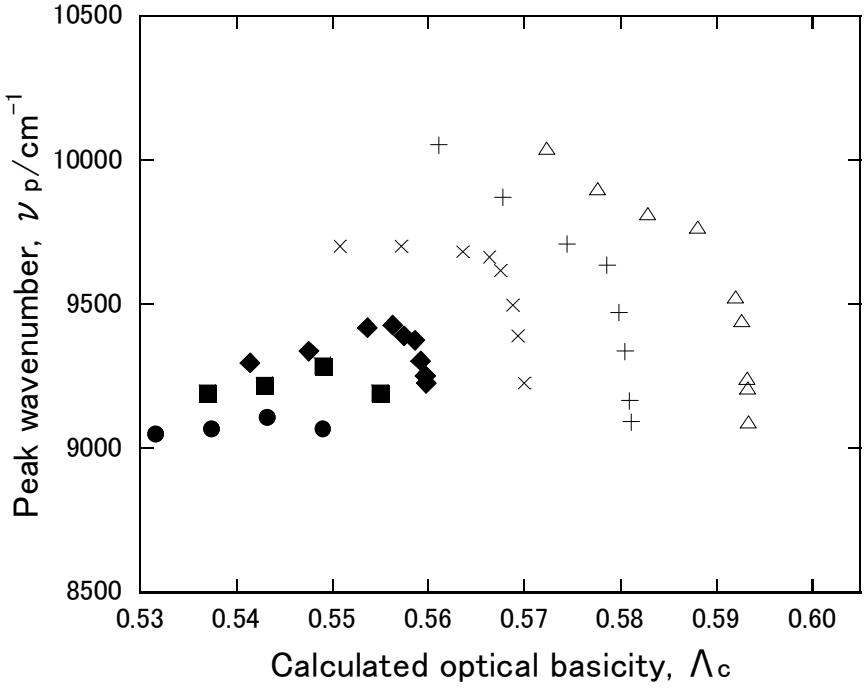

Fig. 3. 4. Absorption-peak wavenumber of Fe^{2+} as a function of calculated optical basicity for S-glass-based alkali-alkaline-earth alumino-silicate glasses: $xCaO{\cdot}(15.8\text{-}x)MgO{\cdot}15.6Al_2O_3{\cdot}68.6SiO_2$ (x = 0-15.8)(●); $yNa_2O{\cdot}xCaO{\cdot}(16\text{-}x)MgO{\cdot}(16\text{-}y)Al_2O_3{\cdot}68SiO_2$ (x = 0-16, y = 2 (■); y = 4(◆); y = 8(×); y = 12(+); y = 16(△)).

Each glass was doped with 0.19 % Fe_2O_3.

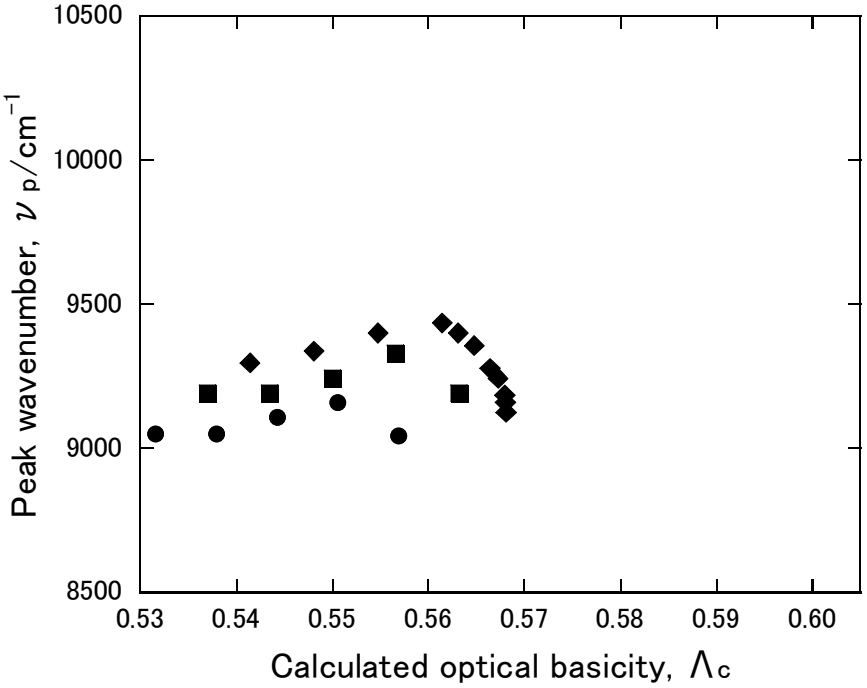

Fig. 3. 5. Absorption-peak wavenumber of Fe^{2+} as a function of calculated optical basicity for S-glass-based alkali-alkaline-earth alumino-silicate glasses: $xSrO{\cdot}(15.8\text{-}x)MgO{\cdot}15.6Al_2O_3{\cdot}68.6SiO_2$ (x = 0-15.8)(●); $yNa_2O{\cdot}xSrO{\cdot}(16\text{-}x)MgO{\cdot}(16\text{-}y)Al_2O_3{\cdot}68SiO_2$ (x = 0-16, y = 2 (■); y = 4(◆)). Each glass was doped with 0.19 % Fe_2O_3.

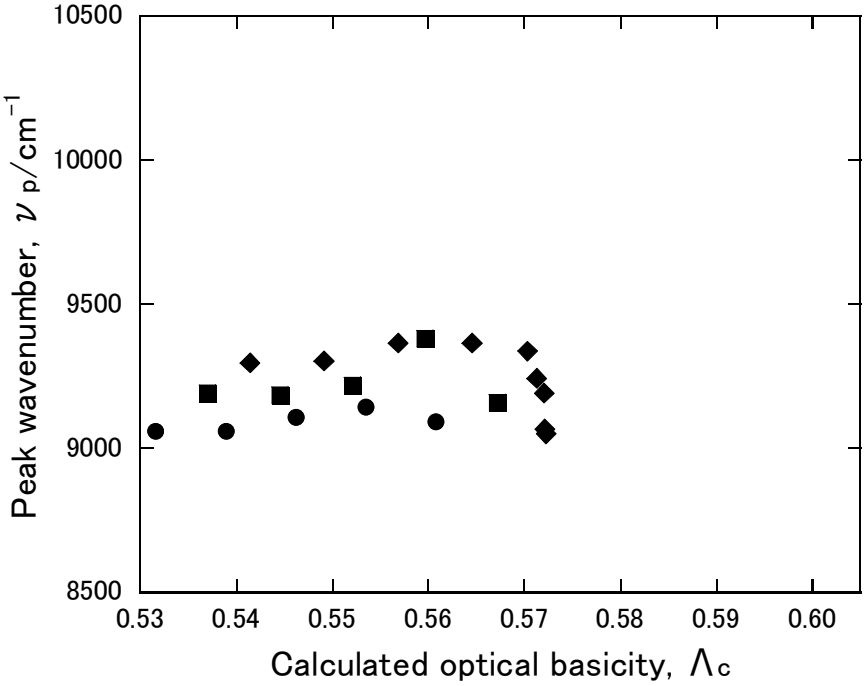

Fig. 3. 6. Absorption-peak wavenumber of Fe^{2+} as a function of calculated optical basicity for S-glass-based alkali-alkaline-earth alumino-silicate glasses: $xBaO{\cdot}(15.8\text{-}x)MgO{\cdot}15.6Al_2O_3{\cdot}68.6SiO_2$ (x = 0-15.8)(●); $yNa_2O{\cdot}xBaO{\cdot}(16\text{-}x)MgO{\cdot}(16\text{-}y)Al_2O_3{\cdot}68SiO_2$ (x = 0-16, y = 2 (■); y = 4(◆)). Each glass was doped with 0.19 % Fe_2O_3.

Na_2O range shown in Fig. 3. 4.

Figure 3. 7. and Fig. 3. 8. show variations of absorption spectra with the Na_2O/Al_2O_3 ratio for glasses containing MgO and CaO, respectively. As can be seen from both figures, the width of the broad absorption band at around 10000 cm^{-1} increased as the Na_2O/Al_2O_3 ratio increased and the degree is large for MgO-containing glasses.

Figures 3. 9. - 3. 12. show changes of absorption spectra when MgO was substituted for CaO for glasses of different Na_2O/Al_2O_3 ratios. For the Na_2O-free glasses (Fig. 3. 9.), changes in the spectral shape are very small. With increase of the Na_2O content, the changes become large. For glasses of 4 % Na_2O (Fig. 3. 10.), we can see that the absorption increased in intensity at around 12000 cm^{-1} with substitution of MgO for CaO and the band width increased. For glasses of 8 % Na_2O (Fig. 3. 11.), the absorption spectra do not vary much with substitution of MgO for CaO except for the full substitution, which markedly increased the absorption below 9000 cm^{-1}. For glasses of 12 % Na_2O (Fig. 3. 12.), the absorption below 9000 cm^{-1} slightly increased with substitution of MgO to CaO, and much increased with full substitution as in the glasses of 8 % Na_2O.

Figure 3. 13. and Fig. 3. 14. show changes of absorption spectra when MgO was substituted for SrO for glasses of different Na_2O/Al_2O_3 ratios. Figure 3. 15. and Fig. 3. 16. show the similar illustration for substitution of MgO for BaO. Basically the same trends as was found for the corresponding glasses of MgO-CaO substitution were confirmed.

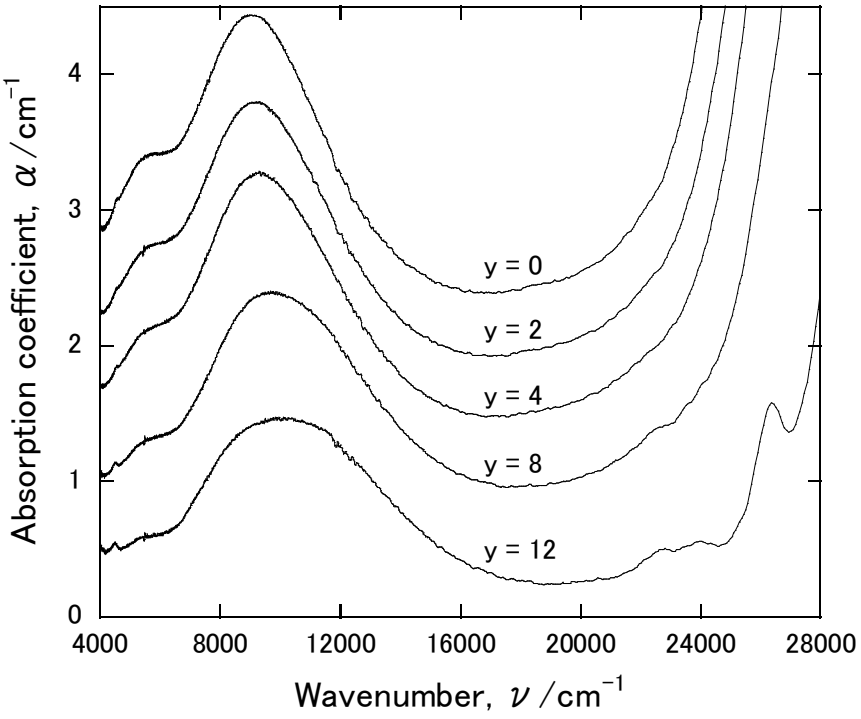

Fig. 3. 7. Absorption spectra for a $15.8MgO{\cdot}15.6Al_2O_3{\cdot}68.7SiO_2$ glass (y = 0) and $yNa_2O{\cdot}16MgO{\cdot}(16\text{-}y)Al_2O_3{\cdot}68SiO_2$ glasses (y = 2, 4, 8 and 12) doped with 0.19 % Fe_2O_3. Spectra are shifted vertically by 0.5 cm^{-1}.

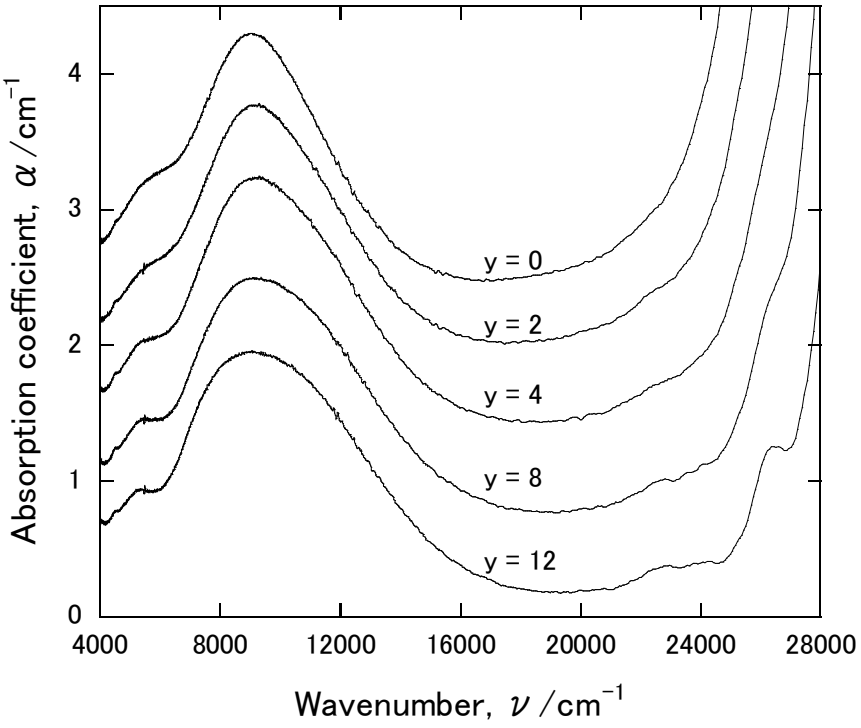

Fig. 3. 8. Absorption spectra for a $15.8CaO{\cdot}15.6Al_2O_3{\cdot}68.7SiO_2$ glass (y = 0) and $yNa_2O{\cdot}16CaO{\cdot}(16\text{-}y)Al_2O_3{\cdot}68SiO_2$ glasses (y = 2, 4, 8 and 12) doped with 0.19 % Fe_2O_3. Spectra are shifted vertically by 0.5 cm^{-1}.

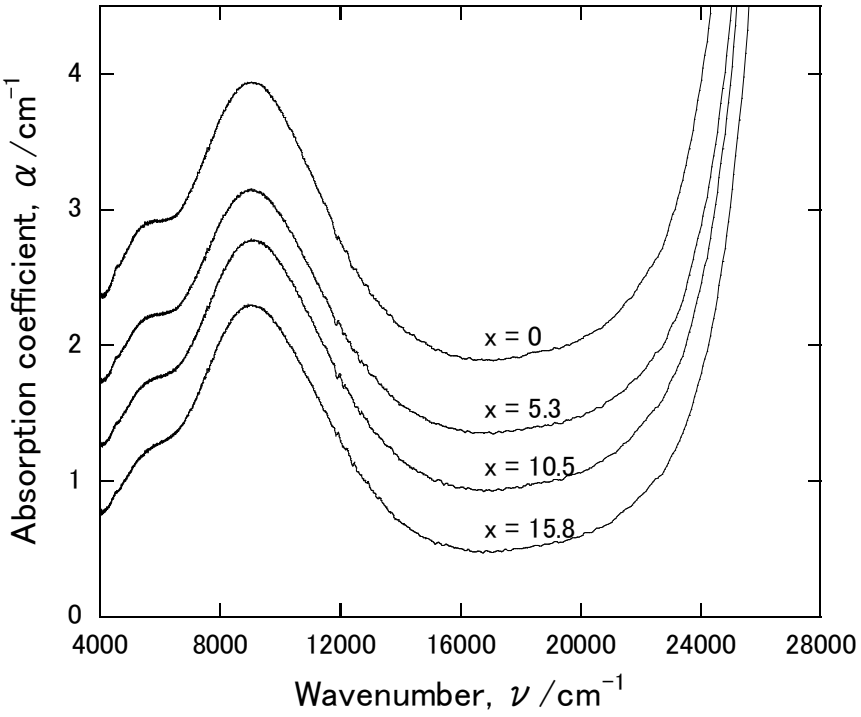

Fig. 3. 9. Absorption spectra for $xCaO{\cdot}(15.8\text{-}x)MgO{\cdot}15.6Al_2O_3{\cdot}68.7SiO_2$ glasses (x = 0-15.8) doped with 0.19 % Fe_2O_3. Spectra are shifted vertically by 0.5 cm^{-1}.

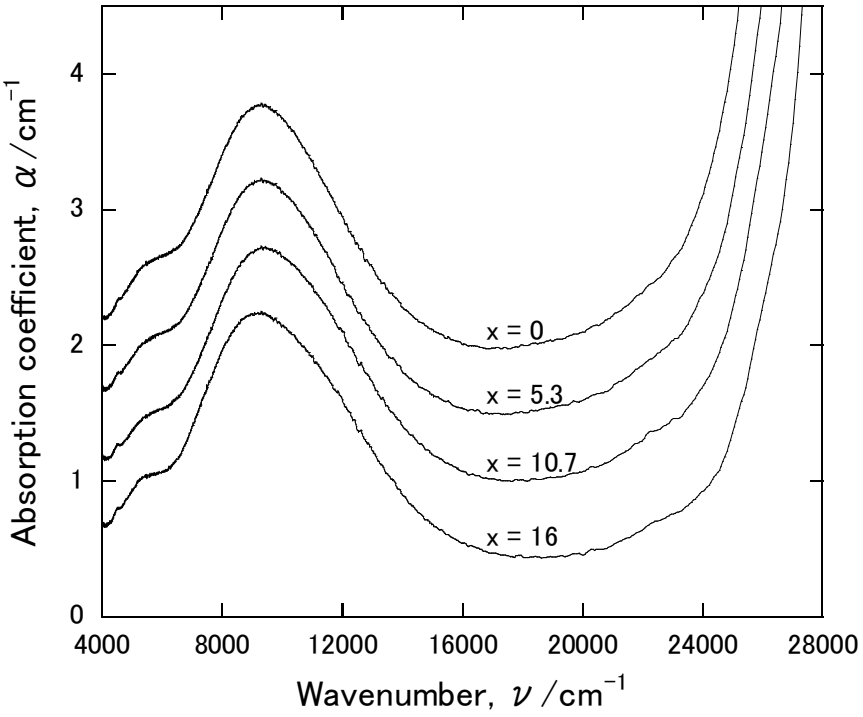

Fig. 3. 10. Absorption spectra for $4Na_2O{\cdot}xCaO{\cdot}(16\text{-}x)MgO{\cdot}12Al_2O_3{\cdot}68SiO_2$ glasses (x = 0-16) doped with 0.19 % Fe_2O_3. Spectra are shifted vertically by 0.5 cm^{-1}.

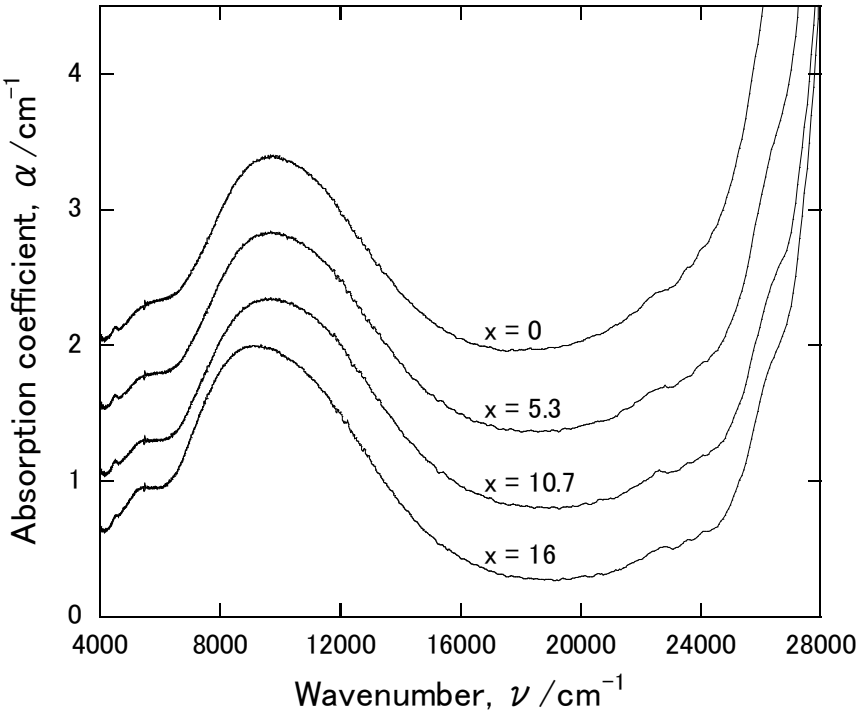

Fig. 3. 11. Absorption spectra for $8Na_2O{\cdot}xCaO{\cdot}(16\text{-}x)MgO{\cdot}8Al_2O_3{\cdot}68SiO_2$ glasses (x = 0-16) doped with 0.19 % Fe_2O_3. Spectra are shifted vertically by 0.5 cm^{-1}.

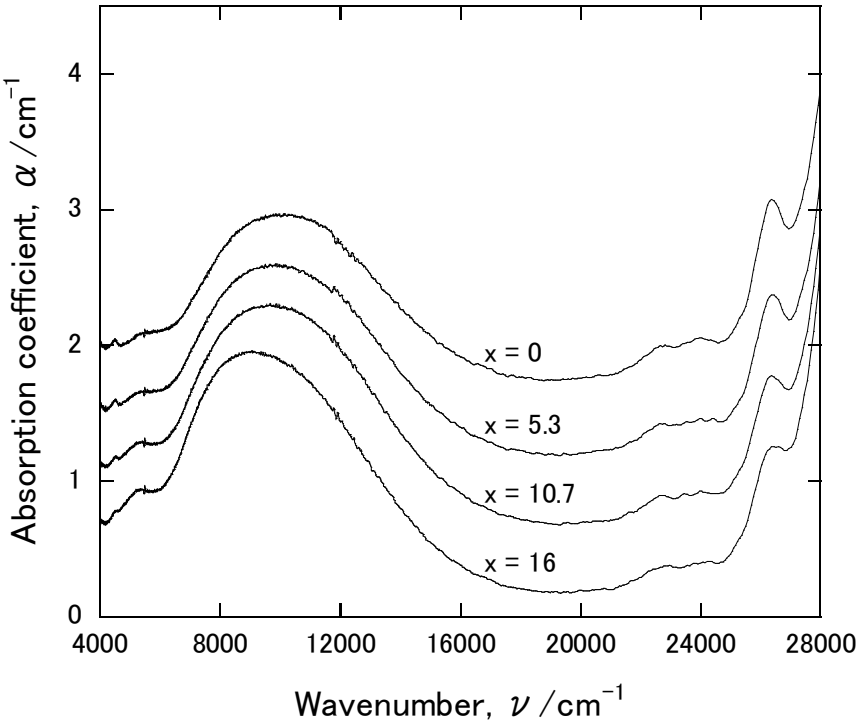

Fig. 3. 12. Absorption spectra for $12Na_2O{\cdot}xCaO{\cdot}(16\text{-}x)MgO{\cdot}4Al_2O_3{\cdot}68SiO_2$ glasses (x = 0-16) doped with 0.19 % Fe_2O_3. Spectra are shifted vertically by 0.5 cm^{-1}.

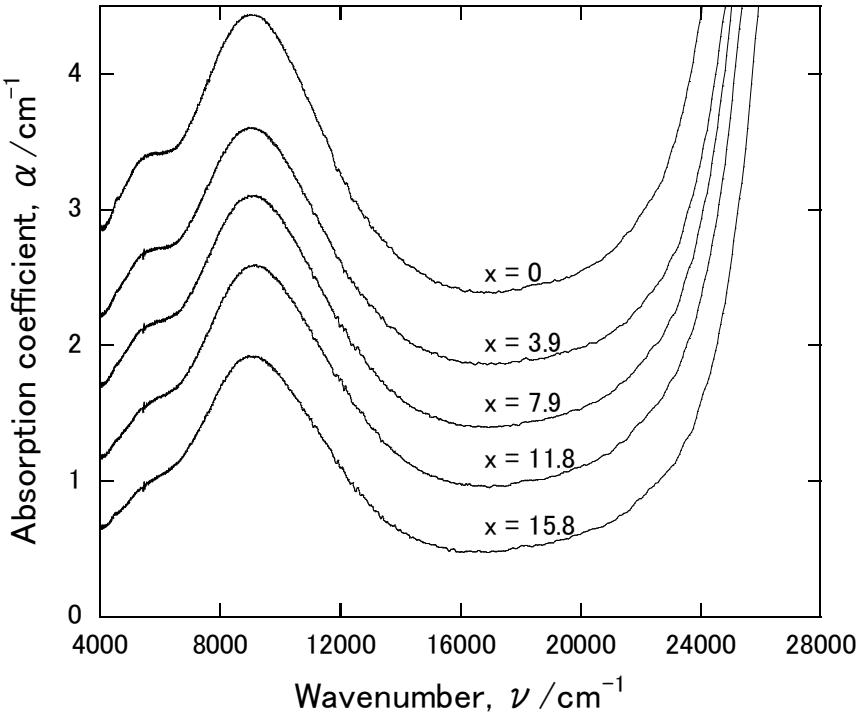

Fig. 3. 13. Absorption spectra for $xSrO{\cdot}(15.8\text{-}x)MgO{\cdot}15.6Al_2O_3{\cdot}68.7SiO_2$ glasses (x = 0-15.8) doped with 0.19 % Fe_2O_3. Spectra are shifted vertically by 0.5 cm^{-1}.

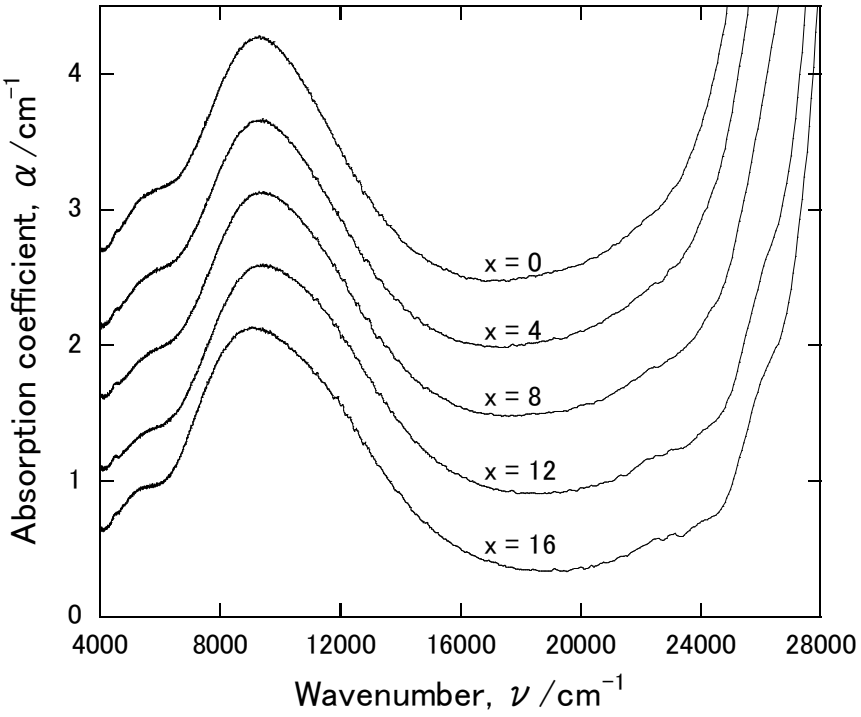

Fig. 3. 14. Absorption spectra for $4Na_2O{\cdot}xSrO{\cdot}(16\text{-}x)MgO{\cdot}12Al_2O_3{\cdot}68SiO_2$ glasses (x = 0-16) doped with 0.19 % Fe_2O_3. Spectra are shifted vertically by 0.5 cm^{-1}.

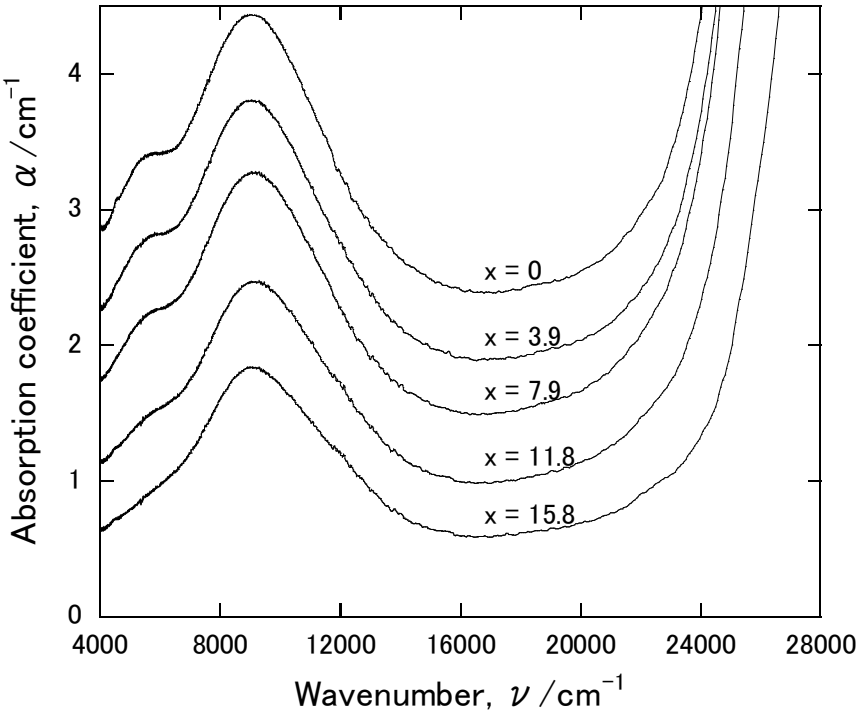

Fig. 3. 15. Absorption spectra for $xBaO{\cdot}(15.8\text{-}x)MgO{\cdot}15.6Al_2O_3{\cdot}68.7SiO_2$ glasses (x = 0-15.8) doped with 0.19 % Fe_2O_3. Spectra are shifted vertically by 0.5 cm^{-1}.

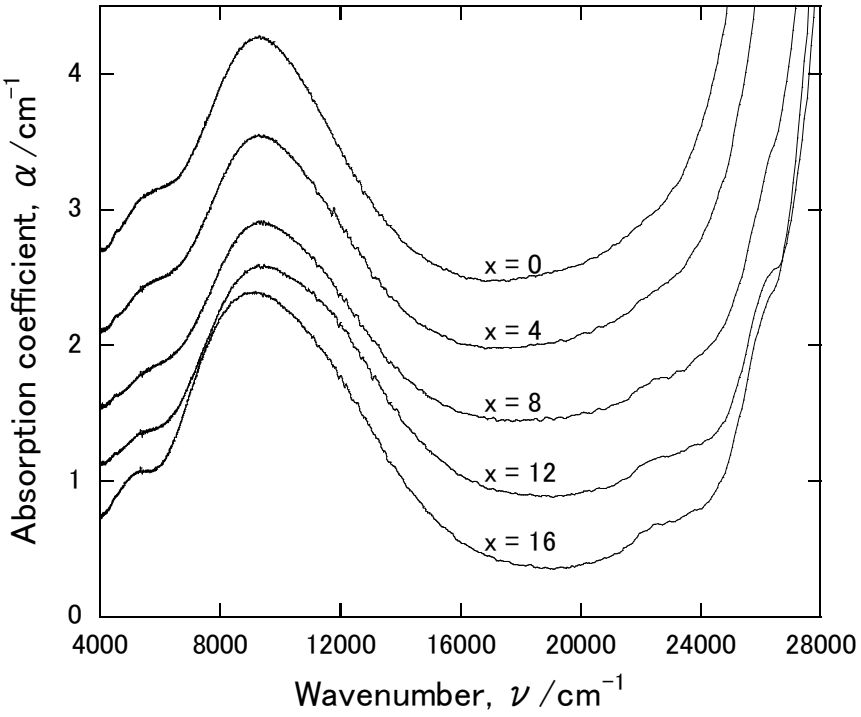

Fig. 3. 16. Absorption spectra for $4Na_2O{\cdot}xBaO{\cdot}(16\text{-}x)MgO{\cdot}12Al_2O_3{\cdot}68SiO_2$ glasses (x = 0-16) doped with 0.19 % Fe_2O_3. Spectra are shifted vertically by 0.5 cm^{-1}.

3. 3. 2. ESR spectra

Figure 3. 17. shows ESR spectra for $0.63K_2O{\cdot}13.0Na_2O{\cdot}8.5CaO{\cdot}5.9MgO{\cdot}0.88Al_2O_3{\cdot}71.0SiO_2$ and $15.8MgO{\cdot}15.6Al_2O_3{\cdot}68.7SiO_2$ glasses both of which doped with 0.19 % of Fe_2O_3. Signals for g = 4.3 were observed for both glasses, but signals for g = 2.0 were confirmed only for the alkali-containing glass.

3. 4. Discussion

For iron-doped soda-lime-silicate glasses, the broad absorption band at around 10000 cm^{-1} has been deconvoluted into three absorption bands [6]; the bands are centered at about 7700 cm^{-1}, 9400 cm^{-1} and 13600 cm^{-1}, which we denote band A, band B and band C, respectively. The structural origin of band A has not been confirmed [6, 10]. Band C has been assigned to tetrahedral Fe^{3+}. Band B is dominant and is attributed to d-d transition of octahedral Fe^{2+}. The ligand field strength, 10*Dq*, corresponds to the energy, 9400 cm^{-1}. Dependence of ν_p on glass composition has been mainly discussed in terms of the ligand field strength [2, 8, 10]. The increase of ν_p with substitution of SiO_2 for R'O or R_2O, depicted in Figs. 1-3, were also reported by Fox et al. [2] and Comes et al. [8] in different representation of their results. As Fox et al. [2] claimed it is probably because effective negative charge on oxygen atoms increases with the increase of network-modifying oxides, increasing the crystal field that the Fe^{2+} ion feels and the distances between the Fe^{2+} ion and surrounding oxygen atoms decrease. Decrease of ν_p observed when substituting an alkali ion or an alkaline-earth ion for a larger ion could be attributed to distortion of the ligand field which deceases 10*Dq*. However, the steep

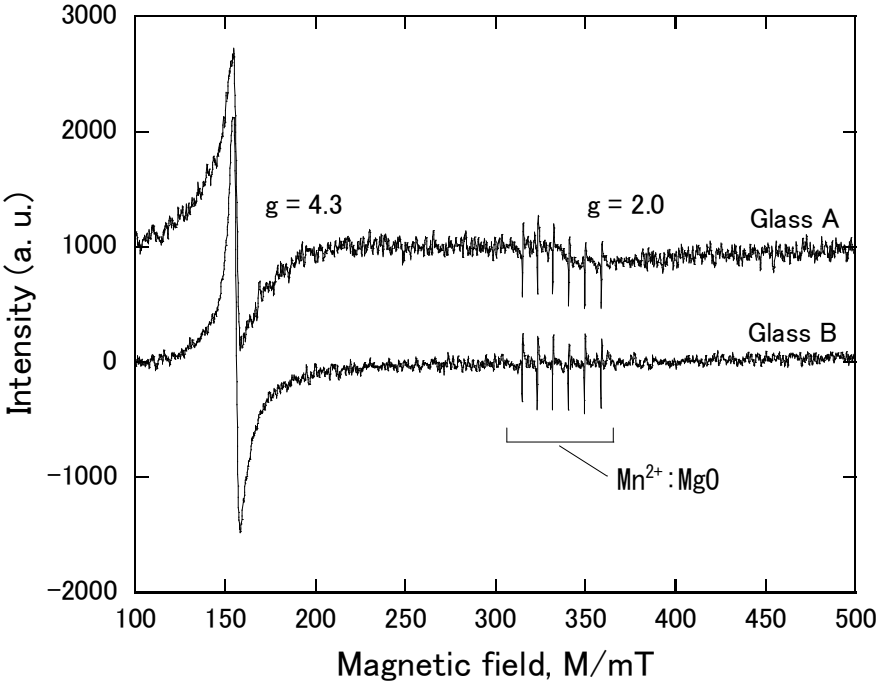

Fig. 3. 17. ESR spectra for glasses doped with 0.19 % Fe_2O_3: $0.63K_2O{\cdot}13.0Na_2O{\cdot}8.5CaO{\cdot}5.9MgO{\cdot}0.88Al_2O_3{\cdot}71.0SiO_2$ (Glass A); $15.8MgO{\cdot}15.6Al_2O_3{\cdot}68.7SiO_2$ (Glass B).

decrease in ν_p depicted in Fig. 3. 1. and Figs. 3. 4 – 3. 6., observed in the regions with a very low or no MgO content, suggests that even a small quantity of Mg^{2+} ions has an effect to change the ligand field strength around Fe^{2+} ions because it occurs in the very narrow range of the composition variation of Mg^{2+} ions and deflection appears in data points in the Λ_c-ν_p diagrams, especially for glasses with low Na_2O content. The effect will be discussed later in the section.

The width of the absorption band is small for Na_2O-free alumino-silicate glasses as depicted in Fig. 3. 9., Fig. 3. 13. and Fig. 3. 15., indicating distortion of the ligand field of Fe^{2+} ions has relatively narrow distribution. Rüssel [12] measured EPR spectra of alkali alkaline-earth silicate glasses and found that the relative peak intensity of signal at g = 2.0 to g = 4.3, increased in the order of lithium-, sodium-, potassium- and cesium-containing glasses. The signal at g = 2.0 was attributed to formation of clusters of Fe^{3+} ions, possibly including Fe^{2+} ions as well [5]. The ESR spectrum for the Na_2O-free alumino-silicate glass in Fig. 3. 17. shows no signal at g = 2.0, suggesting no clustering of Fe^{3+} and Fe^{2+} ions in the glass. One possibility is that the Al^{3+} ion reduces clustering of Fe^{3+} and Fe^{2+} ions by associating with them. This effect will be compromised when the Al^{3+} ion is associated with a network-modifying ion. A typical example is alkali ions, which can compensate the negative charge of AlO_4^-, allowing the Al^{3+} ion to exist as a tetrahedral coordination in the glass network. In this case, interaction between the Al^{3+} ion and Fe^{2+} or Fe^{3+} ions will be reduced, resulting in the clustering of the Fe^{3+} and/or Fe^{2} ions. The observed increase of the width of the absorption band with substitution of Al_2O_3 for Na_2O results possibly from the effect

described above. Montenero et al. [5] observed shift of ν_p to lower energies when the iron content of the glass increased and thought that it was the influence of Fe^{3+} clusters over the Fe^{2+} ions in octahedral coordination. The same argument might apply to our results though the iron content of our glasses is much lower than theirs.

For Na_2O-free alumino-silicate glasses, very small variations of ν_p and the width of the absorption band were found for substitution of MgO for either of CaO, SrO or BaO. With increase of the Na_2O/Al_2O_3 ratio, the variations become large. The result suggests that effects of alkaline-earth ions on glass structures depend on presence and quantity of the Na^+ (alkali) ion.

Rüssel [13] investigated alkali alkaline-earth silicate glasses and claimed that Mg^{2+} is not capable of compensating the negative charge of AlO_4^-, whereas Ca^{2+} compensates one AlO_4^-, not two, which is expected from the nominal charge of the ion. The behaviors of the Na_2O-containing glasses of MgO-CaO series in our investigation can be understood according to this idea. The fraction of tetrahedral Al^{3+} increases with substitution of MgO for CaO. The results shown in Fig. 3. 4. suggest that the ability of the Ca^{2+} ion to compensate AlO_4^- depends on the Na_2O content (Na_2O/Al_2O_3 ratio) and it virtually vanishes in alkali-free glasses, for which almost no variation of ν_p were observed. The similar tendency observed for glasses of MgO-SrO and MgO-BaO series, illustrated in Fig. 3. 5. and 3. 6., allows us to infer that the Fe^{2+} ion strongly associates with the Al^{3+} ion in alkali-free glasses containing any alkaline-earth ion. Increase of the Na_2O/Al_2O_3 ratio compromises the ability of the Al^{3+} ion to associate with and disperse the Fe^{2+} ion in glass by increasing the ability of the Ca^{2+} ion to charge-compensate

AlO_4^-, resulting in increase of ν_p with substitution of MgO for CaO. We consider that the same mechanism applies to the other alkaline-earth oxide series, MgO-SrO and MgO-BaO.

In every series of glasses, distinct steep decrease of ν_p was found in the region with a very low or no MgO content. The phenomenon was observed regardless of the substituted alkaline-earth oxide. Some effect of the Mg^{2+} ion, which can arise with small quantity of the ion, should be responsible for this.

Rüssel [14] investigated standard reduction potential of Fe^{3+}/Fe^{2+} in $Na_2O{\cdot}MgO{\cdot}CaO{\cdot}Al_2O_3{\cdot}SiO_2$ melts and explained its compositional dependency in terms of interaction between the Mg^{2+} ion and the Fe^{2+} ion; both ions have the same valency and similar ionic radii, thus compete for the same kind of sites in glass. Rüssel [14] explained that the Fe^{2+} ion is pushed aside by the Mg^{2+} ion to a site of less stable, higher energy. It means that the ligand field strength of the Fe^{2+} ion decreases, resulting in dropping of ν_p. This is not inconsistent with the tendency that we observed for ν_p in the regions with a very low or no MgO content. Using essentially the same argument of interaction between the Mg^{2+} ion and the Fe^{2+} ion, we can also assume that the Mg^{2+} ion enhances dispersion of the Fe^{2+} ion in glass and the effect causes the steep decrease of ν_p in the regions with a very low or no MgO content. The Mg^{2+} ion reduces clustering of the Fe^{2+} ion, occupying similar sites as the Fe^{2+} ion does. As the number of Mg^{2+} ions decreases to zero, clustering of Fe^{2+} ions markedly increases. As mentioned in the preceding part, this may have an effect to decrease ν_p. Edwards et al. [10] investigated iron-doped $R'O{\cdot}P_2O_5$ glasses (R': Mg, Ca, Sr, Ba) and reported that abrupt change of ν_p

and the Fe^{3+}/Fe^{2+} redox ratio were observed for $MgO{\cdot}P_2O_5$, when changing from the other systems. This also supports the ideas of interaction between the Fe^{2+} and Mg^{2+} described above.

3. 5. Conclusions

Compositional dependence of infrared absorption of iron-doped glasses was investigated. The results were analyzed using Λ_c-ν_p diagrams, in which peak wavenumber of the infrared absorption band ν_p was given as a function of calculated optical basicity Λ_c of glass. We employed Λ_c as glass-composition parameter which represents the complex combination of glass components. Basic variations of glass composition were chosen as substitution of Mg^{2+} for a larger alkaline-earth ion, keeping the total quantity of R'O constant.

For iron-doped alkali alkaline-earth silicate glasses, increase of Λ_c by substitution of SiO_2 for R'O increased ν_p, whereas increasing Λ_c by substituting Mg^{2+} for a larger alkaline-earth ion yielded the opposite trend. We considered that the composition changes vary effective negative charge on oxygen atoms and symmetry of their coordination around the Fe^{2+} ion. For iron-doped (alkali) alkaline-earth (alumino-)silicate glasses, behaviors of the absorption band depended much on the Na_2O/Al_2O_3 ratio. ESR spectra suggested clustering of Fe^{3+} ions (possibly with Fe^{2+} ions) in alkali-containing glasses and no clustering in alkali-free glasses. We estimated that Fe^{3+} and Fe^{2+} ions associate strongly with Al^{3+} ions when the negative charge of AlO_4^- is not compensated by other network-modifying cations.

Steep decrease of the peak wavenumber with increasing Λ_c by substituting Mg^{2+} for Ca^{2+} was observed in the regions with a very low or no MgO content for all series of glasses containing alkali ions. The effect was probably due to direct interaction between the Fe^{2+} ion and the Mg^{2+} ion.

References

[1] F. N. Steel, R. W. Douglas, Phys. Chem. Glasses 6 (1965) 246.

[2] K. E. Fox, T. Furukawa, W. B. White, Phys. Chem. Glasses 23 (1982) 169.

[3] P. S. Danielson, J. W. H. Schreurs, J. Non-Cryst. Solids 38&39 (1980) 177.

[4] K. Nakaguchi, M. Kume, Japanese Patent, JP60215546 (applied Apr. 6, 1984)

[5] A. Montenero, M. Friggeri, D. C. Giori, N. Belkhiria, L. D. Pye, J. Non-Cryst. Solids 84 (1986) 45.

[6] C. Ades, T. Toganidis, J. P. Traverse, J. Non-Cryst. Solids 125 (1990) 272.

[7] J. M. Combes, International Patent, WO9414716 (originally applied in France, Dec. 23, 1992)

[8] J. M. Combes, G. Calas, S. Creux, in : Proc. 17th Int. Congr. Glass, 1995, p.90.

[9] K. Sakaguchi, in: Proc. XIX Int. Congr. Glass, Edinburgh, 1-6 July 2001. Glass Technol. 43C (2002) 245.

[10] R. J. Edwards, A. Paul, R. W. Douglas, Phys. Chem. Glasses 13 (1972) 137.

[11] C. Hirayama, J. G. Castle, Jnr, M. Kuriyama, Phys. Chem. Glasses 9 (1968) 109.

[12] C. Rüssel, Glastech. Ber. 66 (1993) 68.

[13] C. R. Kurkjian, E. A. Sigety, Phys. Chem. Glasses 9 (1968)73.

[14] C. Rüssel, A. Wiedenroth, Chem. Geology 213 (2004) 125.

[15] W. Vogel, Chemistry of Glass, translated and edited by N. Kreidl, The American Ceramic Society Inc., Columbus, OH, 1985, p.179.

[16] J. A. Duffy, M. D. Ingram, J. Am. Chem. Soc. 93 (1971) 6448.

[17] F. G. K. Baucke, J. A. Duffy, Phys. Chem. Glasses 35 (1994) 17.

[18] J. A. Duffy, M. D. Ingram, Optical Basicity in: D. R. Uhlmann, N. J. Kreidl (Eds.), Optical Properties of Glass, American Ceramic Society, Westerville, OH, 1991, p. 159.

[19] K. Morinaga, T. Murata, N. Wada, Yōyūentokōonkagaku (Molten Salts and High-temperature Chemistry) 42 (1999) 145. (in Japanese)

[20] J. A. Duffy, Basicity of Glass-Forming Melts, in: H. Bach, F. G. K. Baucke, D. Krause (Eds.), Electrochemistry of Glasses and Glass Melts, Including Glass Electrodes, Springer-Verlag, Berlin, 2000, p. 275.

Chapter Four

Compositional Dependence of Optical Absorption of Bismuth-Doped Alumino-Silicate Glasses

4. 1. Introduction

Since Fujimoto and Nakatsuka [1] discovered that a $0.3Bi_2O_3 \cdot 2.2Al_2O_3 \cdot 97.5SiO_2$ glass had absorption bands in the visible and infrared regions (peaks at 500 nm, 700 nm and 800 nm) and exhibited broad infrared luminescence, a variety of Bi-doped glasses have been studied. Optical properties of Bi-doped silicate [2-6], borate [7-8], phosphate [9-10] and germanate glasses [11-12], were investigated. Peng et al. [4] reported that Bi_2O_3-Li_2O-ZnO-Al_2O_3-SiO_2 glasses showed absorption peaks at around 485 and 712nm, Meng et al. [7] investigated Bi_2O_3-BaO-Al_2O_3-B_2O_3 glasses and observed absorption bands at 465nm and 700nm, which became obscure with increasing BaO concentration. Sumimiya et al. [8] studied Bi_2O_3-La_2O_3-Al_2O_3-B_2O_3 glasses, which showed an absorption peak at 460 nm. Meng et

al. [10] reported that absorption peaks were at 460nm and 700nm for Al_2O_3-P_2O_5 glasses and 500nm, 700nm, 800nm with a shoulder at 1000nm for Al_2O_3-GeO_2 glasses. Although the previous reports gives the impression that network-formers with high field strength give absorption bands at shorter wavelengths, no systematic investigation has been done to deal with compositional dependence of absorption properties. Bi-doped glasses also sometimes exhibit broad absorption extending from the UV to infrared regions. Kishimoto et al. [2] disclosed that glasses with high basicity showed the broad absorption and no infrared luminescence occurs when excited in the absorption band. However, the result suggests only a general tendency and we need to know how specific combinations of components affect the optical properties of Bi-doped glasses.

In this study, we chose an MgO-Al_2O_3-SiO_2 glass as base composition and investigated changes of the absorption spectrum with composition variation. The obtained spectral changes were interpreted in terms of interactions between the Na^+ ion, alkaline-earth ions and the Al^{3+} ion.

4. 2. Experimental procedure

The experimental glass compositions are based on so-called S-glass for high tensile-strength glass fiber, of which approximate composition is $15.8MgO{\cdot}15.6Al_2O_3{\cdot}68.6SiO_2$. All the glass compositions are expressed in mol% in this chapter. We think that the glass has the lowest basicity among alkali-free multi-component glasses that can be fabricated by conventional melting methods. In each series, we substituted MgO for another alkaline-earth oxide with varying quantities.

For glasses with Al_2O_3/Na_2O substitutions, a slightly modified base-glass composition, $16MgO{\cdot}16Al_2O_3{\cdot}68SiO_2$, was used. Composition variations include substitution between MgO and R'O, where R' is either of Ca, Sr or Ba, and substitution between Al_2O_3 and Na_2O. Thus, the nominal experimental glass compositions are $xR'O{\cdot}(15.8\text{-}x)MgO{\cdot}15.6Al_2O_3{\cdot}68.6SiO_2$ (R': Ca, Sr and Ba; x = 0-15.8) for alkali-free glasses, $yNa_2O{\cdot}xR'O{\cdot}(16\text{-}x)MgO{\cdot}(16\text{-}y)Al_2O_3{\cdot}68SiO_2$ (R': Ca, Sr and Ba; x = 0-16, y = 0, 2 and 4). Each glass was doped with 0.5 % Bi_2O_3. Among the compositions, samples of good quality were not obtained for $15.8BaO{\cdot}15.6Al_2O_3{\cdot}68.6SiO_2$, $2Na_2O{\cdot}16BaO{\cdot}14Al_2O_3{\cdot}68SiO_2$, $4Na_2O{\cdot}12BaO{\cdot}4CaO{\cdot}14Al_2O_3{\cdot}68SiO_2$ and $4Na_2O{\cdot}16BaO{\cdot}14Al_2O_3{\cdot}68SiO_2$, thus no data are presented for the glasses.

For each glass, batch was obtained thoroughly mixing raw materials selected from reagent or high-grade industrial materials of SiO_2, Al_2O_3, MgO, $CaCO_3$, $SrCO_3$, $BaCO_3$, Na_2CO_3 and Bi_2O_3. Each glass batch of 350-g glass was put in a Pt-10% Rh crucible and melted in an electric furnace at 1620 ºC for 6-7 hours in air. The glass melt was stirred with a silica rod several times during melting to enhance its homogeneity. After the melting, the glass melt was poured onto a stainless-steel plate. The glass was annealed at 700 ºC for 30 minutes and cooled at a rate of 1.67 ºC /min or less to room temperature. A sample of 30 mm × 30 mm × 7 mm was cut, ground and polished from each glass block. Transmission spectra were measured in the range from 290 nm to 2500 nm with a Hitachi U-4100 spectrophotometer. After the first transmission measurements, the samples were ground and polished to the thickness of 4.9 mm, and transmission spectra were measured again. For each glass, absorption coefficient at each

wavelength was obtained using Lambert's law from the set of transmittance data for the two thicknesses.

4. 3. Results

Figures 4.1. – 4. 3. show changes of absorption spectra for glasses of MgO-CaO series. As can be seen from Fig. 4. 1., variations of spectra for Na_2O-free glasses are small. With substitution of MgO for CaO, the absorption bands at 20400 cm^{-1} (490 nm) and 14500 cm^{-1} (690 nm) shifted slightly to higher and lower wavenumbers, respectively. From changes of the spectral shapes, we can also see that the absorption intensities at 17800 cm^{-1} (560 nm) and 13000 cm^{-1} (770 nm) decreased and increased, respectively, as the CaO/MgO ratio increased. The broad absorption did not increase with substitution of MgO for CaO, though the composition variation increases glass basicity. As the Na_2O/Al_2O_3 ratio increased, the spectral changes became large. Behaviors of the absorption bands at 20400 cm^{-1} (490 nm) and 14500 cm^{-1} (690 nm) are essentially the same at either Na_2O content. The changes of absorption at 17800 cm^{-1} (560 nm) and 13000 cm^{-1} (770 nm) when MgO was substituted for CaO increased with the Na_2O content. The broad absorption increased with the Na_2O content and with substitution of MgO for CaO. The changes are small at 2 mol% Na_2O, but became markedly large at 4 mol% Na_2O.

Figures 4. 4. – 4. 6. show changes of absorption spectra when MgO was substituted for SrO for glasses of different Na_2O/Al_2O_3 ratios. Figures 4. 7. – 4. 9. show the similar illustration for substitution of MgO for BaO. Basically the same trends as

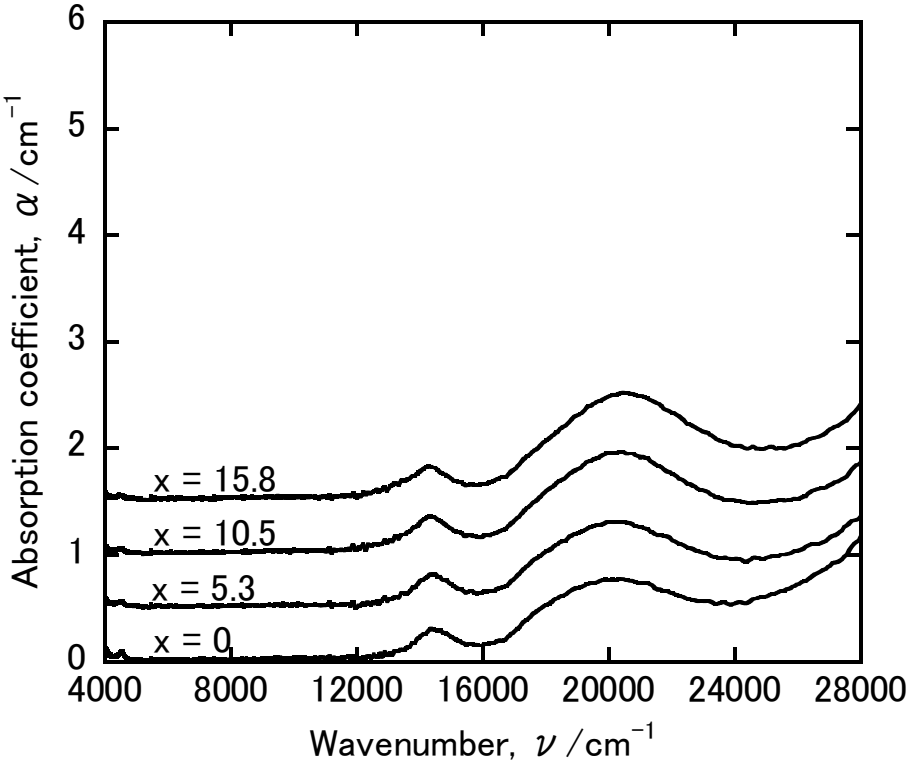

Fig. 4. 1. Absorption spectra for $xCaO{\cdot}(15.8\text{-}x)MgO{\cdot}15.6Al_2O_3{\cdot}68.7SiO_2$ glasses (x = 0-15.8) doped with 0.5 % Bi_2O_3. Spectra are shifted vertically by 0.5 cm^{-1}.

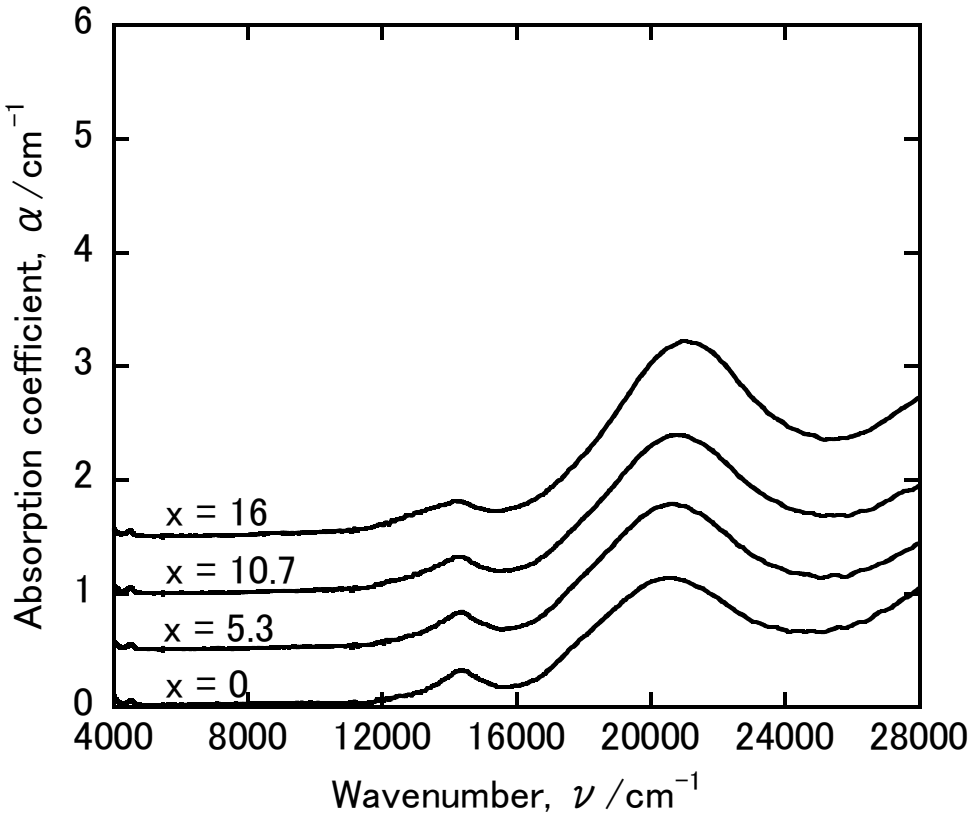

Fig. 4. 2. Absorption spectra for $2Na_2O{\cdot}xCaO{\cdot}(16\text{-}x)MgO{\cdot}14Al_2O_3{\cdot}68SiO_2$ glasses (x = 0-16) doped with 0.5 % Bi_2O_3. Spectra are shifted vertically by 0.5 cm^{-1}.

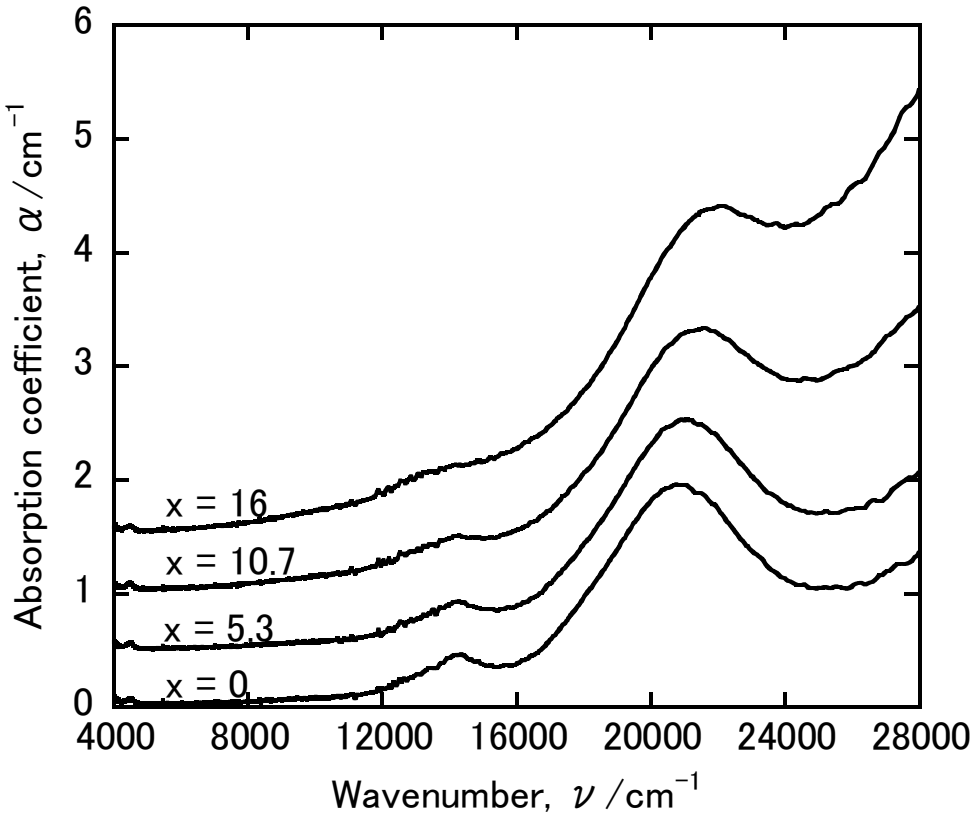

Fig. 4. 3. Absorption spectra for $4Na_2O{\cdot}xCaO{\cdot}(16\text{-}x)MgO{\cdot}12Al_2O_3{\cdot}68SiO_2$ glasses (x = 0-16) doped with 0.5 % of Bi_2O_3. Spectra are shifted vertically by 0.5 cm^{-1}.

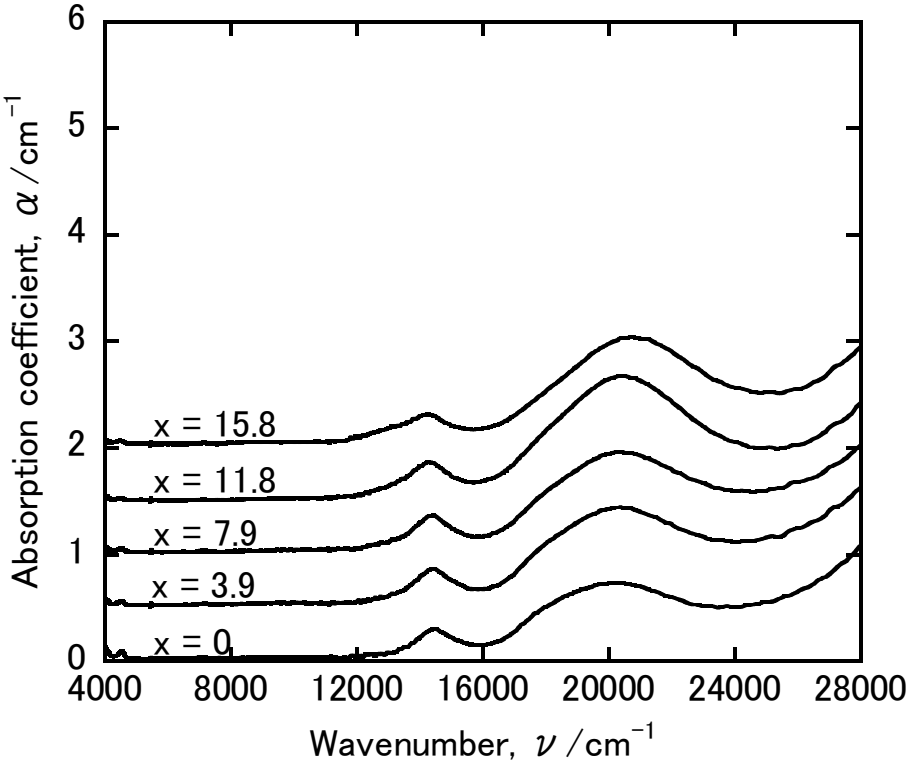

Fig. 4. 4. Absorption spectra for $xSrO{\cdot}(15.8\text{-}x)MgO{\cdot}15.6Al_2O_3{\cdot}68.7SiO_2$ glasses (x = 0-15.8) doped with 0.5 % Bi_2O_3. Spectra are shifted vertically by 0.5 cm^{-1}.

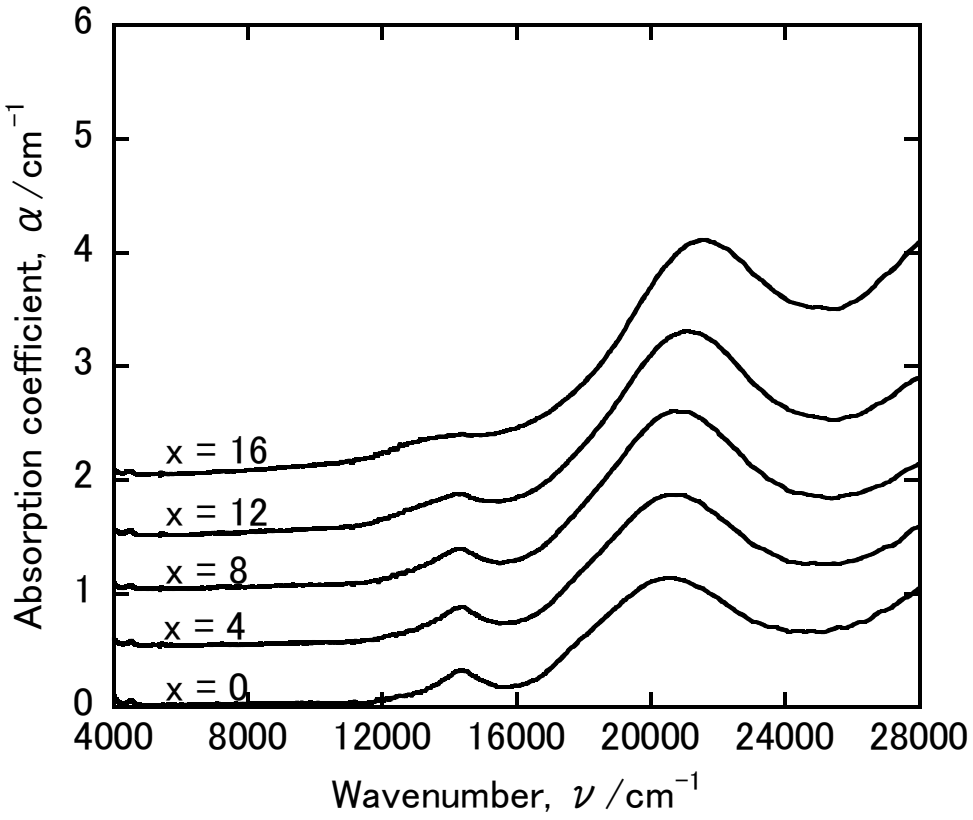

Fig. 4. 5. Absorption spectra for $2Na_2O{\cdot}xSrO{\cdot}(16\text{-}x)MgO{\cdot}14Al_2O_3{\cdot}68SiO_2$ glasses (x = 0-16) doped with 0.5 % Bi_2O_3. Spectra are shifted vertically by 0.5 cm^{-1}.

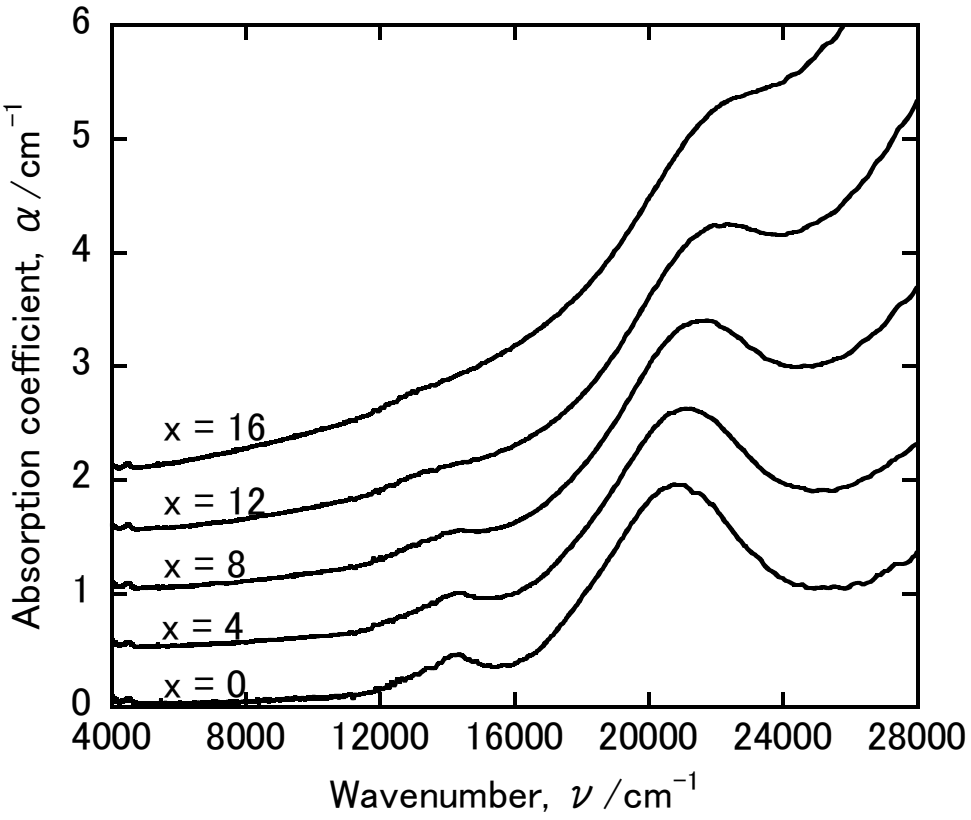

Fig. 4. 6. Absorption spectra for $4Na_2O{\cdot}xSrO{\cdot}(16\text{-}x)MgO{\cdot}12Al_2O_3{\cdot}68SiO_2$ glasses (x = 0-16) doped with 0.5 % Bi_2O_3. Spectra are shifted vertically by 0.5 cm^{-1}.

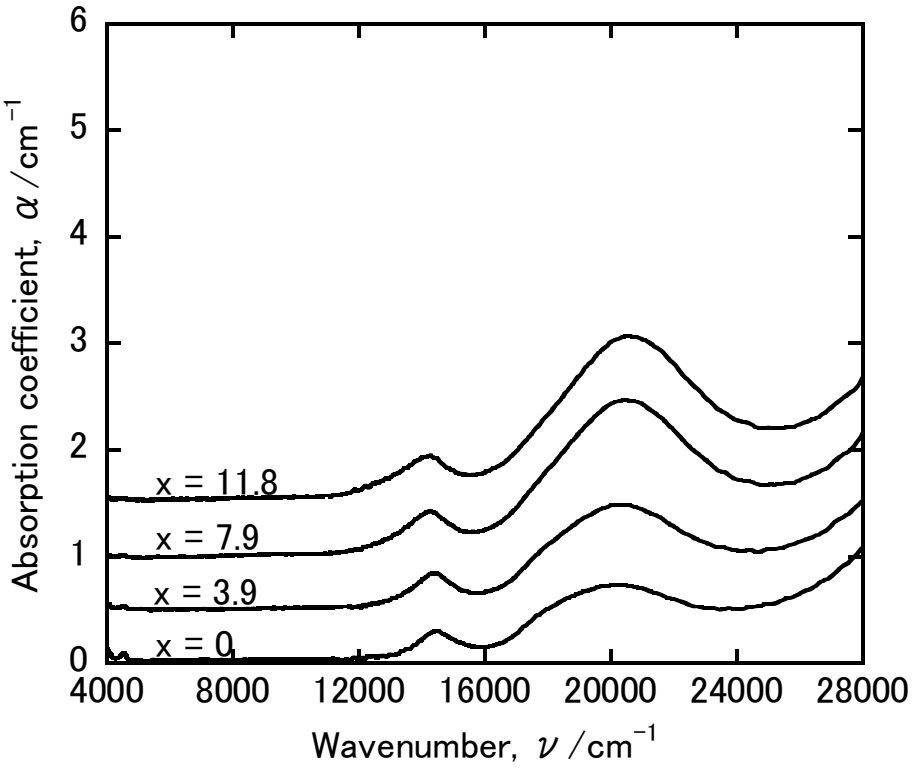

Fig. 4. 7. Absorption spectra for $xBaO{\cdot}(15.8\text{-}x)MgO{\cdot}15.6Al_2O_3{\cdot}68.7SiO_2$ glasses (x = 0-11.8) doped with 0.5 % Bi_2O_3. Spectra are shifted vertically by 0.5 cm^{-1}.

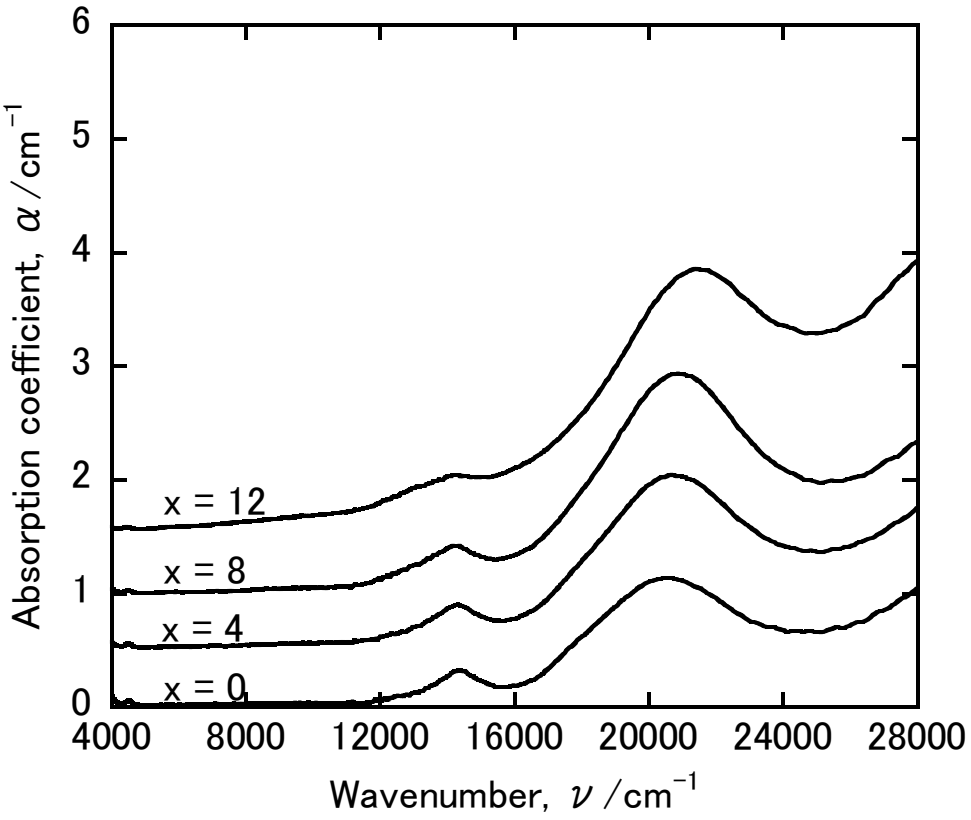

Fig. 4. 8. Absorption spectra for $2Na_2O{\cdot}xBaO{\cdot}(16\text{-}x)MgO{\cdot}14Al_2O_3{\cdot}68SiO_2$ glasses (x = 0-12) doped with 0.5 % Bi_2O_3. Spectra are shifted vertically by 0.5 cm^{-1}.

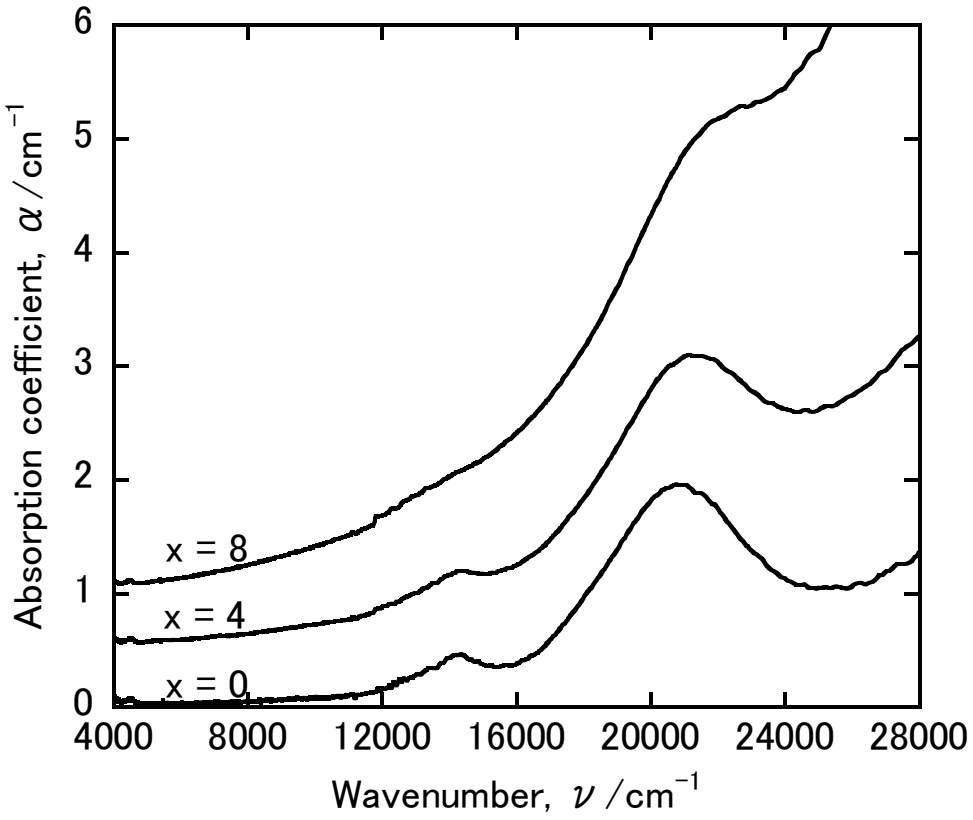

Fig. 4. 9. Absorption spectra for $4Na_2O{\cdot}xBaO{\cdot}(16\text{-}x)MgO{\cdot}12Al_2O_3{\cdot}68SiO_2$ glasses (x = 0-8) doped with 0.5 % Bi_2O_3. Spectra are shifted vertically by 0.5 cm^{-1}.

was found for the corresponding glasses of MgO-CaO substitution were confirmed. The changes with the Na_2O content increased in the order of MgO-CaO, MgO-SrO and MgO-BaO series, especially in the case of the broad absorption band.

4. 4. Discussion

The broad absorption of Bi-doped glasses has been considered to be due to metallic Bi colloids [25, 26]. The reduction reaction, $Bi^{3+} + 3e^- \rightarrow Bi$, was reported to be enhanced by increase of glass basicity [28]. Thus, substitution of MgO for a larger alkaline-earth ion, or substitution of Al_2O_3 for Na_2O, should increase the broad absorption. However, as described in the preceding section, in the case of Na_2O-free alumino-silicate glasses, very small variations the broad absorption band were found for substitution of MgO for either of CaO, SrO or BaO. As the Na_2O/Al_2O_3 ratio increases, the broad absorption increased with the substitutions. The increase becomes large in the order of MgO-CaO, MgO-SrO and MgO-BaO series. The result suggests that effects of alkaline-earth ions on glass structures depend on presence and quantity of the Na^+ (alkali) ion.

Fujimoto and Nakatsuka [1] presented the idea that the Bi^{5+} ion adjacent to the Al^{3+} ion is the origin of the absorption and the luminescence. From their NMR study of the same glass system [16], they concluded that the Al^{3+} ion takes octahedral coordination in the glass. Peng et al. [7] discussed effects of the Al^{3+} ion in their Al-containing borate glasses and claimed that the Bi^+ ion could be stabilized by AlO_4^- just the same way as alkali ions are charge-compensated in the glass. They considered

the Bi^{+} ion as the origin of the characteristic absorption bands and infrared luminescence. Dvoyrin et al. [17] presented essentially the same argument in their report on Bi-doped silica-based fibers. Although these arguments are not conclusive, we can say at least that electron accepting power of the Al^{3+} ion prevents the Bi ion from reduction in glass. If the glass contains ions that decrease the electron-accepting power of the Al^{3+} ion, then the Bi ion is susceptible to reduction. For example, if the glass contains alkali ions, the Al^{3+} ion takes tetrahedral coordination and is stabilized as AlO_4^{-} by the alkali ion. The Bi ion becomes less stable.

Rüssel [18] investigated alkali alkaline-earth silicate glasses and claimed that Mg^{2+} is not capable of compensating the negative charge of AlO_4^{-}, whereas Ca^{2+} compensates one AlO_4^{-}, not two, which is expected from the nominal charge of the ion. The behaviors of the Na_2O-containing glasses of MgO-CaO series in our investigation can be understood according to this idea. The fraction of tetrahedral Al^{3+} increases with substitution of MgO for CaO. The results shown in Figs. 4. 1. – 4. 3. suggest that the ability of the Ca^{2+} ion to compensate AlO_4^{-} depends on the Na_2O content (Na_2O/Al_2O_3 ratio) and it virtually vanishes in alkali-free glasses, for which almost no variation of the broad absorption was observed. Increase of the Na_2O/Al_2O_3 ratio compromises the ability of the Al^{3+} ion to associate with the Bi ion in glass by increasing the ability of the Ca^{2+} ion to charge-compensate AlO_4^{-}, resulting in increase of the broad absorption with substitution of MgO for CaO. We consider that the same mechanism applies to the other alkaline-earth oxide series, MgO-SrO and MgO-BaO. Comparing the changes of the broad absorption between the series, we think that the ability of the alkaline-earth ions

to charge-compensate AlO_4^- increases in the order, $Mg^{2+} < Ca^{2+} < Sr^{2+} < Ba^{2+}$.

4. 5. Conclusions

In Bi-doped alumino-silicate glasses, we consider that the Bi ion is stabilized by the Al^{3+} ion. The broad absorption due to metallic Bi increases when the Al^{3+} ion takes tetrahedral coordination and the negative charge of AlO_4^- is compensated by alkali and alkaline-earth ions. Compositional dependence of the broad absorption indicated that Ca^{2+}, Sr^{2+} and Ba^{2+} need alkali ions to compensate the negative charge of AlO_4^-. From the compositional dependence of the broad absorption, we estimated the ability of the alkaline-earth ions to charge-compensate AlO_4^- increases in the order, $Mg^{2+} < Ca^{2+} < Sr^{2+} < Ba^{2+}$.

References

[1] Y. Fujimoto, M. Nakatsuka, Jpn. J. Appl. Phys. 40 (2001) L279.

[2] S. Kishimoto, K. Sakaguchi, M. Tsuda, S. Nakagaki, S. Yoshii, Y. Fujimoto, M. Nakatsuka, Japanese patent, JP03897170 (applied Jan. 21, 2002).

[3] M. Shigematsu, S. Ishikawa, I. Tsuchiya, T. Murata, Japanese patent JP2004-196649A (applied Dec. 6, 2002).

[4] M. Peng, J. Qiu, D. Chen, X. Meng, C. Zhu, Opt. Express 13 (2005) 6892.

[5] T. Suzuki, Y. Ohishi, Appl. Phys. Lett. 88 (2006) 191912.

[6] N.D. Psaila, R.R. Thomson, H.T. Bookey, A.K. Kar, N. Chiodo, R. Oselllame, G. Cerullo, G. Brown, A. Jha, S. Shen, Opt. Express 14 (2006) 10452.

[7] X. Meng, J. Qiu, M. Peng, D. Chen, Q. Zhao, X. Jiang, C. Zhu, Opt. Express 13 (2005) 1635.

[8] S. Sumimiya, T. Nanba, S. Sakida, Y. Miura, in : Proc. Pacrim 6, 9th Biennial Worldwide Congress on Refractories, Maui, Hawaii, GOM-9-P, September 11-16, 2005.

[9] S. Kishimoto, M. Tsuda, K. Sakaguchi, Y. Fujimoto, M. Nakatsuka, in : Proc. 20th Int. Congr. Glass, paper O-14-029, 2004.

[10] X. Meng, J.Qiu, M.Peng, D.Chen, Q.Zhao, X.Jiang, C.Zhu, Opt. Express, 13 (2005) 1628.

[11] M. Peng, J. Qiu, D. Chen, X. Meng, I. Yang, X. Jiang, C. Zhu, Opt. Lett. 29 (2004) 1998.

[12] M. Peng, J. Qiu, D. Chen, X. Meng, C. Zhu, Opt. Lett. 30 (2005) 2433.

[13] W. Vogel, "Chemistry of Glass", translated and edited by N. Kreidl, The American Ceramic Society Inc., Columbus, OH (1985) p.176.

[14] M. B. Volf, Chemical approach to glass, Vol. 7, Elsevier 1984, p. 465-469.

[15] J. A. Duffy, "Basicity of Glass-Forming Melts", in "Electrochemistry of Glasses and Glass Melts, Including Glass Electrodes", H. Bach, F. G. K. Baucke and D. Krause Eds., Springer-Verlag, Berlin, 2000, p. 299.

[16] Y. Fujimoto, M. Nakatsuka, J. Non-Cryst. Solids 352 (2006) 2254.

[17] V.V. Dvoyrin, V.M. Mashinsky, E.M. Dianov, A.A. Umnikov, M.V. Yashkov, A.N. Guryanov, in : Proc. 31st ECOC, Glasgow, Scotland, vol. 4, paper Th 3.3.5, 2005, p.949.

[18] C. Rüssel, A. Wiedenroth, Chem. Geology 213 (2004) 125.

Chapter Five

Composition and Process Dependence of Optical Absorption and Emission Properties of Bismuth-Containing Zinc-Borate Glasses

5. 1. Introduction

It has been recently found that some groups of Bi-doped glasses exhibit infrared luminescence. Fujimoto and Nakatsuka [1] discovered that a $0.3Bi_2O_3{\cdot}2.2Al_2O_3{\cdot}97.5SiO_2$ glass had absorption bands in the visible and near-infrared regions (peaks at 500 nm, 700 nm and 800 nm) and exhibited broad infrared luminescence when the glasses were excited at either wavelength of the absorption peaks; Luminescence peaks were at about 1140 nm, 1120 nm and 1250 nm, respectively. Since their report, Bi-doped glasses have been attracting great attention because the broad infrared luminescence could be utilized for super-broadband amplifiers and novel lasers [2-21]. Silica-based fibers were fabricated and their optical properties were

reported [13-15, 18, 21]. Multi-component glass systems, including silicate [3, 4, 7, 19, 20], borate [8, 17], phosphate [5, 11] and germanate glasses [10, 12], were investigated as well. Some of the reports include amplification data. However, practical broadband amplifiers have yet to be developed using these glasses.

Several groups of researchers reported properties of Bi-doped glasses and discussed the origin of the characteristic absorption bands and infrared luminescence. There have been arguments especially about the oxidation state of the Bi ion that gives rise to the optical absorption bands at 500 nm, 700 nm and 800 nm. Fujimoto and Nakatsuka [1] presented the idea that the Bi^{5+} ion adjacent to the Al^{3+} ion is the origin of the absorption and the luminescence. They observed no ESR signal for the $0.3Bi_2O_3{\cdot}2.2Al_2O_3{\cdot}97.5SiO_2$ glass, and thus considered that the oxidation state of the Bi ion should be either Bi^{3+} or Bi^{5+}. The latter was considered probable by taking into account of energy levels of the Bi^{5+} ion and the emission properties. From their NMR study of the same glass system [16], they concluded that the Al^{3+} ion takes octahedral coordination in the infrared-emitting glasses. Sumimiya et al. [17] investigated properties and structures of Bi_2O_3-La_2O_3-Al_2O_3-B_2O_3 glasses. They measured ESR signals of the glasses and considered that oxygen defects in the base glass converted Bi^{3+} to Bi^{5+}, which they estimated was responsible for the infrared luminescence. Peng et al. [8] discussed effects of the Al^{3+} ion in their Al-containing borate glasses and claimed that the Bi^{+} ion could be stabilized by AlO_4^- just the same way as alkali ions are charge-compensated in the glass. They considered the Bi^{+} ion as the origin of the characteristic absorption bands and the related infrared luminescence. Dvoyrin et al.

[13] presented essentially the same argument in their report on Bi-doped silica-based fibers. Peng et al. [12] considered more reduced states of Bi ions, namely clustered Bi atoms, as the origin. They irradiated a $1.4Bi_2O_3{\cdot}55B_2O_3{\cdot}12.3PbO{\cdot}12.3SiO_2{\cdot}2Sb_2O_3$ glass with γ-ray and observed a broad absorption band at about 515 nm, which had been earlier reported on a γ-irradiated bismuth-lead-borate glass and had been attributed to metallic Bi [22]. They also observed broad infrared luminescence at about 1300 nm when the γ-irradiated glass was excited at 808 nm. From these results, they considered that Bi_n clusters were the origin of the absorption and infrared luminescence. Dvoyrin et al. [18] claimed in their report on Bi-doped silica-based fibers that they succeeded in explaining most absorption and luminescence properties in terms of energy levels of Bi^{5+}, Bi^{+}, Bi and coordinated oxygen atoms. However, they did not disclose the glass structure in the vicinity of the Bi ions that was used for their calculations. The reactions that brought about the structure are not indicated in their report, either. Summarizing the results reported in the literature, we conclude that the oxidation state of the Bi ion has not been determined conclusively. The two opposite possibilities have been presented: a high oxidation state, Bi^{5+}, and reduced states, Bi^{+} or Bi, including Bi_n clusters.

Previous investigations on Bi-doped glasses have been mainly on optical properties, especially infrared emission and energy levels involved. Optical properties of Bi-doped glasses depend much on glass composition and glass-fabrication conditions. To improve the absorption and emission properties for development of practical amplifiers, it is necessary to elucidate requirements for glass composition and process conditions, which currently are not still clear. Kishimoto et al. [3] disclosed that glasses

with high basicity exhibit broad absorption extending from the visible to the infrared regions and no infrared luminescence occurs when excited in the absorption band. Variation of the optical properties with glass composition is a major difference compared with rare-earth-ion-doped glasses, including Er-doped glasses for amplifiers, which show relatively small changes of properties with glass composition and/or glass-fabrication conditions due to the closed electron-shell structures of the rare earth ions. In the previous reports referred to above, effects of glass composition and glass-fabrication conditions, especially the latter, were not elucidated in detail. The two kinds of effects should be separated to understand what affects the optical properties of Bi-doped glasses. For this purpose, it is beneficial to obtain glasses with an identical composition and varied optical properties, which are obtained from different glass-fabrication conditions.

In this study, we looked at $xBi_2O_3 \cdot (50\text{-}0.5x)ZnO \cdot (50\text{-}0.5x)B_2O_3$ glasses [23] and investigated dependence of optical absorption on glass composition and glass-fabrication conditions. The glasses have low glass basicity that is necessary for the characteristic absorption bands and infrared luminescence of the Bi ion to occur, containing only ZnO as modifier oxide and no alkali ions. The Bi_2O_3-ZnO-B_2O_3 glasses can be melted at low temperatures, typically at 1000-1100°C, and they have low viscosities in the temperature range. This allows us to employ low temperatures for glass melting compared with other glass systems, which require higher melting temperatures for glass-forming and have higher viscosities. For example, a $0.3Bi_2O_3 \cdot 2.2Al_2O_3 \cdot 97.5SiO_2$ glass was fabricated at 1760°C [1], Bi_2O_3-Li_2O-ZnO

-Al_2O_3-SiO_2 glasses at 1600°C [7], Bi_2O_3-BaO-Al_2O_3-B_2O_3 glasses at 1550°C [8], Bi_2O_3-Al_2O_3-P_2O_5 glasses at 1550°C [18] and Bi_2O_3-Al_2O_3-GeO_2 glasses at 1550°C [18]. Low-temperature melting suppresses high temperature reactions including reducing reactions of the Bi ion and glass-structure changes, thus we can elucidate these effects and/or other effects that are hindered.

We investigated effects of composition, melting temperature, raw materials and reducing conditions on absorption of the Bi_2O_3-ZnO-B_2O_3 glasses. We successfully obtained glasses that have an identical composition and varied absorption intensities, which allowed us to infer conditions for the characteristic absorption bands to occur. Infrared luminescence was confirmed for the glasses with the absorption bands. Based on the conditions and using *Ab initio* molecular orbital calculations, we estimated the origin of the characteristic visible-to-near-infrared absorption and the related near-infrared luminescence of Bi-doped glasses.

5. 2. Experimental procedure

5. 2. 1. Glass composition

Nominal glass compositions of the samples are shown in Table 5. 1. The glasses have the compositions defined by the formulae xBi_2O_3-(50-0.5x)ZnO-(50-0.5x)B_2O_3 (x = 1-25). All the glass compositions in this chapter are expressed in mol%. Among the experimental glasses, ZNB1 and ZNB3 were used to investigate effects of glass-fabrication conditions. As a preliminary investigation, thermal expansion was measured for each glass and the glass transition temperature T_g

was determined. Each glass was fabricated by the one-step melting method described in the next section. The glass was annealed at around the temperature estimated to be T_g from the composition, and cooled at a rate of 1.67 °C/min or less to room temperature. A sample of φ5×18 mm was cut from the glass block and used for measurement. Thermal expansion was measured up to slightly above deformation temperature with a Rigaku TMA1000 thermomechanical analyzer. The heating rate was 5°C/min. Glass transition temperature (T_g) was obtained from the temperature-expansion curve. The obtained values for T_g are shown in Table 5. 1.

Table 5. 1.

Nominal glass compositions and measured glass-transition temperatures

Glass no.	Composition (mol%)			T_g
	Bi_2O_3	ZnO	B_2O_3	(°C)
ZNB1	1.00	49.50	49.50	556
ZNB2	3.13	48.44	48.44	517
ZNB3	6.25	46.88	46.88	507
ZNB4	12.50	43.75	43.75	470
ZNB5	25.00	37.50	37.50	418

5. 2. 2. Glass-melting procedures

For each glass, a batch of 400-g glass was obtained by thoroughly mixing adequately weighed reagent grade of Bi_2O_3, ZnO, B_2O_3 and H_3BO_3. Either B_2O_3 or H_3BO_3 was used for each glass batch. In most of the experiments, a platinum crucible of

200 ml was used for melting. Alumina crucibles were used when carbon was added to the batch as reducing agent. Glasses were fabricated according to the following procedures. All the glasses were melted in air.

5. 2. 2. 1. One-step melting method

The glass batch was melted in a platinum crucible at 1000°C -1150°C in an electric furnace. After completing batch feeding, the glass melt was kept at the temperature for 1.5 hours. The glass melt was stirred several times with a silica rod during melting. The glass melt was cast onto a stainless-steel plate and the glass was annealed 10 °C above its T_g for 30 minutes and cooled at a rate of 1.67 °C/min or less to room temperature. At the initial stage of the experiments, to avoid cracking in the glass samples, glasses were cast onto a carbon plate, which was later found to affect the absorption of the glasses (See Discussion). Unless otherwise noted, the glass was cast onto a stainless-steel plate.

In the case of alumina-crucible melting, a glass batch of 50-g glass was used. The glass was melted at a specified temperature for 30 minutes and it was not stirred during melting.

5. 2. 2. 2. Two-step melting methods

To investigate the effects of melting temperature, two-step melting methods were used. The glass was initially melted in an electric furnace at a temperature sufficient for glass-forming and fining. After completing batch feeding, the glass melt

was kept at the temperature for one hour and was stirred once with a silica rod during the melting. After the first-step melting, the crucible was taken out of the furnace and transferred to another furnace kept at a lower temperature. Some glasses were cooled to room temperature between the first and second melting steps. After completing the melting, the glass was annealed and cooled to room temperature as in the case of one-step melted glasses unless otherwise noted.

Table 5. 2.

Glass-fabrication conditions for experiments on melting temperature

Glass	Sample no.	1st-step melting	2nd-step melting	Remark
ZNB1	A	1150°C-1.5 hrs	-	-
ZNB1	B	1100°C-1.5 hrs	-	-
ZNB1		1100°C-1 hr	1000°C-1.5 hrs	-
ZNB1		1100°C-1 hr	800°C-1.5 hrs	-
ZNB1		1100°C-1 hr	700°C-2 hrs	Annealed in a Pt crucible
ZNB1	C	1100°C-1 hr	1000°C-1.5 hrs	Cooled to r. t. after 1st step
ZNB1	D	1100°C-1 hr	800°C-1.5 hrs	Cooled to r. t. after 1st step
ZNB3		1000°C-1.5 hrs	-	-
ZNB3		1000°C-1.5 hrs	750°C-1 hr	-

5. 2. 3. Sample preparation and evaluation

Samples of 30×30×7 mm and 14×30×4.2 mm were cut and polished from each glass block. They were used for optical transmission measurements. The samples of 30×30×7 mm size were also used for luminescence measurement.

Optical transmission spectra were measured with a Hitachi U-4100 spectrophotometer in the range of 290-2500 nm. Absorption coefficient was calculated from transmittance values for the two different thicknesses at each wavelength according to Lambert's law. Infrared luminescence spectra were measured with an Edinburgh Instruments FS-920 spectrofluorimeter with a photomultiplier in 920-1620 nm. The excitation wavelength was 450 nm. All the measurements were carried out at room temperature. X-ray photoelectron spectroscopic (XPS) measurements were carried out with an ULVAC-PHI Inc. ESCA 5600 spectrometer. Samples of 14×30×4.2 mm were used for the measurements. The binding energies were determined relative to the C1s XPS peak for carbon contamination.

5. 3. Results

5. 3. 1. Absorption properties

5. 3. 1. 1. Compositional dependence

Figure 5. 1. shows transmission spectra for $xBi_2O_3 \cdot (50\text{-}0.5x)ZnO \cdot (50\text{-}0.5x)B_2O_3$ (x = 1 - 25) glasses. The absorption edge in the short-wavelength region shifts to longer wavelength with Bi_2O_3 content. An absorption band at 450 nm was observed for glasses of x = 1.0, 3.13 and 6.25. The absorption bands at 1400 nm, 2100 nm and above are due to water in glass and the intensities of the bands increased with decreasing Bi_2O_3 content.

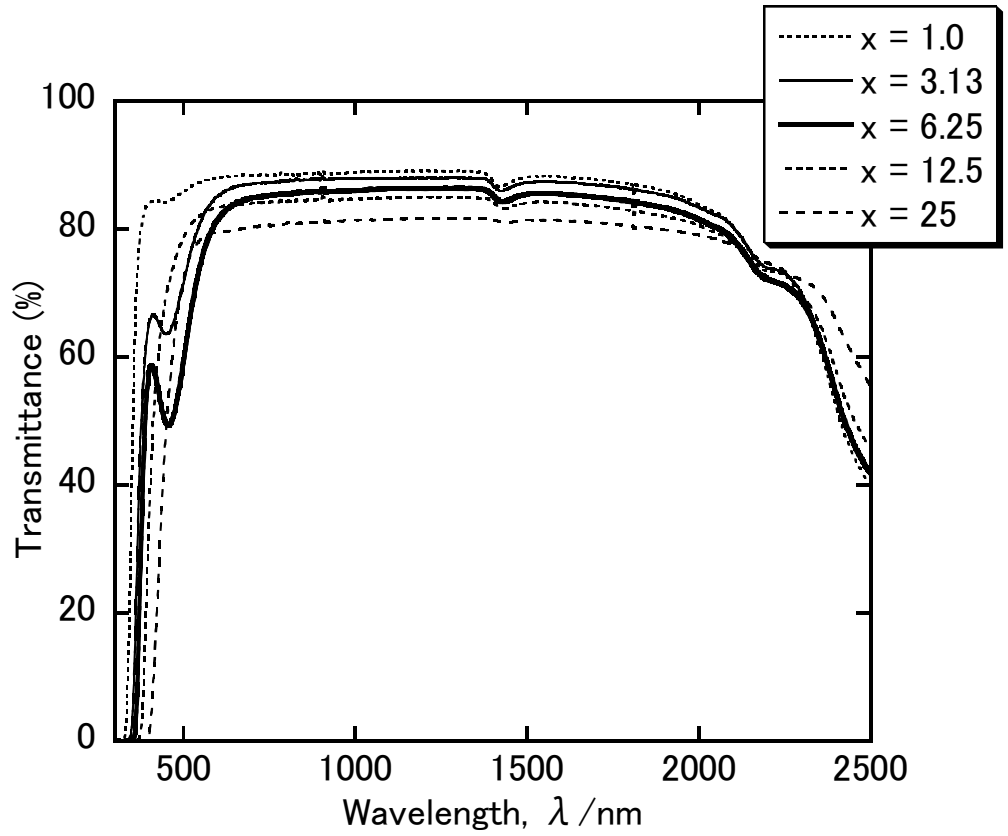

Fig. 5. 1. Transmission spectra for $xBi_2O_3 \cdot (50\text{-}0.5x)ZnO \cdot (50\text{-}0.5x)B_2O_3$ glasses: (a) x = 1; (b) x = 3.13; (c) x = 6.25; (d) x = 12.5; (e) x = 25. The glass-melting temperature was 1100°C for x = 1 and 3.13, and 1000°C for x = 6.25, 12.5 and 25, respectively. Boric acid (H_3BO_3) was used as raw material for B_2O_3. The thickness of the samples was 7 mm.

5. 3. 1. 2. Melting-temperature dependence

Figure 5. 2. shows absorption spectra for $6.25Bi_2O_3 \cdot 46.9ZnO \cdot 46.9B_2O_3$ glasses melted at 1000-1150°C. A broad absorption band, extending from UV to infrared region, intensified with melting temperature. For glasses melted at 1000-1100°C, we can see a weak absorption band at 22200 cm^{-1} (450 nm). The glasses were cast onto a carbon plate, which was later found to enhance the absorption band at 22200 cm^{-1} (450 nm) (See Discussion).

Figure 5. 3. shows absorption spectra for $6.25Bi_2O_3 \cdot 46.9ZnO \cdot 46.9B_2O_3$ glasses melted at different temperatures. The glasses are a glass melted at 1000°C and one melted initially at 1100°C and subsequently at 750°C, using a two-step melting technique. The intensity of the absorption band at 22200 cm^{-1} (450 nm) is larger for the glass melted at the lower temperature.

Figure 5. 4. shows absorption spectra for $1Bi_2O_3 \cdot 49.5ZnO \cdot 49.5B_2O_3$ glasses melted at different temperatures. The fabrication conditions are summarized in Table 5. 2. As the melting temperature decreased, the absorption band at 22200 cm^{-1} (450 nm) increased relative to the broad absorption band. Figure 5. 5. shows absorption coefficient at 22200 cm^{-1} (450 nm) as a function of melting temperature. Simple linear baselines were employed for the band at 22200 cm^{-1} (450 nm), and the corrected absorption coefficients were used for the data plot. An example of the linear base line is shown in Fig. 5. 4. As we can see from Fig. 5. 5., the absorption coefficient at 22200 cm^{-1} (450 nm) increased as the melting temperature decreased in each series of glasses.

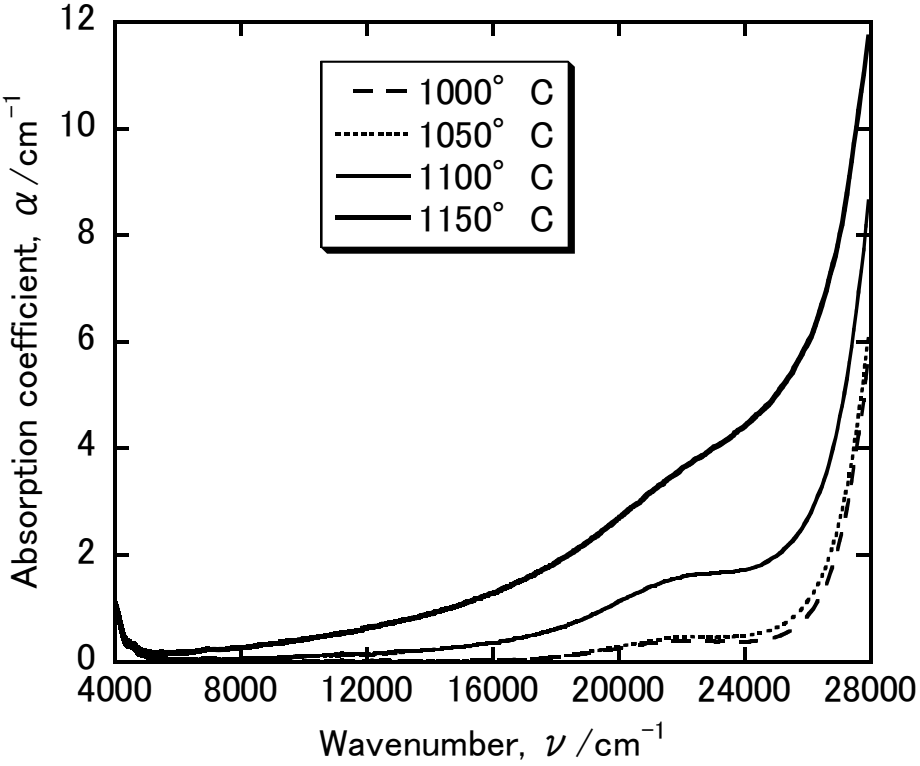

Fig. 5. 2. Absorption spectra for $6.25Bi_2O_3 \cdot 46.9ZnO \cdot 46.9B_2O_3$ glasses melted at different temperatures: (a) 1000°C; (b) 1050°C; (c) 1100°C; (d) 1150°C. Each glass was melted for 1.5 hours and was cast onto a carbon plate.

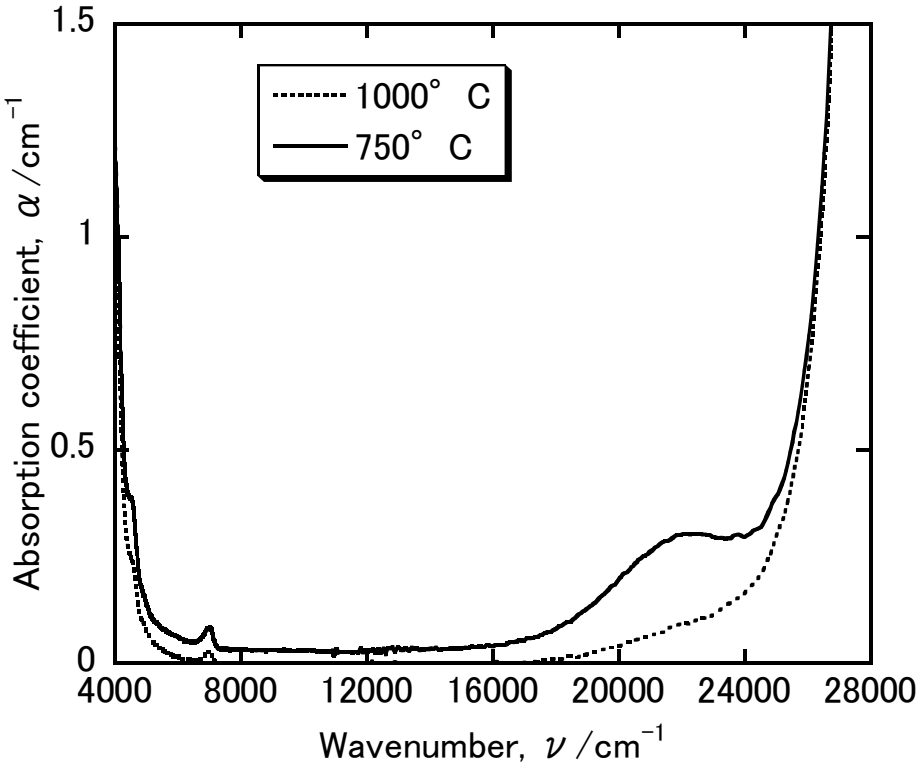

Fig. 5. 3. Absorption spectra for $6.25Bi_2O_3 \cdot 46.88ZnO \cdot 46.88B_2O_3$ glasses. Melting conditions: (a) 1000°C-1.5h; (b) 1000°C-1.5h and 750°C-1h. For each glass, the reagent for B_2O_3 was boric anhydride (B_2O_3).

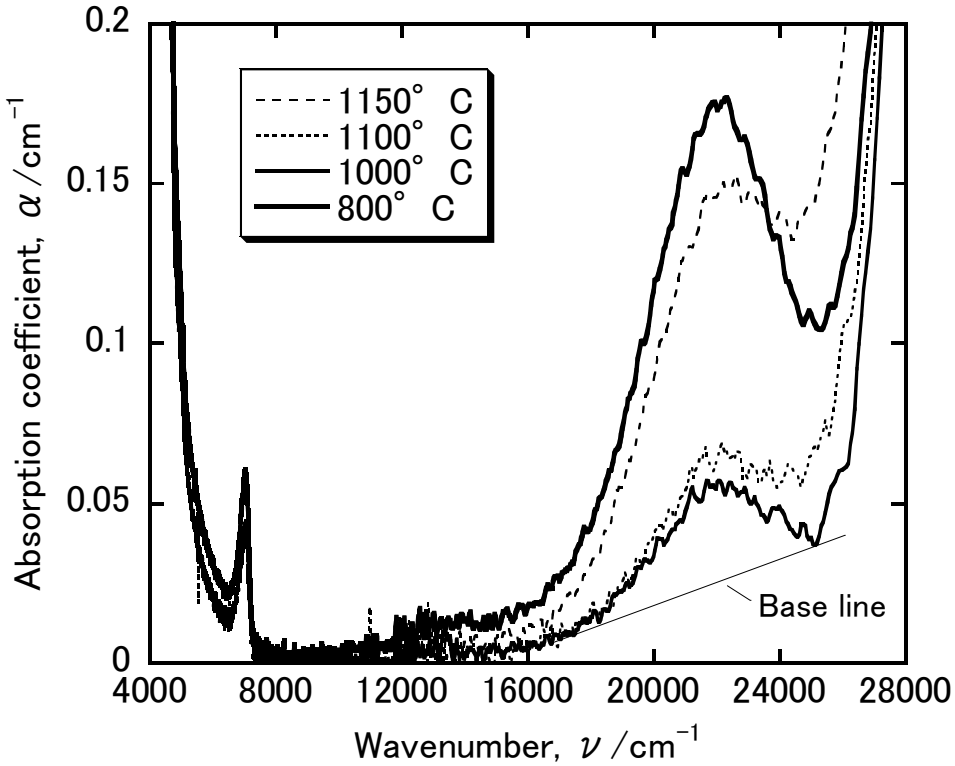

Fig. 5. 4. Absorption spectra for $1Bi_2O_3 \cdot 49.5ZnO \cdot 49.5B_2O_3$ glasses melted at different temperatures (Samples A-D). Melting temperatures are indicated in the figure. A linear base line for calculation of corrected absorption coefficient is drawn for the spectrum of the glass melted at 1000°C. Glass-fabrication conditions are described in Table 5. 2.

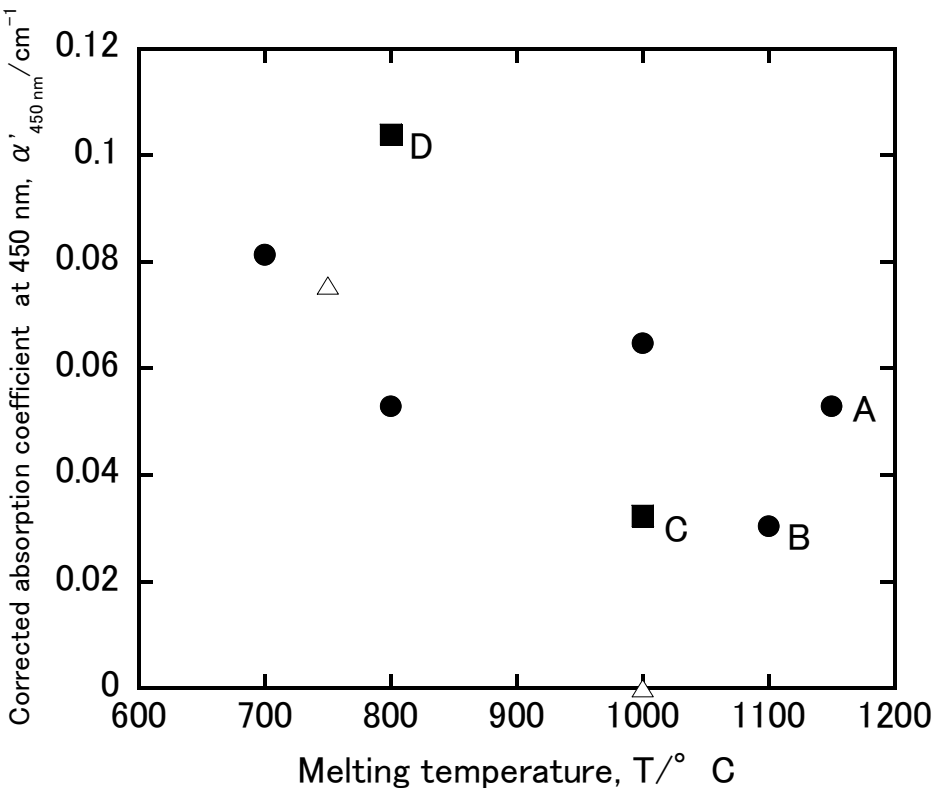

Fig. 5. 5. Base-line-corrected absorption coefficient at 22200cm^{-1} (450 nm) as a function of melting temperature: $1Bi_2O_3{\cdot}49.5ZnO{\cdot}49.5B_2O_3$ glasses (●); $1Bi_2O_3{\cdot}49.5ZnO{\cdot}49.5B_2O_3$ glasses, cooled to room temperature between first and second melting steps (■); $6.25Bi_2O_3{\cdot}46.9ZnO{\cdot}46.9B_2O_3$ glasses (Δ). For glasses melted by two-step melting methods, the melting temperatures of the second step were used in the plot. Glass fabrication conditions are described in Table 5. 2. Sample numbers A-D are indicated in the figure.

5. 3. 1. 3. Effect of reagent for B_2O_3

Figure 5. 6. shows absorption spectra for $6.25Bi_2O_3 \cdot 46.9ZnO \cdot 46.9B_2O_3$ glasses. The reagent for B_2O_3 was either boric anhydride (B_2O_3) or boric acid (H_3BO_3). A largely intensified absorption band at 22200 cm^{-1} (450 nm) was observed for the glass melted from batch containing boric acid.

5. 3. 1. 4. Effect of reducing agent

Figure 5. 7. shows absorption spectra for $6.25Bi_2O_3 \cdot 46.9ZnO \cdot 46.9B_2O_3$ glasses melted from a carbon-free batch and a carbon added batch. A large increase of the absorption band at 22200 cm^{-1} (450 nm) was observed for the glass melted from the carbon-added batch.

5. 3. 2. Emission properties

Figure 5. 8. shows emission spectra for $1Bi_2O_3 \cdot 49.5ZnO \cdot 49.5B_2O_3$ glasses from different fabrication procedures. (Their absorption spectra are shown in Fig. 5. 4.) The intensity of infrared emission was in the order, Sample B ~ Sample C < Sample A < Sample D. The corrected peak-intensity of the emission spectra for Sample A-D were obtained using linear base lines, and are expressed as a function of corrected absorption coefficient at 450 nm in Fig. 5. 9. An almost linear relationship was obtained for the two parameters.

Figure 5. 10. shows the excitation spectra for Sample A and D. Two peaks were observed, one at 20400 cm^{-1} (490 nm) and the other at 13300 cm^{-1} (750 nm).

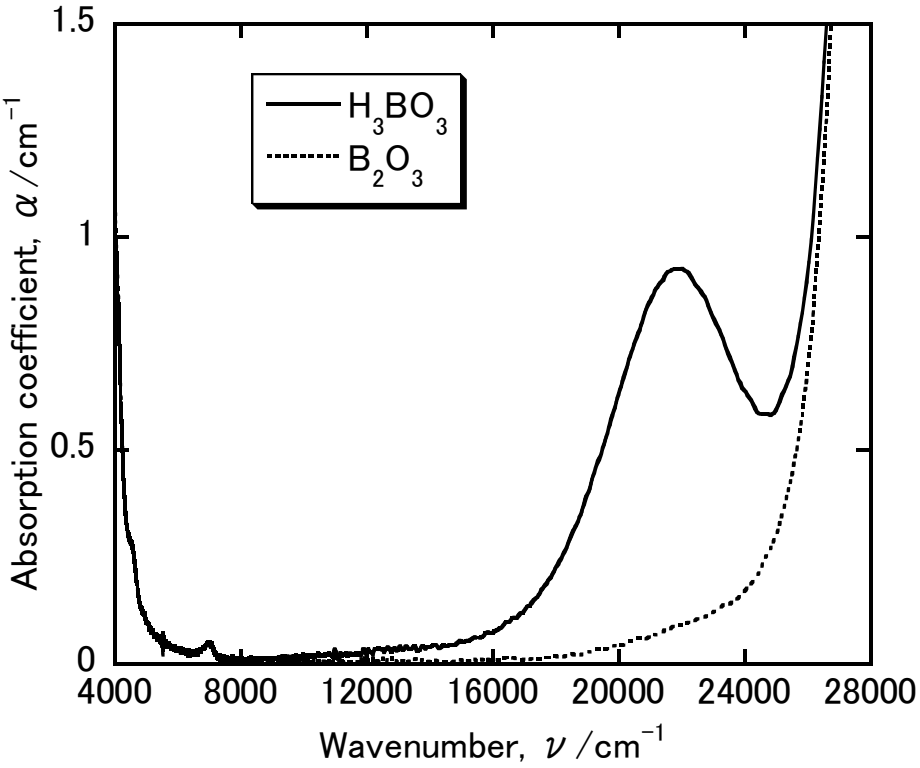

Fig. 5. 6. Absorption spectra for $6.25Bi_2O_3 \cdot 46.9ZnO \cdot 46.9B_2O_3$ glasses with different reagent for B_2O_3: (a) Boric acid (H_3BO_3); (b) Boric anhydride (B_2O_3).

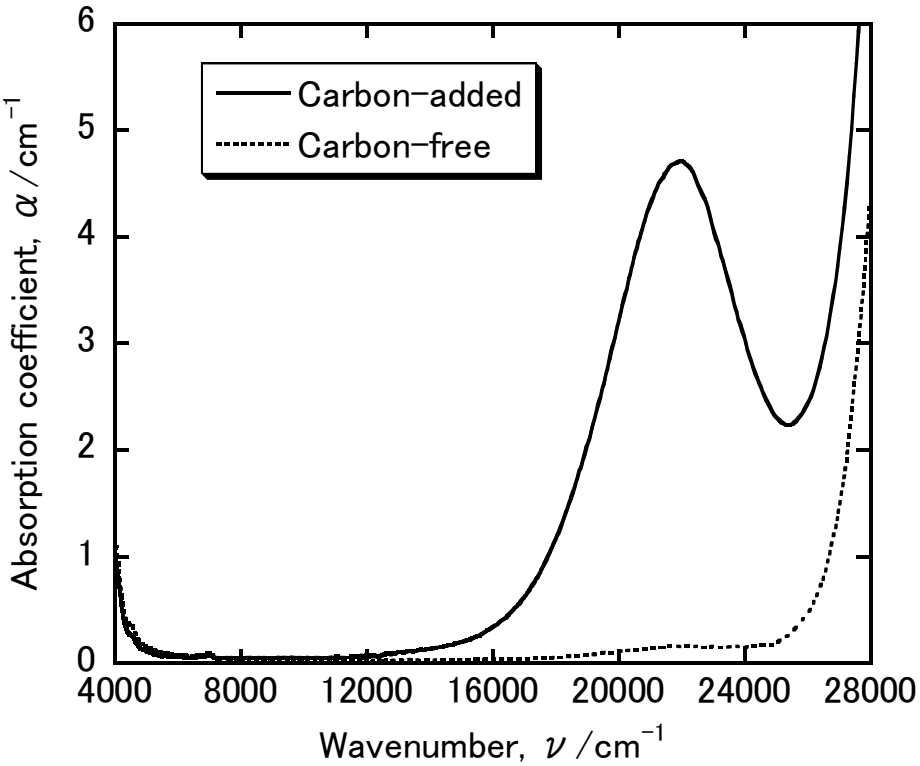

Fig. 5. 7. Absorption spectra for $6.25Bi_2O_3 \cdot 46.9ZnO \cdot 46.9B_2O_3$ glasses: (a) No carbon was added to the batch; (b) Carbon was added to the batch at a ratio of 0.012 g to 100 g of glass. For each glass, the reagent for B_2O_3 was boric anhydride (B_2O_3) and the glass was melted in an alumina crucible at 1000°C for 30 minutes.

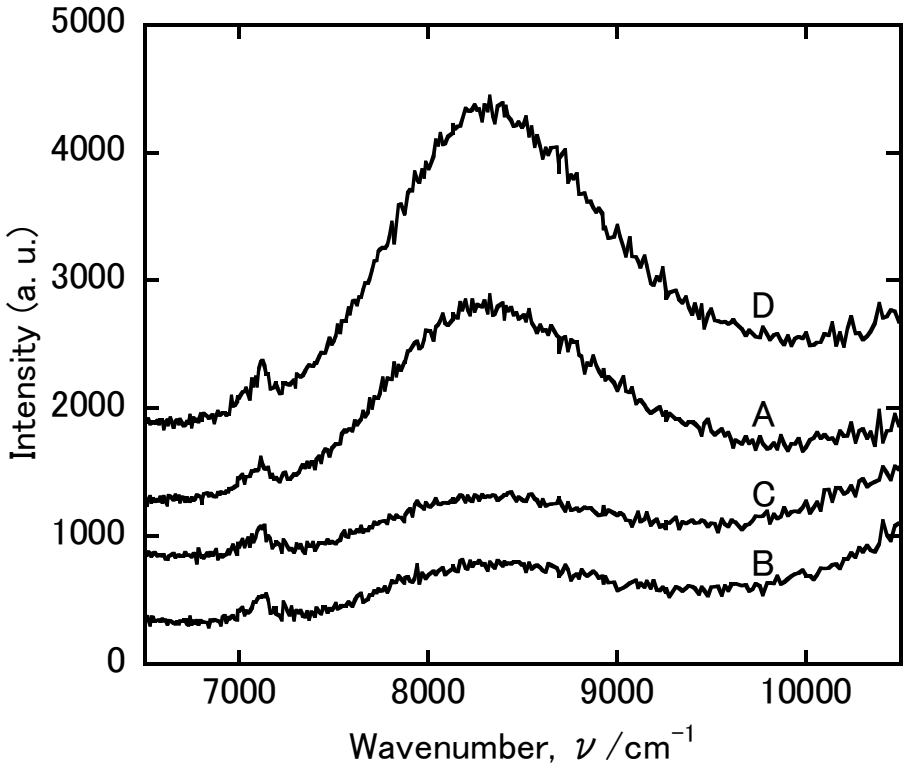

Fig. 5. 8. Emission spectra for $1Bi_2O_3 \cdot 49.5ZnO \cdot 49.5B_2O_3$ glasses excited at 22200 cm^{-1} (450 nm). The samples and melting temperature are as follows: Sample A, 1150°C; Sample B, 1100°C; Sample C, 1000°C; Sample D, 800°C. Detailed glass-fabrication conditions are described in Table 5. 2. The small peaks at around 7300 cm^{-1} are due to sensitivity of the detector and correction procedures, and did not originate from the glasses.

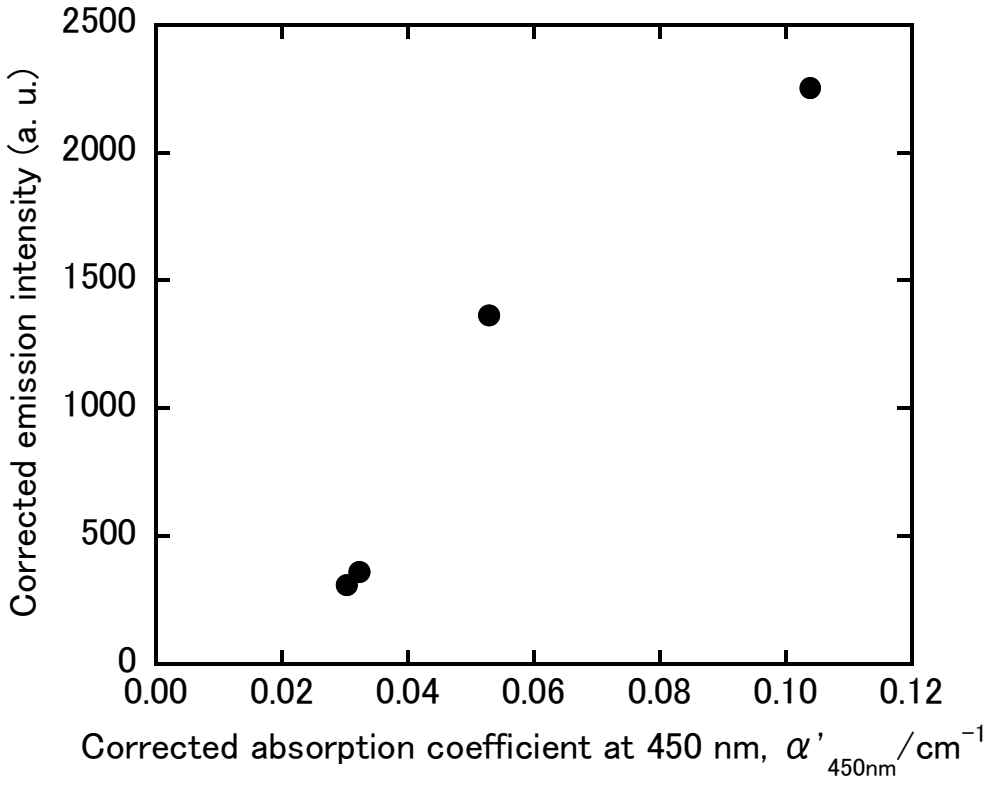

Fig. 5. 9. Corrected emission intensity excited at 22200cm^{-1} (450 nm) as a function of corrected absorption coefficient at 22200cm^{-1} for $1Bi_2O_3 \cdot 49.5ZnO \cdot 49.5B_2O_3$ glasses. Linear base lines were used for the corrections. The plot data are for Sample A-D. The detailed glass-fabrication conditions are described in Table 5. 2.

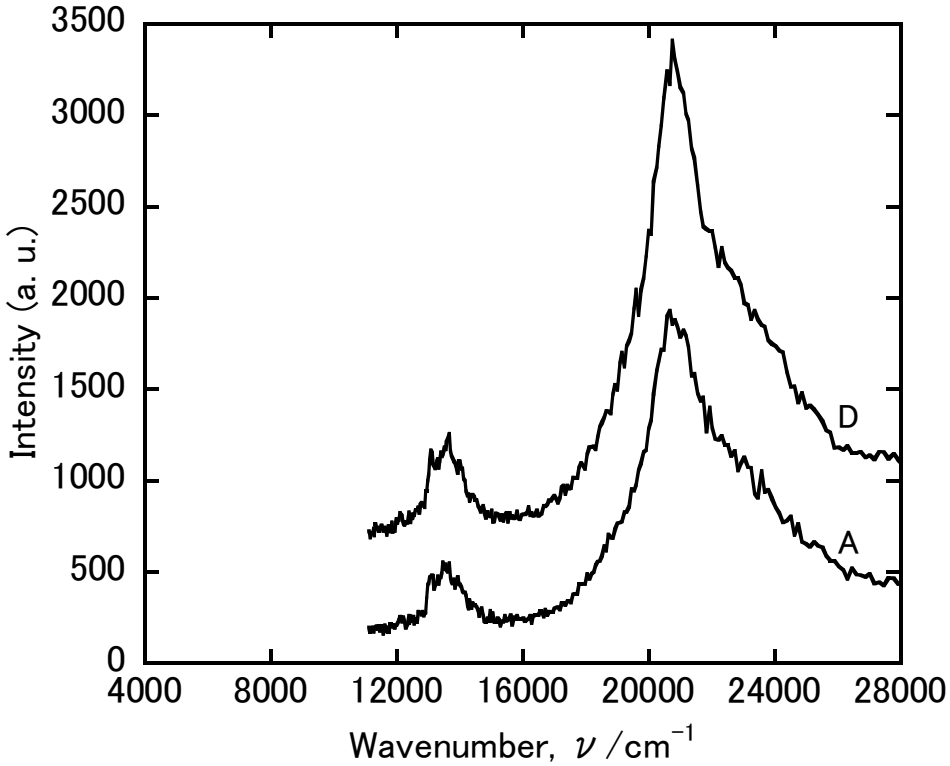

Fig. 5. 10. Excitation spectra for $1Bi_2O_3 \cdot 49.5ZnO \cdot 49.5B_2O_3$ glasses measured at 8333cm^{-1} (1200 nm). Melting temperatures are as follows: Sample A, 1150°C; Sample D, 800°C. Detailed glass-fabrication conditions are described in Table 5. 2.

5. 3. 3. XPS spectra

Figure 5. 11. shows binding-energy spectra of $Bi4f_{5/2}$ and $Bi4f_{7/2}$ for $1Bi_2O_3 \cdot 49.5ZnO \cdot 49.5B_2O_3$ glasses, which showed different corrected absorption coefficients at 22200 cm^{-1} (450 nm), 0.03 cm^{-1}, 0.7 cm^{-1} and 1.1 cm^{-1}. The glasses were fabricated by a two-step melting technique. No appreciable differences were observed between the three glasses in binding-energy peaks of $4f_{5/2}$ and $4f_{7/2}$, at 164.5 eV and 159.3 eV, respectively. These peaks correspond to those of Bi^{3+} [24]. We observed changes of spectra with time during measurement; the intensity at around 157 eV and 162 eV, which correspond to metallic Bi [24], increased with X-ray irradiation time. Figure 5. 11. shows the data after 50 minutes of irradiation.

5. 4. Discussion

5. 4. 1. Glass-fabrication conditions and optical absorption properties

We observed two types of absorption bands for the $xBi_2O_3 \cdot (50\text{-}0.5x)ZnO \cdot (50\text{-}0.5x)B_2O_3$ glasses. One is a broad absorption band extending from the UV- to the infrared regions. The others are the characteristic absorption bands at 22200 cm^{-1} (450 nm) and 13300 cm^{-1} (750 nm). The band at 13300 cm^{-1} (750 nm) was obscure in absorption spectra, but confirmed by excitation spectra shown in Fig. 5. 10. Figure 5. 2. shows the broad absorption band increases and grayish brown color develops as the melting temperature increases. The grayish brown coloration by the broad absorption over the entire visible region has been considered to be due to metallic Bi colloids [25, 26]. Increase of melting temperature generally favors lower oxidation

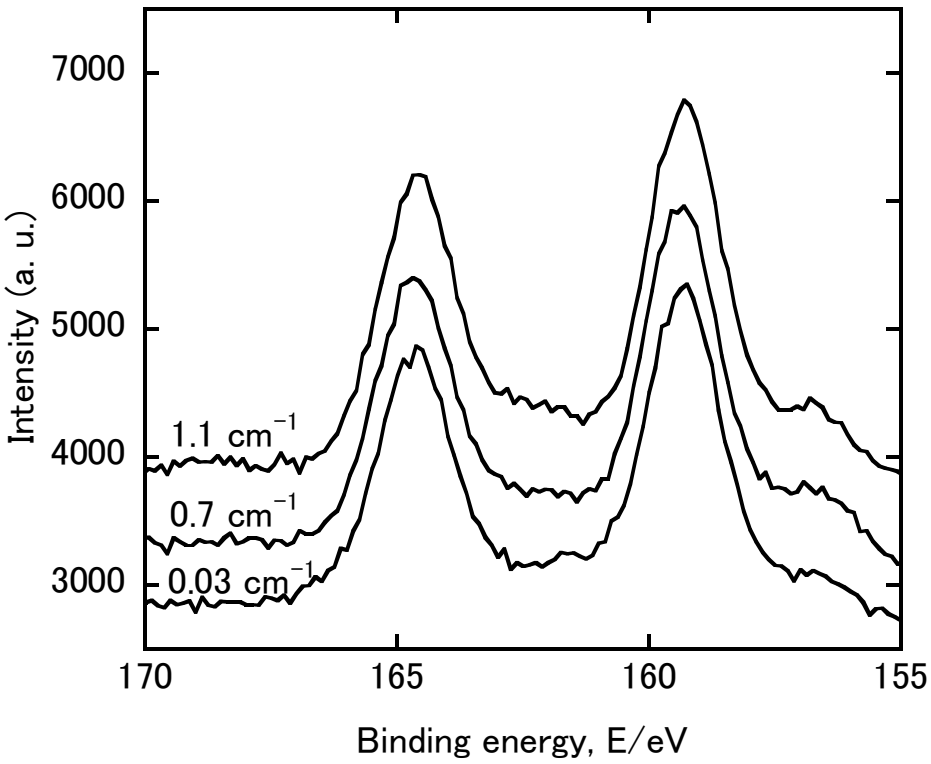

Fig. 5. 11. XPS spectra for $1Bi_2O_3 \cdot 49.5ZnO \cdot 49.5B_2O_3$ glasses. The corrected absorption coefficients at 22200 cm^{-1} (450 nm) of the glasses are indicated in the figure.

states of metal ions in glass [27], and thus the reduction reaction, $Bi^{3+} + 3e^- \rightarrow Bi$, proceeds more at high temperatures. Melting-temperature dependence of the broad absorption of the Bi_2O_3-ZnO-B_2O_3 glasses, depicted in Fig. 5. 2., is consistent with the general tendency. The reduction reaction, $Bi^{3+} + 3e^- \rightarrow Bi$, was also reported to be enhanced by increase of glass basicity [28]. Thus, elevating the melting temperature increases reduction of the Bi ion by increasing electron donation from surrounding oxygen atoms as well. We consider that the broad absorption has no contribution to infrared luminescence as Kishimoto et al. [3] disclosed for alumino-silicate glasses. Sumimiya et al. [17] also reported that glasses melted in a platinum crucible did not exhibit infrared emission and concluded that the glass was reduced more than in the case of alumina-crucible melting. We observed essentially the same phenomena when we melted a glass using carbon as reducing agent. Glasses melted in a platinum crucible showed a much intensified broad absorption compared with a glass melted in an alumina crucible, and the platinum crucibles were often damaged.

On the other hand, the results shown in Fig. 5. 7. clearly indicate that reducing the glass by carbon enhances the absorption band at 22200 cm^{-1} (450 nm). We also observed in our experiments that a glass cast onto a carbon plate showed stronger absorption at 22200 cm^{-1} (450 nm) than a glass cast onto a stainless-steel plate. This is another piece of evidence that reducing reactions contribute to generate specific states of Bi ions which give rise to the characteristic absorption bands. In this case, the duration of contact between the molten glass at high temperatures and the casting plate is very short, but in the narrow reaction window, slight reduction of glass by carbon of

the casting plate may have occurred. These results suggest that Bi^{5+} cannot solely be responsible for the characteristic absorption bands. Summarizing the results concerned with reducing conditions of glass, reducing the glass but not to the extent to generate metallic states of Bi, is desirable to enhance the absorption bands at 22200 cm^{-1} (450 nm) and 13300 cm^{-1} (750 nm).

We found that decreasing the melting temperature increases the absorption band at 22200 cm^{-1} (450 nm) as shown in Fig. 5. 3. - 5. 5. As for oxidation states of the Bi ion, the results seem to contradict with the conclusion above because low melting temperatures generally favor high oxidation states of metal ions as we discussed earlier. Comparing the absorption spectra for the glass melted at 1150°C and the one melted at 800°C in Fig. 5. 4., we can see that the latter has a larger peak at 22200 cm^{-1} (450 nm) and less broad absorption. Thus, the metallic states of the Bi ion decreased in this case. Figure 5. 9. shows baseline-corrected emission intensity is almost proportional to the baseline-corrected absorption coefficient at 22200 cm^{-1} (450 nm). It indicates that the metallic states of the Bi ion, which exhibit the broad absorption, do not contribute to the infrared emission.

Figure 5. 6. shows a large increase in absorption at 22200 cm^{-1} (450 nm) for a glass melted from a batch containing H_3BO_3 compared with one melted from a batch containing B_2O_3. During glass forming reactions, dehydration may work to enhance formation of structures that give rise to the absorption band at 22200 cm^{-1} (450 nm).

We consider that the results referred to above are the first clear demonstration of Bi-doped glasses that have an identical composition and characteristic absorption

bands with varied intensities. The glasses show different optical properties by different states of the Bi ion in the same glass matrix composition.

As a conclusion, we consider the following conditions for the characteristic absorption bands to occur: (a) low melting temperature; (b) reducing condition; (c) dehydration during melting.

5. 4. 2. Structures in the vicinity of the Bi ion

Adding the condition already imposed when we chose the glass system, we summarize the conditions for the characteristic absorption bands to occur as the following four descriptions: 1) low glass basicity; 2) low melting temperature; 3) reducing condition; 4) dehydration during melting. Among these conditions, condition 1 and 2 favor high oxidation states of the Bi ion, whereas condition 3 tends to generates low oxidation states. Condition 1 and 2 also prevent the Bi ion from being reduced to metallic states that give rise to a broad absorption band. We consider that Bi^{+}, Bi^{2+}, and Bi^{4+} ions will not be responsible for the characteristic absorption bands at 500, 700 and 800 nm and the related near-infrared emission bands of Bi-doped glasses because the ESR signals that are attributed to the above cations have not been observed [1]. This suggests that the near-infrared emission centers in Bi-doped glasses result from Bi^{3+} and/or Bi^{5+} cations, which do not have an unpaired electron and are hence ESR inactive. The present XPS spectra shown in Fig. 5. 11. further demonstrate that most of the Bi cations are present in the trivalent state, namely, Bi^{3+}. It is hence reasonable to assume that Bi^{3+} cations are the most probable candidates for the near-infrared emission centers

in Bi-doped glasses.

To get further knowledge about the electronic sates of the Bi^{3+} cations in silicate glasses, we here perform a series of *ab initio* molecular orbital calculations using clusters of atoms, including Bi, Si, O, and Al atoms. Figure 5. 12. shows a cluster of atoms modeling a local structure of the aluminosilicate network containing one Bi^{3+} cation. H atoms are used to terminate the surface dangling bonds of the cluster. In what follows, this cluster is referred to as model I. The structure of model1 was fully optimized at the Hartree-Fock level with the LANL2DZ basis set. The electronic excitation energies for the optimized configuration were calculated using the time-dependent density functional theory (TD-DFT) method [29].

We found that the first singlet-to-singlet electronic excitation energy of model I is calculated to be 5.7 eV (217 nm). This excitation energy is located in the ultraviolet region and is hence much higher than the observed absorption energies of the Bi-doped glasses. The present calculated results indicate that the single Bi^{3+} cation located in the aluminosilicate network does not yield optical absorption bands in the visible region but in the ultraviolet region. It is hence quite likely that this type of Bi^{3+} cation is not responsible for the characteristic absorption bands of Bi-doped glasses and the related near-infrared emission bands.

In this work, we, therefore, propose an alternative structural model of the Bi^{3+} cations to account for the visible-to-near-infrared absorption bands peculiar to Bi-doped glasses. We suggest that the observed visible-to-near-infrared absorptions result from the charge-transfer absorption between two Bi^{3+} cations. However, the charge transfer

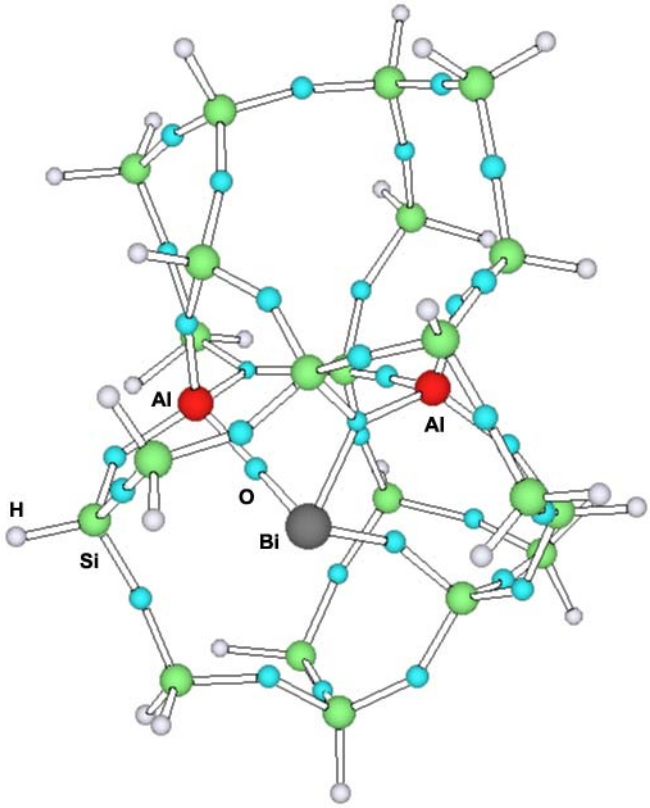

Fig. 5. 12. A cluster of atoms that model the local structure of Bi^{3+} cation (model I) in the aluminosilicate network. The geometry optimization was performed at the Hartree-Fock/LANL2DZ level.

process will not occur between cations with similar charge and structural states. Thus, a pair of two Bi^{3+} cations having different coordination environments is expected to be responsible for the proposed charge-transfer process. We assume that one of the pair is the two-fold coordinated Bi^{3+} cation, and the other is the four-fold coordinated Bi^{3+} cation. The proposed two-fold and four-fold coordinated Bi^{3+} cations have nominal charges of +1 and -1, respectively, since the local charge of the Bi^{3+} cation is fully compensated when the cation is coordinated by three oxygen atoms. It is also interesting to note that these structures can be alternatively viewed as the neutrally charged two-fold coordinated Bi^{2+} and the neutrally charged four-fold coordinated Bi^{4+}. However, the pair of "Bi^{2+}" and "Bi^{4+}" cations will not have an unpaired electron, unlike the case of the isolated Bi^{2+} or Bi^{4+} cation, since the expected two unpaired electrons from "Bi^{2+}" and "Bi^{4+}" will from a pair in this type of coordination state, leading to the singlet electronic state. We, therefore, consider that the present structural model is not inconsistent with the reported ESR measurements [1].

On the basis of the above assumptions, we constructed a cluster having a two-fold coordinated Bi and a four-fold coordinated Bi. We assumed that the total charge and multiplicity of the cluster is zero and singlet, respectively, indicating that both of the Bi cations in the cluster are nominally trivalent and do not have an unpaired electron, as noted earlier. The optimized structure of the cluster, which is called model II, is shown in Fig. 5. 13. We see from Fig. 5. 13. that in the optimized configuration, the assumed four-fold coordinated Bi^{3+} ion is further coordinated to the two bridging oxygen atoms that are originally coordinated to the two-fold coordinated Bi^{3+} cation,

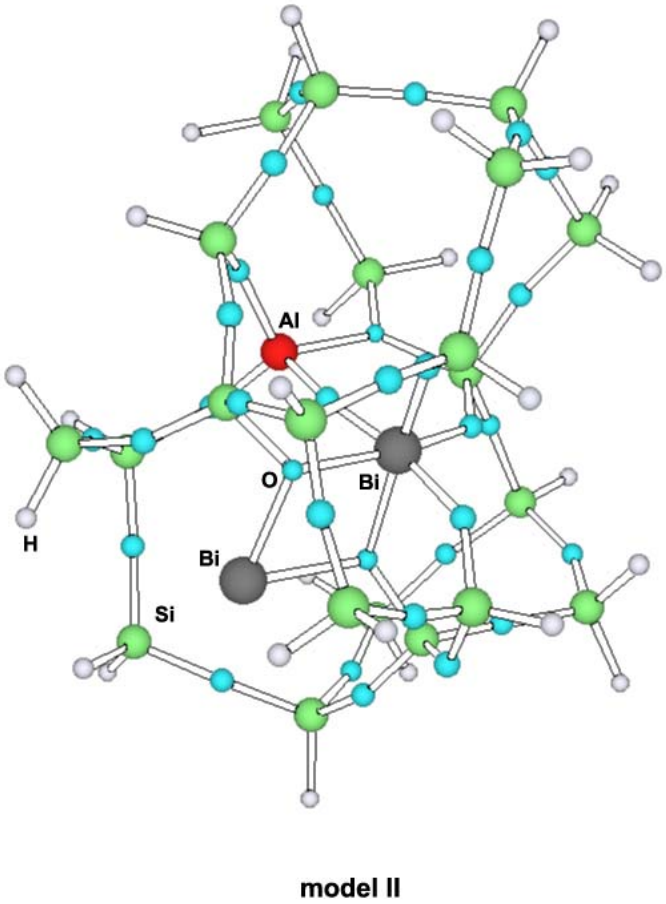

Fig. 5. 13. A cluster of atoms that model the local structure of a pair of Bi^{3+} cations (model II) in the aluminosilicate network. The geometry optimization was performed at the Hartree-Fock/LANL2DZ level.

resulting in the six-fold coordinated Bi^{3+} cation. That is, the resultant Bi pair has an edge-sharing structure, consisting of the six-fold coordinated Bi^{3+} and two-fold coordinated Bi^{3+}. We then calculate the electronic excitation energies on the basis of the TD-DFT method using the optimized configuration obtained. We found that the five lowest excitation energies of model 2 are calculated to be 0.81 eV (1531 nm), 1.04 eV (1184 nm), 2.04 eV (607 nm), 3.38 eV (367 nm), and 3.84 eV (322 nm). Although the calculated excitation energies do not perfectly coincide with those of the observed values, the excitation energies of model II will capture basic underlying optical absorption properties the Bi-doped glasses. From these calculations, we suggest that the characteristic visible-to-near-infrared absorption and the related near-infrared luminescence of Bi-doped glasses originate from the charge-transfer absorption between two Bi^{3+} ions having different coordination states.

Let us discuss how we can understand the conditions that we deduced earlier for occurrence of characteristic absorption bands, in the case of other systems of Bi-doped glass. The first infrared-emitting Bi-doped glass, $0.3Bi_2O_3{\cdot}2.2Al_2O_3{\cdot}97.5SiO_2$ discovered by Fujimoto and Nakatsuka [1], has very small glass basicity. The matrix of the glass has large electron-accepting power, especially by the Al^{3+} ion, which prevents the Bi ion from being reduced and favors to generate high oxidation states. Sample fabrication of the glass requires a high melting temperature, 1760°C, which tends to yield reduced states of the glass. Therefore, the glass and its fabrication process meet the conditions that we described earlier. Most of the infrared-emitting Bi-doped glasses reported in the literature essentially belong to the same category as the Bi-doped

Al_2O_3-SiO_2 glass because they have small quantity of glass-network modifier cations and require high melting temperatures [7, 8, 18].

Summarizing the estimated conditions for characteristic absorption bands to occur in a Bi-doped glass, we consider that the glass should contain Bi^{3+} ions of two different coordination states. The conditions are obtained when the glass has low basicity and is reduced. We can achieve this either by melting a low-basicity glass with high viscosity at a high temperature, or by melting a low-basicity glass with low viscosity at a low temperature under a reducing condition.

5. 5. Conclusions

Composition and process dependence of optical absorption and emission properties were investigated for $xBi_2O_3 \cdot (50\text{-}0.5x)ZnO \cdot (50\text{-}0.5x)B_2O_3$ (x = 1-25) glasses. An absorption band at 450 nm was observed for the glasses of x = 1.0-6.25. The absorption increased in intensity when the glass batch contains carbon or water (H_3BO_3), or by decreasing the melting temperature.

We obtained glasses with an identical composition and varied absorption intensities at 450 nm. From the results, we estimated conditions for the occurrence of the characteristic absorption bands as low glass-basicity and reducing conditions, which tend to generate high oxidation states and low oxidation states of the Bi ion, respectively. Based on the deduced conditions and using *Ab initio* molecular orbital calculations, we estimated that the characteristic visible-to-near-infrared absorption and the related near-infrared luminescence are most likely to originate from two Bi^{3+} ions having

different coordination states, but not different oxidation states.

References

[1] Y. Fujimoto, M. Nakatsuka, Jpn. J. Appl. Phys. 40 (2001) L279.

[2] Y. Fujimoto, M. Nakatsuka, Appl. Phys. Lett. 82 (2003) 3325.

[3] S. Kishimoto, K. Sakaguchi, M. Tsuda, S. Nakagaki, S. Yoshii, Y. Fujimoto, M. Nakatsuka, Japanese patent, JP03897170 (applied Jan. 21, 2002).

[4] M. Shigematsu, S. Ishikawa, I. Tsuchiya, T. Murata, Japanese patent JP2004-196649A (applied Dec. 6, 2002).

[5] S. Kishimoto, M. Tsuda, K. Sakaguchi, Y. Fujimoto, M. Nakatsuka, in : Proc. 20th Int. Congr. Glass, paper O-14-029, 2004.

[6] Y. Fujimoto, M. Nakatsuka, in : Proc. 20th Int. Congr. Glass, paper O-07-77, 2004.

[7] M. Peng, J. Qiu, D. Chen, X. Meng, C. Zhu, Opt. Express 13 (2005) 6892.

[8] X. Meng, J. Qiu, M. Peng, D. Chen, Q. Zhao, X. Jiang, C. Zhu, Opt. Express 13 (2005) 1635.

[9] M. Peng, X. Meng, J. Qiu, Q. Zhao, C. Zhu, Chem. Phys. Lett. 403 (2005) 410.

[10] M. Peng, J. Qiu, D. Chen, X. Meng, I. Yang, X. Jiang, C. Zhu, Opt. Lett. 29 (2004) 1998.

[11] X. Meng, J. Qiu, M. Peng, D. Chen, Q. Zhao, X. Jiang, C. Zhu, Opt. Express, 13 (2005) 1628.

[12] M. Peng, J. Qiu, D. Chen, X. Meng, C. Zhu, Opt. Lett. 30 (2005) 2433.

[13] V.V. Dvoyrin, V.M. Mashinsky, E.M. Dianov, A.A. Umnikov, M.V. Yashkov, A.N.

Guryanov, in : Proc. 31st ECOC, Glasgow, Scotland, vol. 4, paper Th 3.3.5, 2005, p.949.

[14] V.V. Dvoyrin, V.M. Mashinsky, E.M. Dianov, A.A. Umnikov, M.V. Yashkov, A.N. Guryanov, in Optical Fiber Communication Conference and Exposition and The National Fiber Optic Engineers Conference, paper OTuH4 (2006).

[15] E.M. Dianov, V.V. Dvoyrin, V.M. Mashinsky, A.A. Umnikov, M.V. Yashkov, A.N. Guryanov, Quantum Electron, 35 (2005) 1083.

[16] Y. Fujimoto, M. Nakatsuka, J. Non-Cryst. Solids 352 (2006) 2254.

[17] S. Sumimiya, T. Nanba, S. Sakida, Y. Miura, in : Proc. Pacrim 6, 9th Biennial Worldwide Congress on Refractories, Maui, Hawaii, GOM-9-P, September 11-16, 2005.

[18] V. V. Dvoyrin, V. M. Mashinsky, L. I. Bulatov, I. A. Bufetov, A. V. Shubin, M. A. Melkumov, E. F. Kustov, E. M. Dianov, A. A. Umnikov, V F. Khopin, M. V. Yashkov, A. N. Guryanov, Opt. Lett. 31 (2006) 2966.

[19] T. Suzuki, Y. Ohishi, Appl. Phys. Lett. 88 (2006) 191912.

[20] N.D. Psaila, R.R. Thomson, H.T. Bookey, A.K. Kar, N. Chiodo, R. Oselllame, G. Cerullo, G. Brown, A. Jha, S. Shen, Opt. Express 14 (2006) 10452.

[21] Y. S. Seo, Y. Fujimoto, M. Nakatsuka, IEEE Photo. Tech. Lett. 18 (2006) 1901.

[22] A. M. Bishay, Phys. Chem. Glasses 2(1961) 33.

[23] O. Deparis, F.P. Mezzapesa, C. Corbari, P.G. Kazansky, K. Sakaguchi, J. Non-Cryst. Solids 351 (2005) 2166.

[24] C. D. Wagner, W. M. Riggs, L. E. Davis, J. F. Moulder, G. E. Mullenberg, in Handbook of X-ray Photoelectron Spectroscopy, Perkin-Elmer Corp., Eden Prairie, MN,

US (1979), p.190.

[25] W. Vogel, “Chemistry of Glass”, translated and edited by N. Kreidl, The American Ceramic Society Inc., Columbus, OH (1985) p.176.

[26] M. B. Volf, Chemical approach to glass, Vol. 7, Elsevier 1984, p. 465-469.

[27] W. D. Johnston, J. Am. Ceram. Soc. 48 (1965) 184.

[28] J. A. Duffy, “Basicity of Glass-Forming Melts”, in “Electrochemistry of Glasses and Glass Melts, Including Glass Electrodes”, H. Bach, F. G. K. Baucke and D. Krause Eds., Springer-Verlag, Berlin, 2000, p. 299.

[29] M. E. Casida, C. Jomorski, K. C. Casida and D. R. Salahub, J. Chem. Phys. 108 (1998) 4439.

Chapter Six

New Glass-Sealing Method with Lead-Free Solders

6. 1. Introduction

Glass and metal do not join readily due to their different bonding characters, requiring an activation process for joining. For activating the joining interface of glass/ceramics and metal, several technologies were disclosed including ultrasonic vibration [1] and pressure applying [2]. These technologies proved their advantages for joining various metal and glass/ceramics parts. However, for hermetic edge-seal of a pair of glass substrates, which requires filling and joining very small gaps with large sealing lengths as in production of vacuum glazing [3], no commercially applicable technology was proposed. For a simple and cost-effective way of activation, we looked at mechanical friction between glass and metal, using a single-stroke friction-activated capillary soldering step for a high-rate sealing process and demonstrated its

effectiveness.

6. 2. Experimental

6. 2. 1. Materials

We used two kinds of solders. For sealing at around 200 °C, we selected Sn-Zn binary eutectic (Sn 91.2 wt%, Zn 8.8 wt%, the eutectic temperature is 198 °C) as the base alloy and doped small quantity of Ti as activator. The other solder was In-Sn eutectic (In 52 wt%, Sn 48 wt%, the eutectic temperature is 117 °C). Glass substrates were a soda-lime-silicate float glass (FL3, Nippon Sheet Glass Co., Ltd.) and an alkali-free alumino-boro-silicate glass (NA35, NH Techno Glass Corp.). The thicknesses of the substrates were 3 mm and 1.1 mm, respectively. The size of the substrate was 100×100-200×200 mm.

6. 2. 2. Sealing equipment and procedures

Figure 6. 1. shows the schematic illustration of the set-up for friction-activated capillary soldering of paired glass substrates. Molten solder is held in a solder container and flows out from the outlet tube located at the center of the bottom. In this way, incorporation of oxides formed at the surface of the molten solder is avoided: only the inner part of the molten solder, which is separated from the atmosphere, flows out of the solder container to the friction plate. For the friction plate, flat and wave-patterned stainless-steel plates were used. The latter gives stronger friction due to the narrower gap between the plate and the glass substrates.

Sealing experiments were carried out as follows. Glass substrates were paired with a gap of 0.2mm, using stainless pillars for sustaining the gap. They were kept at a specified temperature. The friction plate was inserted to the gap of the paired glass substrates from one of the edges. The insertion depth was 2-5 mm, which would subsequently be the sealing width. During the sealing step, the friction plate slides along the edge of the paired glass substrates, applying the solder to the inner surfaces of the gap. One edge of paired glass substrates was sealed by a single stroke of applying solder. The procedure was repeated four times and the paired glass substrates were edge-sealed entirely. The sealing rate was 25-100 mm/s for each stroke. After the sealing, the paired glass substrates were cooled to room temperature.

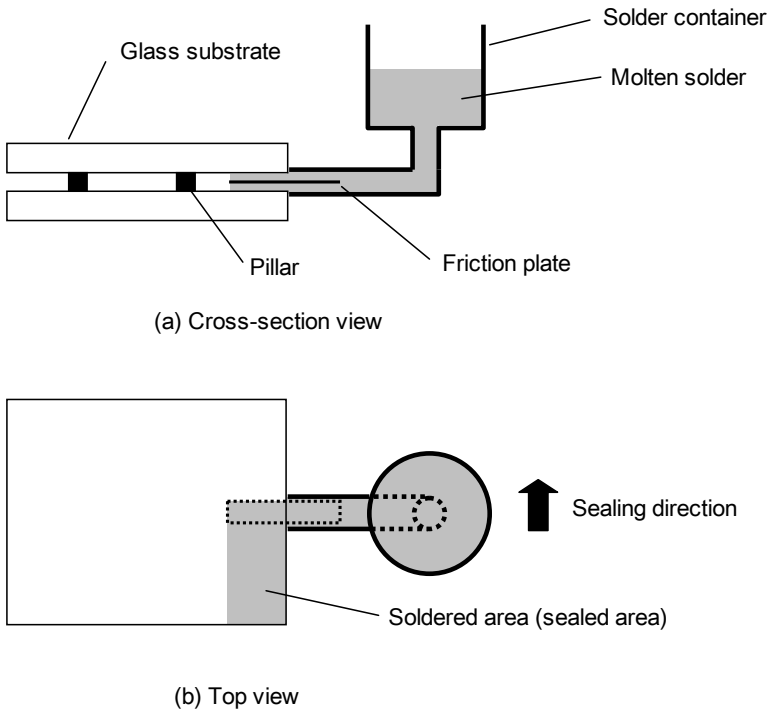

Fig. 6. 1. Schematic illustration of sealing equipment and sealing process.

6. 2. 3. Evaluation of Joining Properties

Hermeticity of joined paired glass substrates was measured using a helium leak detector (Shimazu MSE1001). The sensitivity of the detector was 1×10^{-11}(Pa•m^3/s). As a simple confirmation method of sealed strength of joined solder/glass samples, we carried out a peeling test: the solder layer was peeled by hand and the solder/glass interfaces were later observed.

6. 3. Results and discussion

Table 6. 1. shows the results of edge-sealed samples. For all the successfully sealed samples, the sealed area extends to the traced line of the tip of the friction plate and the inner sealed-edge is clearly defined by a straight line. The soda-lime-silicate float glass yielded very good quality of sealed states. Mirror-surfaces were observed at the solder/glass interfaces, either for the case of flat or wave-patterned friction plate. For sealing at 120 °C, the flat friction plate could not apply In-Sn solder to the glass surface sufficiently. However, the wave-patterned friction plate yielded good joined interfaces. We understand that the wave-patterned friction plate generates stronger friction at the glass/solder interface, thus it gives additional activation energy which is needed to compensate the low sealing temperature. For oxide glasses, we think that the joining is bond formation between metal components (such as Ti and In) and oxygen atoms. The oxygen atoms in glass have bonds with cations in the glass thus rearrangement is required for the new bond formation with the metal components. Comparing the results for the float soda-lime-silicate glass and the alkali-free alumino-boro-silicate glass, we observed no marked difference between the two for their sealed-state qualities. It is

rather amazing considering the difference between their glass-network strengths: the glass transition temperatures are 550 °C and 640 °C, respectively. The joining process does not seem to be bond-breaking and bond-formation at the interface, where the friction contributes to breaking the bonds between cations and oxygen atoms in glass. We think that friction induces chemical reactions involving the glass surface and components in the solder when adequate rubbing by the friction plate works as some kind of catalyst.

Table 6. 1. Sealed states of edge-sealed paired glass substrates

Glass/solder	Temperature[a)] (°C)	Friction plate	He-leak test[b)]	Peeling strength[c)]
FL3/Sn-Zn-Ti	200	Flat	Passed	Strong
FL3/Sn-Zn-Ti	200	Wave-patterned	Passed	Strong
NA35/Sn-Zn-Ti	200	Wave-patterned	Passed	Strong
FL3/In-Sn	120	Flat	Failed	Weak
FL3/In-Sn	120	Wave-patterned	Passed	Strong
FL3/In-Sn	100	Wave-patterned	Passed	Strong
FL3/In-Sn	80	Wave-patterned	Failed	Weak
NA35/In-Sn	120	Wave-patterned	Passed	Strong

a) Approximate temperature at the edge of the paired glass substrates.

b) The detection sensitivity was 1×10^{-11} ($Pa\bullet m^3/s$).

c) The sealed pair of glass substrates was pulled apart by hand. “Weak” means that the solder layer was removed without breaking glass substrates. “Strong” means that the glass substrates were at least partially fractured when the solder layer was peeled.

6. 4. Summary

We have developed a novel process for hermetic seal of paired glass substrates. We used Ti-doped Sn-Zn eutectic solder and In-Sn eutectic solder for sealing materials. The sealing process is based on friction-activated capillary action. The sealing machine is equipped with a solder container and a solder outlet with a friction plate. We successfully fabricated hermetically edge-sealed samples of float soda-lime-silicate glass and alkali-free alumino-boro-silicate glass. The sealing edge is clearly defined as a straight line. The developed process is commercially applicable to sealing of large substrates. The sealing process assumed to involve tribologically induced chemical reactions.

References

[1] K. Nagano et al., Reports Res. Lab. Asahi Glass Co., Ltd., 21 (1971) 177.

[2] K. Suganuma, J. Mater. Sci., 61 (1991) 6144.

[3] R. E. Collins et al., Building and Environment, 30 (1995) 459.

Chapter Seven

Conclusions

In the foregoing chapters, we have shown composition and process dependence of absorption of iron-doped glasses and bismuth-doped glasses. Also, as a phenomenon concerning glass basicity, we have demonstrated that lead-free solders can be utilized for hermetic sealing of glass sheets. We give our findings as follows.

7. 1. Process dependence of absorption of iron-doped alkali-silicate glasses

Heat treatment experiments of an iron-containing float glass revealed that Fe^{2+} absorption peak at around 1080nm shifted to shorter wavelengths and Fe^{3+} absorption in the 420-440nm region increased in intensity. It is due to relaxation of the glass structure. For heat treatments below T_g, only peak shifts of Fe^{2+} occurred, while no changes were observed in Fe^{3+} absorption. The peak shift of Fe^{2+} showed the largest change around

200 ºC below T_g, suggesting that the rearrangement of alkali ions may cause the absorption change.

7. 2. Compositional dependence of absorption of iron-doped silicate glasses

Compositional dependence of infrared absorption of iron-doped glasses was investigated and analyzed using Λ_c-ν_p diagrams, in which peak wavenumber of the infrared absorption band ν_p was given as a function of calculated optical basicity Λ_c of glass. We employed Λ_c as glass-composition parameter which represents the complex combination of glass components. Basic variations of glass composition were chosen as substitution of Mg^{2+} for a larger alkaline-earth ion, keeping the total quantity of R'O constant. For iron-doped alkali alkaline-earth silicate glasses, increase of Λ_c by substitution of SiO_2 for R'O increased ν_p, whereas increasing Λ_c by substituting Mg^{2+} for a larger alkaline-earth ion yielded the opposite trend. We considered that the composition changes vary effective negative charge on oxygen atoms and symmetry of their coordination around the Fe^{2+} ion. For iron-doped (alkali) alkaline-earth (alumino-)silicate glasses, behaviors of the absorption band depended much on the Na_2O/Al_2O_3 ratio. ESR spectra suggested clustering of Fe^{3+} ions (possibly with Fe^{2+} ions) in alkali-containing glasses and no clustering in alkali-free glasses. We estimated that Fe^{3+} and Fe^{2+} ions associate strongly with Al^{3+} ions when the negative charge of AlO_4^- is not compensated by other network-modifying cations.

Steep decrease of the peak wavenumber with increasing Λ_c by substituting Mg^{2+} for Ca^{2+} was observed in the regions with a very low or no MgO content for all

series of glasses containing alkali ions. The effect was probably due to direct interaction between the Fe^{2+} ion and the Mg^{2+} ion.

7. 3. Compositional dependence of absorption of Bi-doped alumino-silicate glasses

In Bi-doped alumino-silicate glasses, we consider that the Bi ion is stabilized by the Al^{3+} ion. The broad absorption due to metallic Bi increases when the Al^{3+} ion takes tetrahedral coordination and the negative charge of AlO_4^- is compensated by alkali and alkaline-earth ions. Compositional dependence of the broad absorption indicated that Ca^{2+}, Sr^{2+} and Ba^{2+} need alkali ions to compensate the negative charge of AlO_4^-. From the compositional dependence of the broad absorption, we estimated the ability of the alkaline-earth ions to charge-compensate AlO_4^- increases in the order, $Mg^{2+} < Ca^{2+} < Sr^{2+} < Ba^{2+}$.

7. 4. Process dependence of absorption of Bi-doped zinc-borate glasses

Process dependence of optical absorption and emission properties were investigated for $xBi_2O_3 \cdot (50\text{-}0.5x)ZnO \cdot (50\text{-}0.5x)B_2O_3$ (x = 1-25) glasses. An absorption band at 450 nm was observed for the glasses of x = 1.0-6.25. The absorption increased in intensity when the glass batch contains carbon or water (H_3BO_3), and when the melting temperature was decreased. We obtained glasses with an identical composition and varied absorption intensities at 450 nm. This is the first clear demonstration of process dependence of the characteristic absorption bands of Bi-doped glasses. From the results, we estimated conditions for the occurrence of the characteristic absorption

bands as low glass-basicity and reducing conditions, which tend to generate high oxidation states and low oxidation states of the Bi ion, respectively. Based on the deduced conditions and using *Ab initio* molecular orbital calculations, we estimated that the characteristic visible-to-near-infrared absorption and the related near-infrared luminescence are most likely to originate from two Bi^{3+} ions having different coordination states, but not different oxidation states.

7. 5. Glass/metal joining for hermetic sealing

We have developed a novel process for hermetic seal of paired glass substrates. We used Ti-doped Sn-Zn eutectic solder and In-Sn eutectic solder for sealing materials. The sealing process is based on friction-activated capillary action. We successfully fabricated hermetically edge-sealed samples of float soda-lime-silicate glass and alkali-free alumino-boro-silicate glass. The sealing process assumed to involve tribologically induced chemical reactions.

Publication List

Chapter 2, 3, 4, 5 and *6* are based on the following papers published or submitted or to be submitted.

Chapter 2: K. Sakaguchi, “Effect of heat treatment on optical absorption of iron in float glass”, Glass Technol., 43C(2002)245-247.

Chapter 3: K. Sakaguchi and T. Uchino, “Compositional dependence of infrared absorption of iron-doped silicate glasses”, submitted to J. Non-Cryst. Solids.

Chapter 4: K. Sakaguchi and T. Uchino, “Compositional dependence of optical absorption of bismuth-doped alumino-silicate glasses”, to be submitted to J. Ceram. Soc. Jpn.

Chapter 5: K. Sakaguchi, M. Tsuda and T. Uchino, “Composition and process dependence of optical absorption and emission properties of bismuth-containing zinc-borate glasses”, to be submitted to J. Non-Cryst. Solids.

Chapter 6: K. Sakaguchi, S. Domi and K. Suganuma, “New Glass Sealing Method with Lead-free Solders”, Advances in Science and Technology, 45 (2006) 1604-1607.